Beneath the Trees: The Influence of Natural Capital on Shadow Price Dynamics in a Macroeconomic Model with Uncertainty*

Ghassane Benmir[1] Aditya Mori[2,5] Josselin Roman[3] Romano Tarsia[4]

July 28, 2025

Abstract

We investigate how incorporating natural capital into a macroeconomic framework affects optimal economic allocation and climate policy under uncertainty. We develop a dynamic stochastic general equilibrium model in which output depends on both conventional inputs as well as renewable and non-renewable natural capitals. Rising temperatures degrade these stocks through input-specific climate damage functions. We estimate both the elasticities of substitution between natural capital and other inputs, and the magnitude of climate-induced damages. Using these estimates, we quantify the impact of natural capital dynamics on shadow prices and the social cost of carbon (SCC). We find that incorporating natural capital increases the SCC by approximately 12% relative to a benchmark DICE-***type*** model. In addition, SCC estimates are highly sensitive to the elasticity of substitution between production inputs. Under stochastic productivity and temperature shocks, the SCC rises by 39% in our baseline parametrization.

Keywords: Natural Capital, Shadow Prices, Social Cost of Carbon, Uncertainty.

JEL: *E6, Q2, Q5*

*This draft has benefited from comments and suggestions by V. Bosetti, V. Botelho, S. Dietz, M. Giuzio, S. Maso, E. Pappa, M. Parker, F. Venmans, S. Wei, participants at the CEPR Symposium on Climate Change and the Environment, the CIVICA Advancing Climate Economics Conference, the IAERE Conference, the 2025 RCEA International Conference on Economics, Econometrics, and Finance, the ECB-DG Economics Seminar, and the LSE Applied Economics WIP Seminar.

[1]IE University and Business School, P. de la Castellana, 259, Madrid, Spain; E-mail: ghassane.benmir@ie.edu.

[2]University of Oxford, Manor Road, Oxford OX1 3UQ, UK

[3]European Commission – Joint Research Centre; E-mail: josselin.roman@ec.europa.eu.

[4]London School of Economics and Political Science, Houghton Street, London WC2A 2AE, UK; E-mail: r.tarsia@lse.ac.uk.

[5]King's Business School and Qatar Centre for Global Banking & Finance, Strand, London WC2B 4BG, UK; E-mail: aditya_babubhai.mori@kcl.ac.uk.

1 Introduction

Natural capital, which includes ecosystems, natural resources, and the services they provide, underpins virtually all economic activity. It encompasses renewable and non-renewable assets such as forests, cropland, water, minerals, fossil fuels, and biodiversity, as well as the ecosystem services they generate, including climate regulation, soil fertility, pollination, and the provision of clean air and water. Despite its central role, natural capital remains largely absent from standard macroeconomic models. This omission leads to an underestimation of climate change impacts and distorts the cost-benefit analysis of climate policy.

In this paper, we develop a dynamic stochastic general equilibrium (DSGE) model that integrates natural capital and input-specific climate damages into the production structure. We introduce multiple forms of renewable and non-renewable natural capital and allow their degradation to depend on rising temperatures. Production technologies are governed by Constant Elasticity of Substitution (CES) aggregators, which enable us to estimate and explore substitution patterns between natural capital and conventional inputs such as labor and produced capital. Crucially, we also introduce stochastic shocks to productivity and climate dynamics, allowing us to compute expectation-based shadow prices for each form of natural capital under uncertainty.

We make two main contributions. First, we provide new empirical estimates of (i) climate-induced damage functions for different types of natural capital, and (ii) substitutability between these inputs. Second, we use these estimates in our macroeconomic model to quantify how shadow prices and the social cost of carbon (SCC) respond to uncertainty and structural assumptions. We compare our framework to a benchmark DICE-***type*** model without natural capital.

Our results indicate that including natural capital raises the SCC by approximately 12% in a deterministic setting. More strikingly, we show that SCC estimates are highly sensitive to substitution elasticities in the production function, more so than to commonly discussed parameters such as damage functions or discount rates. Under stochastic productivity and temperature shocks, the SCC increases by 39% under our baseline calibration. We also find that while unexpected fossil-fuel discoveries can spur a short-term output surge, they ultimately undermine long-run growth and erode social welfare.

This paper contributes to three main strands of the literature. First, we add to the growing body of climate econometrics that quantifies the economic damages associated with temperature shocks. While much of this literature focuses on outcomes such as agriculture (Deschênes and Greenstone, 2007; Schlenker and Roberts, 2009; Burke and Emerick, 2016), mortality (Deschênes and Greenstone, 2011; Barreca, 2012; Carleton, Jina, Delgado, Greenstone, Houser, Hsiang, Hultgren, Kopp, McCusker, Nath, et al., 2022), or aggregate GDP (Dell, Jones, and Olken, 2012; Burke, Hsiang, and Miguel, 2015; Klenow, Nath, and Ramey, 2023; Bilal and Känzig, 2024), we shift the focus to the effects of temperature on the stocks of natural capital. A closely related contribution by Bastien-Olvera, Conte, Dong, Briceno, Batker, Emmerling, Tavoni, Granella, and Moore (2024) estimates how climate change–induced changes in terrestrial vegetation cover affect economic output and the value of non-market ecosystem services. In contrast, we employ methods from the climate econometrics literature to estimate the impact of rising temperatures on a broader range of natural capital stocks. Specifically, we provide novel estimates of the economic costs of climate change stemming from damages to cropland, forest ecosystems, minerals, coal, gas, oil, fossil fuels, and renewable energy

sources.

Second, we contribute to the empirical literature on CES production functions within environmental economics. Previous studies, such as Acemoglu, Aghion, Bursztyn, and Hemous (2012); Papageorgiou, Saam, and Schulte (2017), and more recently Jo and Miftakhova (2024) have emphasized the importance of substitutability between clean and dirty energy inputs for green growth and provided estimates of CES functions within this context. Our modeling framework adopts a more disaggregated approach, requiring the estimation of elasticities both between different types of natural capital and between natural capital and conventional production inputs. Following Papageorgiou et al. (2017), we utilize a range of estimation techniques to assess the robustness of our results.

Third, we contribute to the literature on integrated assessment and macroeconomic climate models. The inclusion of climate dynamics in macroeconomic frameworks dates back to Nordhaus (1991), which laid the foundation for a wide range of Integrated Assessment Models (IAMs). However, this literature has primarily focused on the carbon cycle and the effects of rising temperatures on optimal economic allocation, often without explicitly modeling natural capital.[1] Studies such as Sterner and Persson (2008), Drupp (2018), and Drupp and Hänsel (2021) introduce natural capital or ecosystem services into the utility function focusing on willingness to pay. By contrast, we incorporate natural capital directly into the production function. In similar fashion, Dasgupta (2021), Bastien-Olvera and Moore (2021), and Bastien-Olvera et al. (2024) incorporate the evolution of natural capital stocks into their analyses within the production function and estimate their related climate damages for the latter, while Giglio, Kuchler, Stroebel, and Wang (2025) propose a stylized model highlighting the feedback loops between climate change and nature loss. Relatedly, Giglio, Kuchler, Stroebel, and Wang (2024) model a production function that captures the complementarity between produced capital and ecosystem services, emphasizing the role of biodiversity in sustaining the latter. Our modeling approach differs in three key respects. First, rather than imposing unitary elasticity of substitution (*i.e.*, a Cobb-Douglas structure), we estimate substitution parameters empirically. Second, we incorporate multiple forms of natural capital in the production function and allow for distinct damage functions and dynamics for each. Third, we extend the analysis beyond deterministic optimal allocation by examining how stochastic fluctuations in temperature and productivity affect the shadow prices of natural capital and the social cost of carbon.

The rest of the paper is organized as follows. Section 2 presents the macroeconomic model, including the role of natural capital and climate damages. Section 3 describes the data and estimation of damage functions and substitution elasticities. Section 4 presents simulation results, including long-run scenarios under optimal policy, SCC and shadow prices estimates, and the impacts of uncertainty. Section 5 concludes.

2 The Model

We develop a DSGE model that integrates multiple forms of natural capital and climate dynamics into a macroeconomic production structure. The model captures how rising temperatures affect different input types—produced capital, labor, and a range of renewable and non-renewable natural capital stocks including cropland, energy resources, minerals, and forest ecosystems.[2]

[1] Schubert (2018) offers a comprehensive review of the environmental macroeconomics literature.
[2] We detail and justify our choice of natural capital stocks in section 2.2 and section 3.1.

A visual representation of the model is provided in figure 1. Final output is produced through a nested CES production function that combines human capital, manufactured capital, and various forms of natural capital. Each aggregation node (shown in green) allows for a flexible elasticity of substitution, ranging from perfect complements to perfect substitutes. This setup enables us to empirically estimate substitution elasticities and evaluate how they shape the economy's response to climate damages and influence shadow prices and the social cost of carbon.

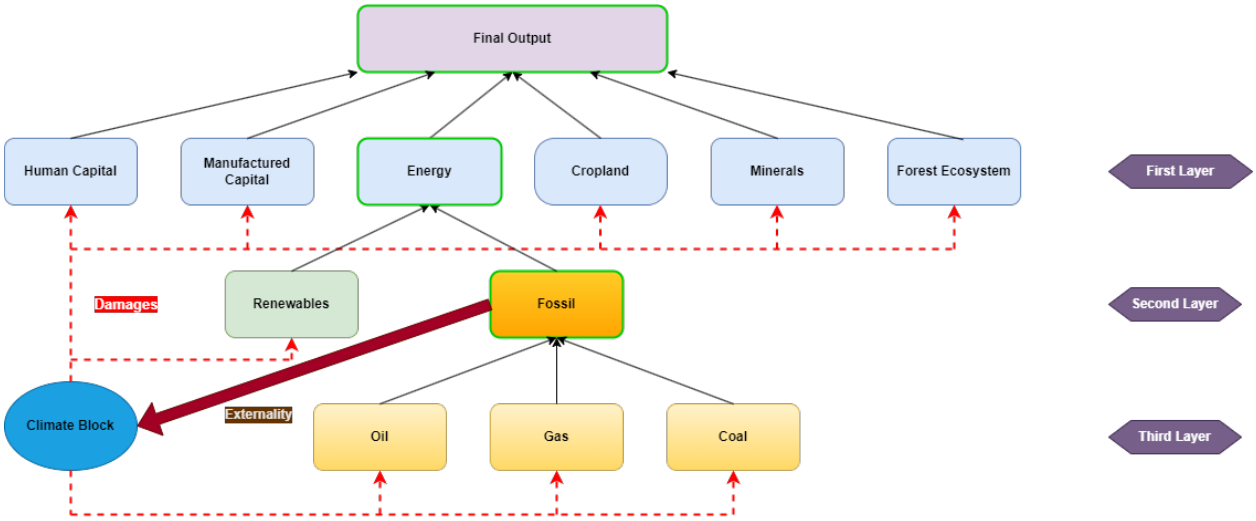

Figure 1: Structure of the Model

Energy can be produced using fossil fuels (coal, oil, and gas) or renewable sources. Fossil fuel use emits CO_2, which accumulates in the atmosphere and drives up global temperatures. In turn, temperature increases cause input-specific climate damages that lower the productivity of both natural and conventional production factors. A central part of our analysis involves estimating these damage functions empirically and exploring their implications for optimal climate policy.

We assume the economy operates in discrete time with annual periods and an infinite horizon. To derive optimal policy results, we adopt a social planner framework in which a benevolent planner internalizes the climate externality and allocates all available resources to maximize the lifetime utility of a representative household.

We now present the core building blocks of the model. We begin with the climate module and the carbon cycle, followed by the production structure and the household's optimization problem. We then turn to the social planner's problem, which yields the equilibrium allocation and the social cost of carbon.

2.1 Climate Dynamics

Building on the foundations of standard IAMs such as those proposed by Nordhaus (1991) and Nordhaus and Yang (1996), we integrate climate dynamics into our natural capital macroeconomic framework. We model the processes governing the atmospheric concentration of carbon dioxide and global temperature as follows. The global temperature T_t is assumed to be linearly proportional to the stock of CO_2 emissions,

representing the cumulative emissions over time, as established by Matthews, Gillett, Stott, and Zickfeld (2009):

$$T_{t+1} = \epsilon_t^T \phi_1 (\phi_2 X_t - T_t) + T_t, \tag{1}$$

with ϕ_1 and ϕ_2 being the climate transient parameters, calibrated to match both the temperature at the start of the simulation (i.e. 2018), and the temperature dynamics with respect to cumulative emissions and the initial.

Following Matthews et al. (2009), cumulative CO_2 emissions, denoted as X_t, reads as:

$$X_{t+1} = X_t + E_t, \tag{2}$$

ϵ_t^T is a temperature shock, which captures exogenous variations in temperature and is assumed to follow an AR(1) process $log(\epsilon_t^T) = \rho_T log(\epsilon_{t-1}^T) + \eta_t^T$ where ρ_T is the persistence of the shock and $\eta_t^T \sim N(0, \sigma^{T^2})$. X_{t+1} is the concentration of gases in the atmosphere, $E_t \geq 0$ anthropogenic emissions of CO_2 stemming from fossil fuel production Y_t^{FE} where:

$$E_t = \phi_E Y_t^{FE}. \tag{3}$$

with ϕ_E the emission intensity to fossil energy output.

In the spirit of Nordhaus (1991), temperature damages production. However the novelty in our work, is that: i) temperature damages are specific to each input in our production function and ii) feature temperature lags. The damage function reads as:

$$d_{\mathrm{h}}(\cdot) = \sum_m \beta_m^h T_{t-m}. \tag{4}$$

where β_m^h are the estimated betas for each natural capital. m represents temperature lags, while h represents all inputs impacted by climate raising temperatures, namely: oil, gas, coal, renewable energy, minerals, cropland, forest ecosystem, as well as the capital/labor inputs.

2.2 Natural Capital and Production

The World Bank's Changing Wealth of Nations (CWON) dataset classifies natural capital into nine categories: energy, minerals, cropland, forest ecosystem, timber provision, mangroves, fisheries, and protected areas. We focus on energy, minerals, cropland, and forest ecosystem, as well as the decomposition of energy resources.

We expand the traditional Cobb-Douglas production function with capital and labor to include the following natural capitals: energy Y_t^E, minerals Y_t^M, cropland Y_t^L, forest ecosystem services Y_t^{FO}, fossil energy Y_t^{FE}, renewable energy Y_t^{RE}, oil Y_t^O, gas Y_t^G, and coal Y_t^C. The following subsections detail the nested CES structure of our model and the laws of motion for the various stocks in our economy.

2.2.1 First Nest CES: Final Output

Final output Y_t^T is a CES function of the following aggregates: (i) produced capital Y_t^K, (ii) energy Y_t^E, (iii) minerals Y_t^M, (iv) cropland Y_t^L, (v) forest ecosystem services Y_t^{FO}, and (vi) human capital (labor

augmenting technology) Y_t^{AL}.

$$Y_t^T = \epsilon_t^A g_Y \left(\sum_k \theta_k \left(Y_t^k\right)^{\frac{\theta-1}{\theta}} \right)^{\frac{\theta}{1-\theta}}, \tag{5}$$

where $k \in \left\{Y_t^{\text{K}}, Y_t^E, Y_t^M, Y_t^L, Y_t^{\text{FO}}, Y_t^{\text{AL}}\right\}$. θ_k represents the production share of each input (with $\sum_k \theta_k = 1$), while θ is the elasticity of substitution and $g_Y > 0$ a scaling parameter to final output. ϵ_t^A is a TFP shock and is assumed to follow an AR(1) process $log(\epsilon_t^A) = \rho_A log(\epsilon_{t-1}^A) + \eta_t^A$ where ρ_A is the persistence of the shock and $\eta_t^A \sim N(0, \sigma^{A^2})$.

The choice of production function in this nest is guided by the natural capital data available from the CWON dataset. While a more comprehensive nesting such as composites of produced and human capital or cropland and minerals would be desirable, the absence of output data for such composites limits our specification. Furthermore, without such data, we cannot estimate the substitution elasticities needed to calibrate a more granular structure, justifying the more parsimonious specification employed here.

Human capital production function reads as:

$$Y_t^{\text{AL}} = e^{d_{\text{AL}}(\cdot)} A_t L_t, \tag{6}$$

where A_t is labor-augmenting productivity and L_t labor input, which is subject to an exogenous growth trend $\Gamma_t = \gamma^\Gamma \Gamma_{t-1}$.[3]

Natural capital production is assumed to rely on an exhaustible, finite stock S_t^j for each natural capital type j, following the framework of van der Ploeg and Rezai (2021). In the same spirit of van den Bijgaart and Rodriguez (2023), both passive and active regeneration is captured by D_t, encompassing processes such as mineral discovery, land transformation, natural regeneration or investment in forest ecosystem services. In addition, it captures the accumulation of non-depreciated produced capital through capital investment in line with standard macroeconomic models. This flexible specification allows us to represent the laws of motion for both renewable and non-renewable natural capital in the same form:

$$S_{t+1}^j = S_t^j - F(Y_t^j) + \epsilon_t^{D_i} \alpha_j D_t^j, \tag{7}$$

with: where $j \in \left\{Y_t^K, Y_t^{FO}, Y_t^L, Y_t^M\right\}$, $F(Y_t^j) = \delta_j S_t^j$, δ_j the depreciation rate, and α_j the share of discovery[4], that is subject to an AR(1) shock $\epsilon_t^{D_i}$.[5] Natural capital Y_t^j production is assumed to use the stock S_t^j and subject to non-linear climate damages $d_j(\cdot)$:

$$Y_t^j = e^{d_j(\cdot)} S_t^j. \tag{8}$$

2.2.2 Second Nest CES: Energy

Energy is a CES function of fossil energy and renewable energy:

[3] With $\gamma^\Gamma = 1 + \tilde{\gamma}^\Gamma$, where $\tilde{\gamma}^\Gamma$ the actual growth rate of the economy. In the online appendix C and appendix D we present both the non-detrended economy equilibrium and the balanced growth path equilibrium, respectively.

[4] In our framework, only a fraction of "discoveries" of new natural-resource stocks is usable to expand the productive stock of natural capital, as the rest (1-α_j) is often lost in beneficiation, processing, or applied at unrealizable rates and never contributes to long-run soil capital (Cordell, Drangert, and White (2009)).

[5] The AR(1) shock to discovery reads as: $log(\epsilon_t^{D_j}) = \rho_D log(\epsilon_{t-1}^{D_j}) + \eta_t^{D_i}$, with $\eta_t^{D_i} \sim \mathcal{N}(0, \sigma_{D_j}^2)$.

$$Y_t^E = g_E \left(\sigma_{\text{FE}} \left(Y_t^{\text{FE}}\right)^{\frac{\sigma-1}{\sigma}} + \sigma_{\text{RE}} \left(Y_t^{\text{RE}}\right)^{\frac{\sigma-1}{\sigma}} \right)^{\frac{\sigma}{1-\sigma}}, \tag{9}$$

with Y_t^{FE} and Y_t^{RE} being the production of fossil and renewable energy, respectively. σ_{FE} and σ_{RE} represents the production share of each input (with $\sigma_{\text{FE}} + \sigma_{\text{RE}} = 1$), while σ is the elasticity of substitution and $g_E > 0$ a scaling parameter to aggregate energy output.

As with the other types of natural capital, renewable energy production relies on a finite stock S_t^{RE}. This stock can be increased through investment D_t^{RE} and part of it is used in the production process:

$$S_{t+1}^{\text{RE}} = S_t^{\text{RE}} - F(Y_t^{\text{RE}}) + \epsilon_t^{D_{\text{RE}}} \alpha_{\text{RE}} D_t^{\text{RE}}, \tag{10}$$

with α_{RE} the share of renewable investment, $\epsilon_t^{D_{\text{RE}}}$ an AR(1) investment shock, and $F(Y_t^{\text{RE}}) = \delta_{\text{RE}} S_t^{\text{RE}}$. Renewable energy production Y_t^{RE} is again assumed to use the stock S_t^{RE} and is subject to climate damages d_{RE}:

$$Y_t^{\text{RE}} = e^{d_{\text{RE}}(\cdot)} S_t^{\text{RE}}. \tag{11}$$

2.2.3 Third Nest CES: Fossil Energy

Fossil energy is, in turn, a CES function of oil, gas, and coal:

$$Y_t^{\text{FE}} = g_F \left(\sum_i \epsilon_i \left(Y_t^i\right)^{\frac{\epsilon-1}{\epsilon}} \right)^{\frac{\epsilon}{1-\epsilon}}, \tag{12}$$

where $i \in \left\{Y_t^O, Y_t^G, Y_t^C\right\}$. ϵ_{FE} and ϵ_i is the production share of each input (with $\epsilon_O + \epsilon_G + \epsilon_C = 1$), while ϵ is the elasticity of substitution between oil, gas, and coal, and $g_F > 0$ a scaling parameter to aggregate fossil energy output.

Similar to the previous natural capitals, oil, gas, and coal each have a finite stock S_t^i, and discoveries D_t^i can be made over time, allowing these natural capital stocks to increase:

$$S_{t+1}^i = S_t^i - F(Y_t^i) + \epsilon_t^{D_i} \alpha_i D_t^i, \tag{13}$$

with $\epsilon_t^{D_i} \alpha_i$ the stochastic share of discovery as for the first nest, and $F(Y_t^i) = \delta_i S_t^i$ and natural capital Y_t^j production is assumed to use total stock S_t^i and subject to the same type of climate damages discussed above:

$$Y_t^i = e^{d_i(\cdot)} S_t^i. \tag{14}$$

2.3 Households

The representative household problem features a constant relative risk aversion (CRRA) utility function with habits formation:

$$\text{Welfare}_t = \mathbb{E}_0 \sum_{t=0}^{\infty} \beta^t \left\{ \frac{\left(C_t - \gamma_H H_t\right)^{1-\sigma^H}}{1-\sigma^H} \right\}, \tag{15}$$

where β represents household time preference and σ^H is the risk aversion parameter, while $\gamma_H \in (0,1)$ is the degree of habits.[6]

The household derive utility from consumption expenditures C_t subject to habit formation H_t and inelastic labor hours $\frac{L_t}{\Gamma_t} = \bar{L}$.

$$H_{t+1} = \bar{m}H_t + (1-\bar{m})C_t. \tag{16}$$

Where $\bar{m}$ is the degree of habit formation persistence. As argued in Benmir, Jaccard, and Vermandel (2020), we introduce internal habit formation to maximize our macro-finance model's ability to generate realistic asset-pricing dynamics and macroeconomic implications. Internal habit formation has been shown to play a central role in accurately matching asset-price dynamics and variations in macroeconomic aggregates, as well as in driving carbon-pricing responses to different shocks. Habits lead to greater volatility in carbon prices compared with standard CRRA utility or recursive preferences. This elevated volatility over the business cycle has important implications for policy design and for optimal carbon pricing.

2.4 The Aggregate Resource Constraint

We close the model with the aggregate resource constraint of the economy, which reads as follows:

$$Y_t^T = C_t + \sum_h D_t^h. \tag{17}$$

2.5 The Social Cost of Carbon Under The Presence of Natural Capital

We now characterize the first-best allocation, considering the optimal plan a benevolent social planner would choose to maximize welfare.[7]

Definition 1 *The optimal policy problem for the social planner is to maximize total welfare in equation (15) by choosing a sequence of allocations for the quantities* $\{H_{t+1}, X_{t+1}, T_{t+1}, C_t, E_t, Y_t^{AL}, Y_t^{FE}, Y_t^E, Y_t^T, Y_t^h, D_t^h, S_{t+1}^h\}$, *for given initial conditions for the eleven endogenous state variables* H_0, S_0^h,[8] T_0 *and* X_0 *as well as all the stochastic shocks that satisfy equation (1), equation (2), equation (3), equation (5), equation (6), equation (7), equation (8), equation (9), equation (10), equation (11), equation (12), equation (13), equation (14), and equation (16).*

Definition 2 *In a centralized equilibrium, the planner fully internalizes the SCC (i.e. the shadow price of* CO_2 *emission* V_t^E*, ensuring that the marginal cost of emissions matches the shadow price of* CO_2 *emissions.*

Solving the optimal policy problem, the SCC under the presence of natural capital reads as:

$$V_t^E = \beta \mathbb{E}_t \left\{ \frac{\lambda_{t+1}^C}{\lambda_t^C} \left[V_{t+1}^E + \epsilon_{t+1}^T \phi_1 \phi_2 V_{t+1}^T \right] \right\}, \tag{18}$$

[6] We set γ_H very close to 1, as habits persistence will be captured by m. γ_H main role is to ensure non-zero utility at the steady state.

[7] Refer to the online appendix C for the full derivations.

[8] Where $h \in \{i\} \cup \{j\} \cup \{\text{RE}\}$.

where V_t^T represents the discounted sum of future temperature climate damages:

$$V_t^T = \mathbb{E}_t \left\{ \beta \frac{\lambda_{t+1}^C}{\lambda_t^C} \left[(1 - \epsilon_{t+1}^T \phi_1) \right] V_{t+1}^T \right\} - \sum_h \sum_m \mathbb{E}_{t+m} \left\{ \left[\left(\prod_{o=0}^{m-1} \beta \frac{\lambda_{t+1+o}^C}{\lambda_{t+o}^C} \right) \Psi_{t+m}^h \beta_m^h Y_{t+m}^h \right] \right\}. \tag{19}$$

3 Parameterization and Empirical Estimation

This section starts by presenting the data used in this paper, followed by the calibration of the representative economy and lastly, we present the estimation of the CES production function and the climate damages.

3.1 Data

The data employed in this paper is drawn from four sources: the World Bank Changing Wealth of Nations (CWON), the World Bank Database, Our World in Data (OWID) Energy Dataset, and the Climate Change Knowledge Portal (CCKP).[9]

The CWON dataset provides a comprehensive measure of national wealth by reporting stock estimates of produced, natural, and human capital for approximately 150 countries from 1995 to 2018. We adopt CWON's classification of natural capital throughout our analysis. Of the natural capitals available in CWON, we do not include mangroves and fisheries as they are not directly relevant to the aggregate production of a representative global economy. In addition, forest timber is not included because it has an estimated zero production share. Importantly, CWON reports these stocks in monetary terms, reflecting market valuations rather than physical quantities. For the purposes of estimating climate damages, it is crucial not to conflate the effects of temperature on the quantity of natural capital with changes in its market value. To address this, we use quantity-based measures of natural capital wherever feasible. For example, for cropland we rely on the World Bank's Arable Land data (measured in hectares per capita), which we convert to total hectares using population data from CWON. Similarly, in estimating CES production functions, we resort to market valuations only when quantity measures are unavailable, as is the case for the first layer of the CES production function. GDP data is sourced from the World Bank.

The OWID Energy Dataset offers a panel of country-level energy production and consumption figures disaggregated by energy source and reported in physical units, which is essential for the calibration, accurate CES production function estimation and the analysis of climate damages. Finally, temperature and precipitation data are obtained from the CCKP, which provides country-level aggregates of the ERA5 grid-level data.

A summary of the variables used in the analysis is presented in table 1. Descriptive statistics for the data underlying the CES production function estimation and the natural capital climate damage assessment are provided in table 5 and table 6, respectively.

[9] We also draw on a few additional sources—cited where used—to calibrate the investment and discovery rates of our natural capital.

Variable	Description	Unit	Source
GDP	GDP at purchaser's prices	2018 USD	World Bank
Capital	Value of buildings and equipment	2018 USD	CWON
Human Capital	PV of future earnings for the population	2018 USD	CWON
Ecosystem	Forest ecosystem services	2018 USD	CWON
Cropland	Agricultural Land	2018 USD	CWON
Minerals	Composite of different minerals	2018 USD	CWON
Fossil Energy	Oil, gas, hard and soft coal	2018 USD	CWON
Electricity Demand	Demand for electricity	Terawatt hours	OWID
Fossil Fuel Electricity	Electricity generation from fossil fuels	Terawatt hours	OWID
Renewable Electricity	Electricity generation from renewables	Terawatt hours	OWID
Oil Production	Oil production	Terawatt hours	OWID
Gas Production	Gas production	Terawatt hours	OWID
Coal Production	Coal production	Terawatt hours	OWID
Coal Electricity	Electricity generation from coal	Terawatt hours	OWID
Gas Electricity	Electricity generation from gas	Terawatt hours	OWID
Oil Electricity	Electricity generation from oil	Terawatt hours	OWID
Energy	Primary energy consumption	Kilowatt hours	OWID
Temperature	Average mean surface-air temperature	Celsius	CCKP
Precipitation	Average precipitation	mm	CCKP

Table 1: Variable Description and Sources

3.2 Calibration

Following conventional practice, we calibrate the parameters with annual time intervals. We customize the calibration process to match key observed aggregates such as temperature, global CO_2 emissions, and the value of each natural capital stock, all within the world context. This meticulous calibration ensures that our model accurately captures the real-world dynamics and trends of these critical environmental and economic indicators. Table 7 lists the values of all parameter calibrations, while table 8 summarizes the moments we match.

The parameters pertaining to the business cycle structure of our model are conventional. For the standard parameters in these models, such as the discount factor β and the risk aversion σ^H, we align with typical values used in macroeconomic modeling. Specifically, the discount factor β is set at 0.968 to match a 3.3 percent world GDP-weighted interest rate, while the risk aversion σ^H is set at 2, following Stern (2008). Labor $\bar{L}$ hours worked are set at $1/3$ (which corresponds to daily mean of 8 hours). The productivity of labor A is calibrated to match the level of human capital in 2018 as reported in the matching moments table (see table 8). The habits level parameter $\bar{m}$ is set at 0.9, following Benmir et al. (2020). The parameter γ_H takes two values: i) $\gamma_H = 1$ in the case of stationary equilibrium (i.e., the discovery/investment exercise), and ii) $\gamma_H = 0.975$ in the case of the non-detrended economy, to avoid utility going to zero with consumption equal to habits at the steady state. Finally, the AR(1) shock process persistence parameter is set at 0.9, as is standard in the literature, and the growth rate of the world economy $\tilde{\gamma}^\Gamma$ is set at 3 percent, corresponding to the average world growth rate over the past 10 years.

All specific capital production values are set according to data taken from the World Bank database. In particular, parameters such as the weights for aggregating fossil energy, aggregate energy, and final outputs (denoted as g_F, g_E, and g_Y, respectively) are calibrated to match the values of Y^{FE}, Y^E, and Y^T presented in table 8.

We set the output of renewable energy to $542.7 billion, based on the global average cost of electricity

from renewable sources ($81 per megawatt-hour, MWh) in 2018, relative to total production of 6,700,000,000 MWh.[10]

For the remaining specific outputs, which are set according to the World Bank, we use the production share of capital stocks, δ_s, to match the values in the corresponding data in table 8. Regarding discovery and investment, we use the discovery/investment share, α_s, to precisely match the level of discovery/investment relative to specific capital production in table 8.[11] The ratio of discovery/investment to each specific capital production is calibrated using estimates from the International Energy Agency (IEA). In particular, the investment/discovery-to-output ratios for renewable energy, oil, gas, and coal are set to 156%, 0.46%, 0.14%, and 1%, respectively. For produced capital, mining, cropland, and forest ecosystem services, the investment/discovery-to-output ratios are set to 3%.[12] In addition, we calibrate the damages to human capital following the standard DICE calibration of damages to output since these are not estimated.

In calibrating the climate block of the model, we follow Dietz and Venmans (2019) and set the parameters for the global temperature function as $\zeta_1^o = 0.50$ and ζ_2^o to retrieve the initial temperature level of 1^{o}C at the start of the transition. Finally, the emission intensity parameter ϕ_E is set to 0.0014 to match the initial state of emissions with respect to fossil fuel production. Finally, we estimate the CES production parameters and natural capital damages, which are presented below.

3.2.1 Natural Capital CES Estimation

The model introduces a nested CES production function with three nests, corresponding to the production of final goods, energy, and fossil energy, respectively. To calibrate the production functions, we estimate both the elasticities of substitution and the share parameters. Our estimation method closely follows the approach of Papageorgiou et al. (2017), using both non-linear least squares (NLS) and the linear approximation proposed by Kmenta (1967). For the NLS estimation, we use Adam, a stochastic gradient descent (SGD) method and Sequential Quadratic Programming (SQP) method to verify the robustness of our result to the method employed.[13] NLS is applied across all three nests, while the Kmenta approximation is restricted to the second and third nests, each of which involves only two inputs. This follows Hoff (2004), who highlights that the parameter constraints required by the Kmenta method grow prohibitively complex as the number of inputs increases.

Following Papageorgiou et al. (2017), we note that our results should be seen as associations rather than causal due to endogeneity concerns arising from unobserved productivity shocks that may influence input choices. Additionally, there is simultaneity between input and output decisions. Studies such as Jo (2025), Jo and Miftakhova (2024) and Atalay (2017) among others have addressed this issue using price instruments or exogenous price shifters.[14] However, we are unable to implement this method here given the lack of price data for natural capital inputs. For brevity, we present only the baseline results in the main

[10] The global total production of renewable energy in 2018 was between 6.7 and 7.4 petawatt-hours (PWh). The average price is based on the International Renewable Energy Agency (IRENA): i) onshore ($50 to $70 per MWh) and offshore ($120 to $150 per MWh) wind, ii) solar photovoltaic ($85 per megawatt-hour), iii) hydropower ($40 to $80 per MWh), and iv) Bioenergy and Geothermal ($70 to $150 per MWh). See https://www.irena.org/-/media/Files/IRENA/Agency/Publication/2018/Apr/IRENA_Report_GET_2018.pdf.

[11] We also consider cases where these intensity shares change unexpectedly in the context of our stochastic shock analysis.

[12] Due to data limitations, we set them all to 3%, representing the lower bound of produced capital investment as a share of output.

[13] For the second and third nest, we implement Adam within Wei and Jiang (2025)'s neural network method as it generates smaller mean squared errors. Implementing this in the first nest proved more challenging due to the multiplicity of inputs.

[14] Lagomarsino (2020) provides a comprehensive review of the literature employing different methods including this approach.

text. In these specifications, the returns to scale parameter υ is fixed at 1 in the first nest and thereafter, set to the value estimated using the Kmenta approximation, following the recommendation of Corbo (1976), who find that the Kmenta method yields a consistent estimate of returns to scale. Further details, including a review of the relevant CES estimation literature, a description of the estimation procedures, validation of our results using multiple estimation approaches and a comparison of our results with existing findings are provided in appendix section B.2.

Table 2 presents the estimates for all three nests in Panels A, B and C respectively. In the first nest, in addition to estimating the full CES production function as in equation (5), we also estimate a CES production function including only human capital, produced capital and energy inputs to compare it to a DICE-***type*** production function. Panel A of table 2 shows that, consistent with macroeconomic literature, human capital contributes the largest share to output followed by produced capital and energy across both production functions. In addition, the results indicate that natural capitals are substitutable. Table 11 demonstrates that elasticity is robust across specifications and alternative estimation methods, ranging from 1.65 to 1.79.

Panel A: First nest

	θ_{K}	θ_{AL}	θ_{FO}	θ_{L}	θ_{M}	θ_{E}	g_Y	υ_Y	$\theta = \frac{1}{1+\rho_Y}$	MSE
Full Model	0.2278	0.4261	0.0366	0.1178	0.0155	0.1764	0.3565	1.0000	1.7368	0.1028
	(0.0195)	(0.0293)	(0.0204)	(0.0135)	(0.0072)	(0.0101)	(0.0147)			
Energy-Only Model	0.2531	0.5426	–	–	–	0.2043	0.2739	1.0000	1.7274	0.1114
	(0.0215)	(0.0227)				(0.0138)	(0.0049)			

Panel B: Second nest

	σ_{FE}	σ_{RE}	g_E	υ_E	$\sigma = \frac{1}{1+\rho_E}$	MSE
ADAM Fixed υ	0.5226	0.4774	1.0473	0.8126	5.1256	0.0153
	(0.0602)	(0.0602)	(0.0332)			
Kmenta-OLS	0.5076	0.4924	4.0316	0.8126	1.7156	0.0186
	(0.0540)	(0.0540)	(0.0575)	(0.0117)		

Panel C: Third nest

	ϵ_{G}	ϵ_{C}	g_F	υ_F	$\epsilon = \frac{1}{1+\rho_F}$	MSE
ADAM Fixed υ	0.3990	0.6010	1.2630	0.4149	1.6670	0.0075
	(0.0127)	(0.0127)	(0.0399)			
Kmenta-OLS	0.5013	0.4924	52.1997	0.4149	1.2643	0.1326
	(0.0512)	(0.0512)	(0.2446)	(0.0425)		

Note: Numbers in parentheses are bootstrapped standard errors. Blank cells denote parameters not estimated in that specification.

Table 2: CES Estimates All nests

For the second nest, we disaggregate the energy input in the first nest into renewable and fossil energy inputs. Panel B of table 2 reports the estimation results from both methods, indicating a greater share assigned to fossil energy relative to renewable energy. Moreover, both approaches yield elasticity estimates greater than one, suggesting that fossil and renewable energy are substitutable. These findings are broadly consistent with the estimates provided by Papageorgiou et al. (2017), Jo (2025) and Jo and Miftakhova (2024). As shown in table 13, elasticity estimates range from 1.72 to 5.69 across methods and specifications, with both consistently assigning a higher share to fossil energy inputs.

Lastly, fossil energy is a CES aggregate of oil, gas and coal inputs. However, noting that fossil electricity

generation (the dependent variable) is primarily driven by gas and coal, we sum oil and gas production into a single input. Panel C of table 2 presents the resulting estimates, which suggest that coal and gas are substitutable although only moderately so. As shown in table 14, elasticity estimates across methods and specifications range from 1.13 to 1.67. In addition, coal tends to receive a higher estimated share relative to oil-gas composite.

3.2.2 Natural Capital Climate Damages Estimation

Rising temperatures affect natural capital through multiple mechanisms. For cropland, higher temperatures accelerate soil degradation, reduce water availability, and increase evaporation, leading to a decline in total arable land. Besides impacting food production and economic stability in agrarian regions, these changes feedback on regional climate systems, influencing warming patterns and exacerbating the intensity, frequency, and duration of extreme events (IPCC, 2019). Forest ecosystems, vital for carbon sequestration and biodiversity conservation, are particularly vulnerable to warming (Graham, Turner, and Dale, 1990), as intensified evapotranspiration increases forests susceptibility to wildfires, pest outbreaks, and disease (Seidl, Thom, Kautz, Martin-Benito, Peltoniemi, Vacchiano, Wild, Ascoli, Petr, Honkaniemi, et al., 2017). The resulting decline in forest cover compromises ecosystem services and amplifies climate change impacts. Mineral resources are also affected, as rising temperatures raise cooling costs in mining. Roy, Mishra, Bhattacharjee, and Agrawal (2022) highlights the reduction of extraction efficiency due to heat related stress on underground miners.[15]

This study further explores the vulnerabilities of fossil fuels—coal, gas, and oil. Higher temperatures can reduce the efficiency of extraction and processing, while increasing the risk of disruptions due to extreme weather events. This increases production costs and threatens the stability of energy supplies. Climate change can also influence the supply of renewable energy, particularly for the hydro and wind power generation.[16] Furthermore, higher temperatures can influence the demand for energy consumption. Warmer years result in greater cooling requirements during warm months, while simultaneously reducing energy demand for heating in colder months. The net effect of these opposing forces depends on the intra-annual distribution of daily temperatures and the degree of seasonal variability.

The economic implications of these impacts are extensive. Reduced agricultural capacity affects food security and increases volatility in food prices, with cascading effects on economies dependent on agriculture. The decline in forest health and cover affects industries reliant on forest products and services, from timber to tourism. Increased operational costs in mining and energy sectors lead to higher prices for these essential resources, impacting a wide range of industrial activities and economic outputs. In this section, we present novel estimates of the impact of temperature on the considered natural capitals.

Identification Strategy. The estimation of climate damages draws on the latest advancements in the climate econometrics literature.[17] The current methodological frontier relies on panel data analysis, that exploits spatial and time fixed effects to isolate plausibly random variations in weather with (Hsiang, 2016).

[15] These dynamics remain mostly unexplored in the economics literature.

[16] For a review of the various dynamics through which climate change can affect energy supply see Schaeffer, Szklo, de Lucena, Borba, Nogueira, Fleming, Troccoli, Harrison, and Boulahya (2012).

[17] The literature has evolved from cross-country studies (Nordhaus, 2006) to panel data approaches (Dell et al., 2012; Burke et al., 2015; Kotz, Levermann, and Wenz, 2024), enabling the identification of idiosyncratic weather shocks (Hsiang, 2016).

Two primary approaches have emerged to ascertain the causal impact of temperature on socioeconomic factors: yearly average temperature and temperature bins.[18] In this study, we adopt the former approach as it aligns more coherently with the climate damages incorporated into our macroeconomic model. For a discussion of these methodologies in the context of economic damages, see Tarsia (2023).

Our empirical strategy adopts an agnostic approach towards model selection, aiming to identify the most appropriate model guided by empirical evidence. Hence, we initially define each variable of interest as a flexible function of temperature and precipitation:

$$y_{i,t} = g(T_{i,t}) + f(P_{i,t}) + \sum_{\ell \geq 1} h(T_{i,t-\ell}) + \delta_i + \lambda_t + \varepsilon_{i,t} \tag{20}$$

where $y_{i,t}$ represents the natural logarithm of country i's variable of interest in year t, $g(T_{i,t})$ denotes a flexible function capturing the impact of yearly average temperature on $y_{i,t}$ for country i in year t, $f(P_{i,t})$ represents a flexible function capturing the impact of yearly total precipitation on $y_{i,t}$, $\sum_{\ell \geq 1} h(T_{i,t-\ell})$ is defined as the sum over ℓ lags of a flexible function of yearly average temperature, δ_i stands for a country fixed effect that accounts for country-specific unobserved constant components, λ_t denotes a year fixed effect that accounts for time-specific unobserved constant components such as economic and climate trends or shocks, and $\varepsilon_{i,t}$ represents the autocorrelated and spatially correlated error component. In appendix section B.3, we report the details of the model selection procedure used to identify the model outlined in equation (20).

As a result, we estimate the marginal effect of an additional $1°C$ in yearly average temperature on our variables of interest using the following model:

$$y_{i,t} = \alpha + \beta_0 T_{i,t} + \sum_{\ell=1}^{2} \beta_\ell T_{i,t-\ell} + \psi_0 P_{i,t} + \delta_i + \lambda_t + \varepsilon_{i,t} \tag{21}$$

where the variables are defined as in equation (20). In this framework $y_{i,t}$ is the log of the various natural capital variables of interest, defined in levels if stationary or in first difference otherwise, according to the results of online appendix B.2. The marginal effects identified by the estimates β_ℓ are the average percentage change in $y_{i,t-\ell}$ due to an additional $1°C$ in yearly average temperature $T_{i,t-\ell}$ for $\ell = \{0, 1, 2\}$. Table 3 reports the estimates from the analysis based on equation (21) for each variable of interest. All variables, except oil, are negatively affected by higher temperatures, though with different timing.

The estimates are negative and statistically significant across all lags $\ell = \{0, 1, 2\}$ for produced capital, gas, and fossil fuel, in lags $\ell = \{0, 1\}$ for forest ecosystem, in lags $\ell = \{1, 2\}$ for cropland and minerals, and only in lag $\ell = 0$ for aggregate energy and renewable energy. The estimates for coal are statistically significant only in period $t-2$ and positive, though small in magnitude. Given the negative contemporaneous estimate, this suggests a sign reversal and points to the absence of persistent growth effects. Since the estimates for coal are inconsistent with those for the other variables, and mostly not statistically significant, we rely on the fossil fuel estimates to calibrate the coal-specific damage function in the model.

[18] The former method estimates the impact of changes in yearly average temperature (Dell et al., 2012; Burke et al., 2015), whereas the latter evaluates the impact of an additional day with average temperature within a specific range (Deschênes, Greenstone, and Guryan, 2009).

	(1) Produced Capital	(2) Cropland	(3) Forest Ecosystem	(4) Minerals	(5) Δ Agg. Energy	(6) Δ Coal	(7) Gas	(8) Oil	(9) Fossil Fuel	(10) Renewable Energy
T	-0.0297**	-0.015	-0.011**	-0.027			-0.084**	-0.041	-0.063**	-0.062**
	(0.0084)	(0.012)	(0.0036)	(0.017)			(0.029)	(0.048)	(0.020)	(0.020)
$(\ell 1)\ T$	-0.0396***	-0.051***	-0.011**	-0.082**			-0.088***	-0.011	-0.057**	-0.029
	(0.0088)	(0.0081)	(0.0038)	(0.026)			(0.023)	(0.051)	(0.019)	(0.018)
$(\ell 2)\ T$	-0.0357***	-0.047***	-0.0078	-0.160***			-0.098***	0.031	-0.039**	-0.045
	(0.0086)	(0.010)	(0.0070)	(0.027)			(0.017)	(0.032)	(0.015)	(0.024)
ΔT					-0.016***	-0.0037				
					(0.0035)	(0.020)				
$(\ell 1)\ \Delta T$					-0.0056	0.021				
					(0.0034)	(0.018)				
$(\ell 2)\ \Delta T$					-0.0013	0.014**				
					(0.0024)	(0.0041)				
P	0.00001	0.0001	-0.00001	0.0001			-0.0003**	-0.0004*	-0.0001	0.0002**
	(0.00002)	(0.00006)	(0.00002)	(0.0001)			(0.0001)	(0.0002)	(0.0001)	(0.0001)
ΔP					0.00001	-0.00011**				
					(0.00001)	(0.00004)				
Country FE	Yes	Yes	Yes	Yes	Yes	Yes	Yes	Yes	Yes	Yes
Year FE	Yes	Yes	Yes	Yes	Yes	Yes	Yes	Yes	Yes	Yes
R^2	1.00	1.00	1.00	0.93	0.26	0.14	0.92	0.89	0.97	0.96
N	1584	1584	1562	1254	1512	1067	1452	1423	1504	1483

Standard errors in parentheses
* $p < 0.10$, ** $p < 0.05$, *** $p < 0.01$

Table 3: Point estimates and standard errors from the regressions of weather variables on the natural capital variables belonging to the first nest. Results from the linear model of temperature with all variables expressed in differences, country and year FE, and standard errors clustered at the regional level as identified by the World Bank.

The estimates indicate that these sources of natural capital are consistently negatively affected by higher temperatures, although with different magnitudes. Among the variables in the first nest the marginal effect of an additional $1°C$ in yearly average temperature ranges between approximately -1% for forest ecosystem and aggregate energy to approximately -16% for minerals (in year $t-1$), whereas the effect is approximately -3% across all years for produced capital and approximately -5% for cropland (in years $t-1$ and $t-2$). The variables in nests two and three are characterized by larger effects: between -4% and -6% for fossil fuel, between -8% and -10% for gas, and approximately -6% for renewable energy (in year t). The energy sector exhibits larger estimates as it is subject not only to supply-side shocks but also to demand-side fluctuations, insofar as higher temperatures influence both heating and cooling needs. In addition, while large estimates of climate damages are not uncommon in the literature (Ricke, Drouet, Caldeira, and Tavoni, 2018; Bilal and Känzig, 2024; Kotz et al., 2024), it is important to emphasize that these marginal effects correspond to a 1°C increase in temperature, whereas yearly average temperatures typically fluctuate by only a fraction of a degree.

The estimates for lagged temperature suggest that these effects are generally non-transitory. With the exception of coal, the estimates are negative or not statistically significant, emphasizing the presence of persistent growth effects. This implies that the negative shocks on natural capital induced by higher temperature are not recovered, but instead affect countries' ability to grow. This result is not surprising given the variables we are analyzing. Unlike GDP studied in previous work, natural capital is not as dynamic and regenerates at slow rates. Therefore, any negative shock is unlikely to be recovered in the medium term.

4 Quantitative Analysis

In this section, we use the parameter estimates from section 3 to explore the quantitative implications of the model detailed in section 2. The primary objective is to highlight two main findings: first, the sensitivity of the social cost of carbon and natural capital shadow prices to key structural parameters, particularly the elasticity of substitution between production inputs; and second, the importance of accounting for uncertainty—especially in the presence of habit formation—for optimal valuation and social welfare. Before turning to these core results, we examine the long-run transition trajectories implied by the model under optimal allocation. While not a central contribution of the paper, this exercise serves to illustrate the internal mechanics of the model and to verify that the inclusion of natural capital, along with the estimated parameter values, yields plausible macroeconomic dynamics consistent with the broader climate-economics literature.

4.1 Model Solution

Our modeling framework extends the familiar solution techniques used in DICE-***type*** integrated assessment models to handle both long-run growth dynamics and medium/shorter-term cyclical fluctuations (*e.g.* stochastic shocks) in a unified way. In particular, we employ a perfect-foresight solver to compute deterministic transition paths for the economy and climate system under specified policy trajectories or exogenous trend shocks. This approach preserves the ability of non-linear solution methods to accurately capture transition dynamics even far from the steady state, while retaining the computational tractability needed for high-dimensional, non-linear systems, whereas usual local approximation techniques do not perform as well in the presence of such non-linearities, especially in the context of highly non-linear climate dynamics. By directly solving the full non-linear model over the entire transition horizon, we ensure that regime shifts, such as those induced by climate damages, are faithfully represented in our long-run transitions.

To analyze the medium- and short-term business cycle effects of discovery and investment shocks, we rely on perturbation methods around the initial deterministic steady state to compute impulse response functions (IRFs). This stochastic component allows us to capture the effects of transitory shocks, such as temporary changes in total factor productivity or resource discoveries, on the cyclical dynamics of the economy. To ensure the validity of the approximation, we apply a stationary transformation by detrending all variables around their respective trends, thereby recovering a balanced growth path (BGP). This guarantees that shocks are mean-zero and variance-bounded, and allows us to decompose the IRFs into contributions from each individual driver.

4.2 Model Long-Run Properties

We begin by illustrating the model's long-run dynamics under the assumption of optimal allocation. From 2018 to 2125, the economy is projected to grow at an annual rate of 3 percent in human capital,[19] and all trajectories are computed using a perfect foresight solution method. The purpose of this exercise is not to

[19] This growth rate can be interpreted as reflecting improvements in labor-augmenting technology and/or population growth. Endogenous growth is not modeled in our framework and is left for future research.

provide policy projections, but to verify that the inclusion of natural capital and the estimated parameters yields internally consistent and plausible macroeconomic dynamics.

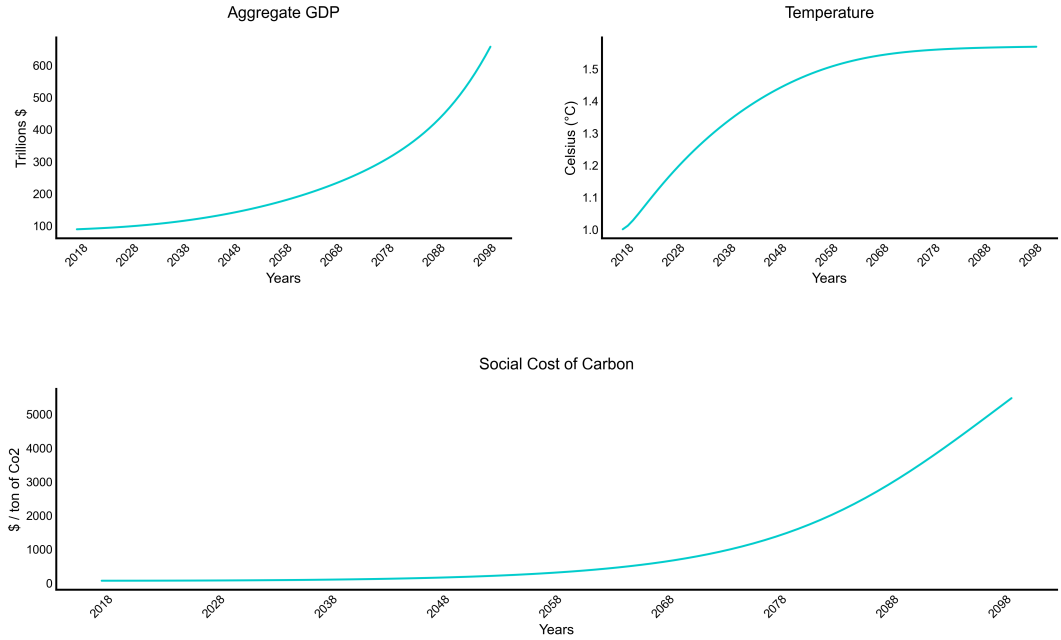

Figure 2: Long-Run Transition: Social Cost of Carbon

Notes: This figure illustrates the long-run transition over 82 years (up to 2100) with a 3 percent growth rate in human capital.

Figure 2 displays the evolution of aggregate output, temperature, and the social cost of carbon. As human capital grows exogenously, aggregate output increases, which raises emissions and exerts upward pressure on temperature. In response, the SCC rises steadily, reflecting the planner's internalization of the climate externality. The increase in the SCC drives a gradual shift away from fossil energy toward renewable sources, as shown in figure 3.

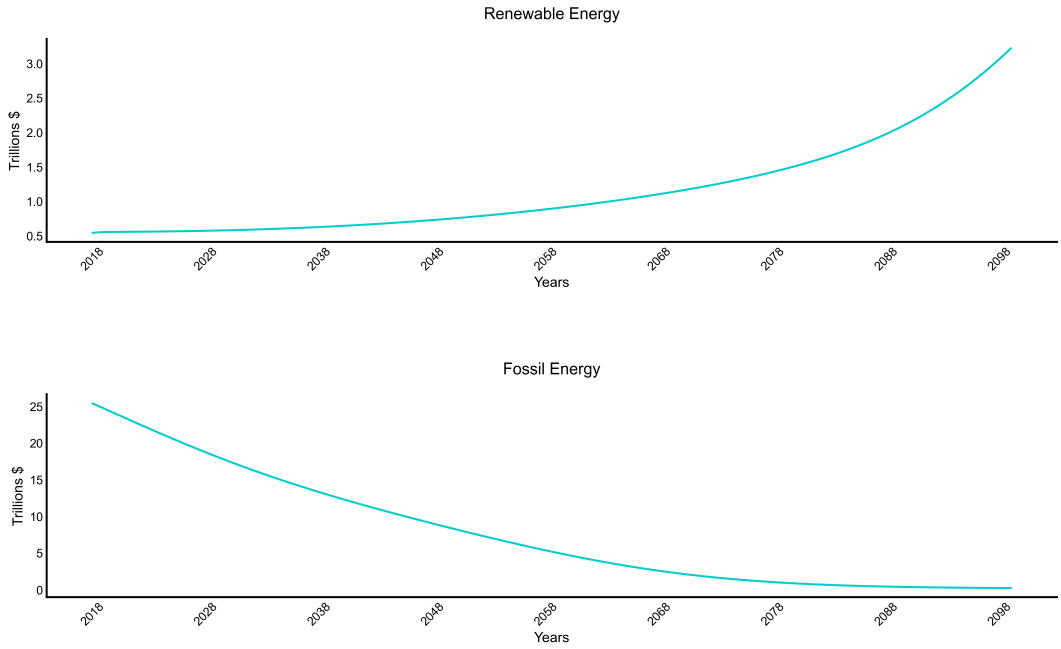

Figure 3: Long-Run Transition: Energy Components

Notes: This figure illustrates the gradual shift from fossil fuels to renewable energy in response to the rising social cost of carbon.

The planner's response ensures that the climate constraint is met: by the end of the horizon, temperature remains close to 1.5°C. This outcome is achieved through a steady decline in fossil energy use, with each of its components (oil, gas, and coal) decreasing over time and a complete phaseout occurring around 2090 (see figure 14).

In the short run, we observe a temporary decline in all types of natural capital and produced capital (see figure 12 and figure 13), driven by substitution toward human capital, whose productivity grows exogenously. As human capital becomes more efficient, the demand for other inputs is temporarily reduced. However, this effect is short-lived. In the long run, the model ensures a gradual reaccumulation of natural capital and a smooth transition to a cleaner and more balanced resource allocation.

Overall, these trajectories confirm that the model behaves in a stable and economically plausible manner, with the dynamics of natural capital, energy use, and carbon pricing evolving in line with established mechanisms in the literature. Notably, the temperature trajectory generated by our model is broadly consistent with that of Bastien-Olvera and Moore (2021), despite several key differences in model structure. While their framework assumes a CES specification for consumption and Cobb-Douglas functions on the production side, we adopt a nested CES structure that allows for more flexible substitution patterns in production. In addition, whereas they aggregate all ecosystem services into a single variable, we explicitly model multiple forms of natural capital. This opens the door to a richer analysis of sector-specific dependencies on different types of natural capital in future work.

4.3 Shadow Prices Estimates

In this section, we present estimates of the social cost of carbon and shadow prices of natural capital, comparing our natural capital macro framework with a standard DICE-***type*** benchmark. In the benchmark model, final output Y_t^T is produced using a CES aggregator of produced capital, human capital, and energy, with climate damages applied only to these three inputs.[20]

$$Y_t^T = \left(\gamma_{\text{K}} (Y_t^{\text{K}})^{\frac{\theta-1}{\theta}} + \gamma_{\text{FE}} (Y_t^{\text{FE}})^{\frac{\theta-1}{\theta}} + \gamma_{\text{AL}} (Y_t^{\text{AL}})^{\frac{\theta-1}{\theta}} \right)^{\frac{\theta}{\theta-1}}. \tag{22}$$

A large body of climate macroeconomic research uses DICE-***type*** models to estimate the SCC in dollars per ton of CO_2. These studies typically identify three key drivers of the carbon price: i) the discount rate, ii) the damage function, and iii) climate sensitivity to emissions and cumulative CO_2. As a result, SCC estimates in the literature span a wide range, from \$10 to over \$1000 per ton (e.g., Traeger (2023)).

While these parameters are unquestionably important, we show that the elasticity of substitution between production inputs can also be a major determinant of both the SCC and the shadow prices of natural capital—an area that has received comparatively little attention. To illustrate this point, we compare our full framework with the benchmark DICE-***type*** model augmented with energy, as defined above.

4.3.1 Sensitivity of the Social Cost of Carbon

We evaluate the SCC's sensitivity to four key parameters: i) climate damages β_m^h, ii) the climate transition parameter ζ_1, iii) the discount rate β, and iv) the elasticity of substitution in the first CES nest, θ.[21] We first examine the role of the first three parameters, which are well covered in the literature, before turning to the elasticity of substitution, which is less explored.

Climate Damages, Discounting, and Climate Dynamics. Our baseline calibration is shown by the dashed vertical line in figure 4, yielding an SCC of \$63 per tCO_2 in the full model with natural capital, and \$56 per tCO_2 in the energy-only specification. The 12 percent difference highlights the role of natural capital damages in amplifying the optimal carbon price and suggests that DICE-***type*** models without natural capital may systematically undervalue the SCC by omitting these effects.

We also find that uncertainty in the damage function can have large effects. Doubling or quadrupling the climate damage parameters leads to a proportional increase in the SCC in both models. This outcome reflects the form of our damage specification and is consistent with prior results in the literature.[22] The discount rate also has a strong impact, with SCC estimates ranging from \$25 to over \$200 per tCO_2 across the tested range of β. This is a well-documented and contentious aspect of climate valuation (Stern, 2008; Nordhaus, 2008).

In contrast, the influence of climate sensitivity (ζ_1) is relatively muted. This is due to two factors: i) emissions and temperatures are calibrated to match observed 2018 values, which limits the effect of ζ_1

[20] The social planner problem and all equilibrium conditions are detailed in the appendix.

[21] While our empirical estimates for the elasticity of substitution in the lower CES nests fall within the range reported in the literature, there is limited empirical guidance for the elasticity across production inputs when including natural capitals. We therefore conduct a sensitivity analysis of θ in the first CES layer, which aggregates produced capital, human capital, minerals, energy, forest ecosystem services, and cropland.

[22] Note that we do not model tipping points explicitly. However, their inclusion would likely amplify our results.

on near-term SCC estimates; and ii) the analysis presented in this subsection focuses on static allocations, which attenuate the dynamic amplification channels associated with ζ_1 (as emphasized in Folini, Friedl, Kübler, and Scheidegger (2024)).

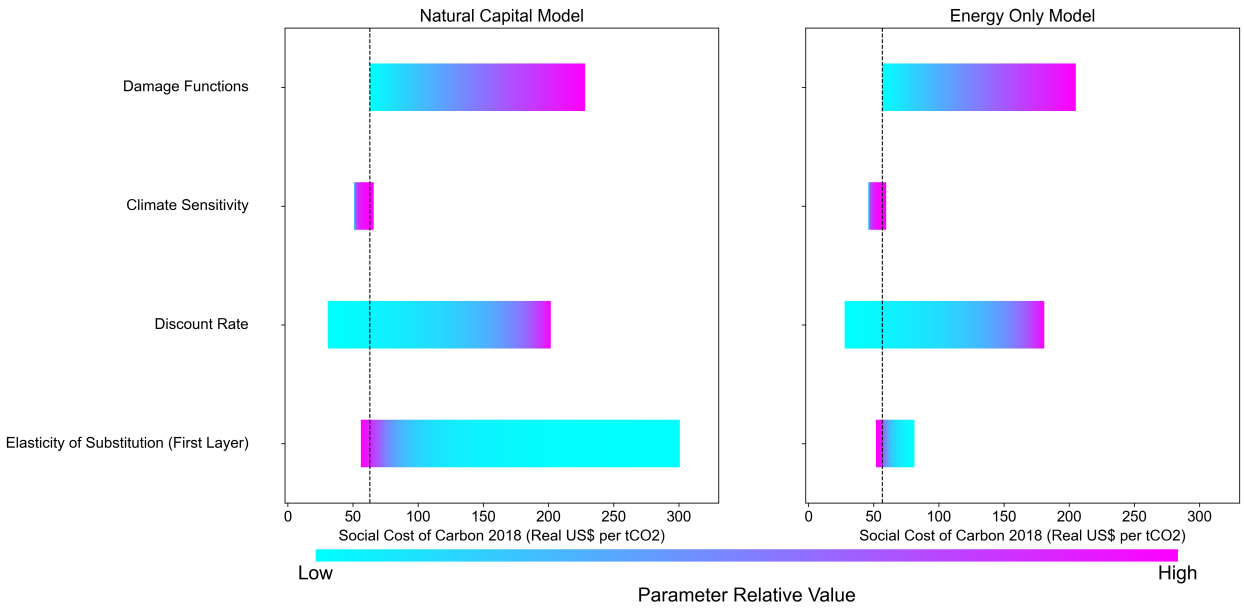

Figure 4: Social Cost of Carbon Sensitivity

Notes: This figure shows the SCC under two model specifications for different parameter values. Monte Carlo draws are performed over uniformly distributed values for each parameter. The ranges are: $\beta_m^h \in (\text{Baseline}, 4 \times \text{Baseline})$, $\theta \in (0.2, 3.5)$, $\beta \in (0.94, 0.99)$, and $\zeta_1 \in (0.1, 2)$.

Elasticity of Substitution Between Production Factors. The role of natural capital becomes even more pronounced when examining the SCC's sensitivity to the elasticity of substitution, θ. In the full model, the SCC rises sharply as θ decreases—that is, as natural capital becomes more complementary to other inputs. For example, with $\theta = 0.85$, the SCC is approximately 4.5 times higher than in the baseline case with $\theta = 1.7$. The response is highly non-linear across the range of values considered, with disproportionately large increases in the SCC at lower elasticity levels. In contrast, the energy-only model exhibits a much more muted response: the SCC increases by only about 50 percent between the same extremes.

These findings highlight two important points. First, accounting for multiple forms of natural capital is essential for accurate policy valuation in macro-climate models. Second, more work is needed to better estimate substitution elasticities across regions and income groups, especially where complementarity may be strong.

4.3.2 Sensitivity of Shadow Prices

We now examine how the shadow prices of production inputs respond to the same four parameters. As in the SCC analysis, we first consider the effects of climate damages, discounting, and climate dynamics before turning to the elasticity of substitution.

Climate Damages, Discounting, and Climate Dynamics. In our static setting, climate-related parameters only affect the shadow prices of fossil energy and its components (oil, gas, and coal) as shown in figure 9, figure 10, and figure 11. This is expected as all other shadow prices in our static exercise can only be impacted by the various components of the production function of the nest to which they belong. In the case of fossil energy and its components, however, the optimal price of carbon enters the formula for shadow prices. As the social cost of carbon grows, fossil inputs become undesirable for the social planner, and their respective shadow prices fall. The effect is thus only indirect, through the impact on the SCC discussed in the previous subsection. The reason is that we target specific levels of production for each type of production input to match the observed levels in 2018. Hence, even though the social planner would theoretically like to reduce the economy's reliance on fossil fuels, the static analysis does not allow it. This limitation is lifted when we study transition dynamics (section 4.2), where shadow prices, stocks, and flows are allowed to move freely.

Elasticity of Substitution Between Production Factors. Figure 5 displays the sensitivity of shadow prices to changes in θ. In the full model, all natural capital shadow prices rise substantially as substitution becomes more difficult. Each more-than-doubles relative to the baseline case with $\theta = 1.7$. This reflects the increasing marginal value of less abundant resources in an economy where substitution across inputs is constrained.

In the energy-only model, this effect is even more pronounced in relative terms. With only three production inputs, reduced substitutability leaves the planner with fewer adjustment margins. As a result, fossil inputs retain high shadow values, and the SCC becomes less responsive to elasticity changes than in the full model. This also helps explain the muted SCC response observed earlier.

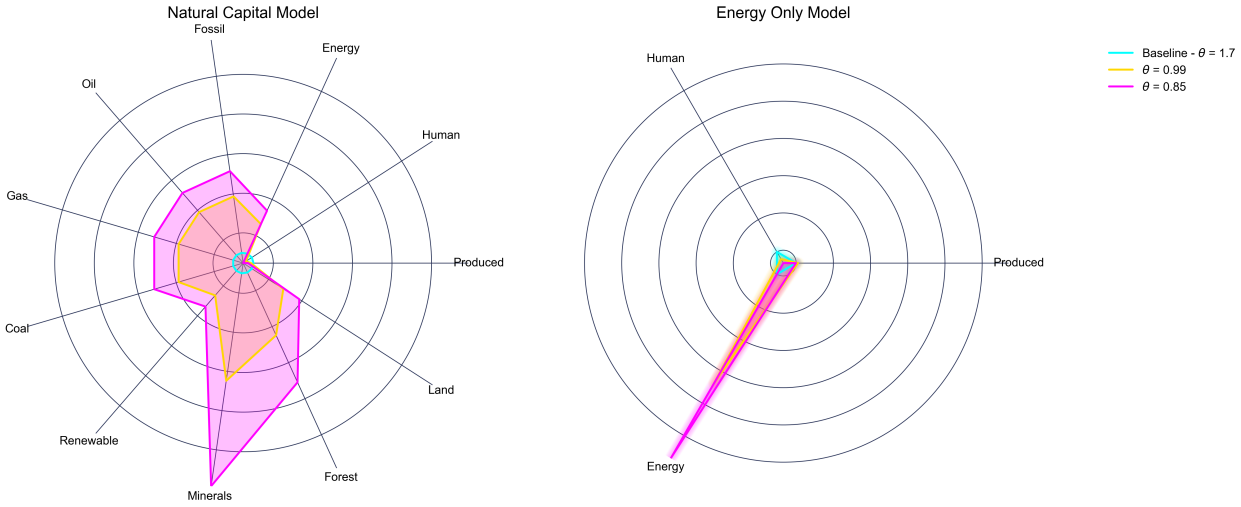

Figure 5: Sensitivity of Shadow Prices to Elasticity of Substitution

Notes: This figure shows the shadow prices of production factors under two model specifications for three elasticity scenarios: baseline, Cobb-Douglas ($\theta \approx 1$), and low substitution ($\theta = 0.85$). Shadow prices are normalized to one at baseline. The center of each circle corresponds to the lowest value observed.

4.4 The Role of Uncertainty

This section examines how aggregate uncertainty affects key outcomes in a macro-climate model with natural capital. We focus on two sources of uncertainty: TFP and temperature. We show that their impact on the SCC and shadow prices is significantly amplified in the presence of habit formation, highlighting the importance of modeling preferences and stochastic discounting. We also explore the consequences of unexpected fossil energy discoveries and trace the transmission channels through which they influence a set of policy-relevant variables.

4.4.1 Uncertainty and Shadow Prices

Recent literature (Golosov, Hassler, Krusell, and Tsyvinski, 2014; Cai and Lontzek, 2019; Benmir et al., 2020; Barnett, Brock, and Hansen, 2021; Folini et al., 2024) emphasizes that uncertainty is a critical factor when assessing the optimal value of carbon pricing. In particular, economic uncertainty can significantly affect the stochastic discount factor, a key element in climate valuation (Stern, 2008; Nordhaus, 2008). The discount factor is highly sensitive to both the structure of preferences and the rate of time discounting. Benmir et al. (2020) argue that habit formation plays a dual role: while it improves the consistency of macroeconomic models with observed financial and macroeconomic data, it also amplifies the sensitivity of the social cost of carbon to uncertainty. Following this insight, we contrast the results of our model with and without habit formation, as in Jaccard (2014).

We focus on the effect of uncertainty in TFP and temperature, computing the (theoretical) conditional mean of the SCC and natural capital shadow prices using second-order perturbation methods. Both shocks are standardized to have a one percent standard deviation,[23] and all results are reported as percentage deviations from the deterministic benchmark.

The results in table 4 show how shadow prices respond to stochastic TFP shocks across three values of the elasticity of substitution, θ. Focusing first on the SCC, we find that accounting for TFP uncertainty increases the planner's valuation of potential climate damages. The SCC rises by 22 to 68 percent relative to the deterministic case, depending on the degree of substitutability. When substitution is higher, the optimal allocation shifts toward inputs that do not generate environmental externalities.[24] As these cleaner inputs become more abundant, their marginal value—and thus their shadow price—declines. In contrast, the overall stock of energy remains largely unchanged, and given its significant role in production, its shadow price rises.

Relative to a DICE-*type* model, the effect of uncertainty on the SCC can be up to 4.7 times larger when natural capital is explicitly included, especially in cases with low substitution elasticity. This highlights the importance of incorporating natural capital into macro-climate models, as omitting it can lead to significant underestimation of uncertainty-related effects.

Standard deviations of shadow prices also increase under uncertainty, and the spread widens as θ decreases. This suggests that TFP shocks generate stronger co-movement among production inputs when those inputs are more complementary.

[23] This corresponds to annual output fluctuations of approximately one percent and temperature variations of about 0.01°C.
[24] While not reported in the table, the conditional mean of non-fossil natural capital stocks increases sharply.

Name	Variable	All Natural Capital			Only Energy		
		$\theta = 0.85$	$\theta = 0.99$	$\theta = 1.70$	$\theta = 0.85$	$\theta = 0.99$	$\theta = 1.70$
Shadow Price of Emission	$\mathbb{E}(V^{\mathrm{E}})$	68.04	22.12	39.67	14.39	15.62	31.22
		(68.66)	(45.14)	(26.73)	(41.39)	(41.05)	(33.35)
Shadow Price of Energy	$\mathbb{E}(\Psi^{\mathrm{E}})$	11.61	2.17	7.45	0.36	-0.51	-11.31
		(20.67)	(11.70)	(6.14)	(29.37)	(31.37)	(25.72)
Shadow Price of Fossil	$\mathbb{E}(\Psi^{\mathrm{FE}})$	-0.09	-3.11	-16.04	-	-	-
		(53.79)	(30.54)	(25.15)	-	-	-
Shadow Price of Oil	$\mathbb{E}(\Psi^{\mathrm{O}})$	0.13	-2.93	-15.78	-	-	-
		(53.07)	(30.10)	(24.03)	-	-	-
Shadow Price of Gas	$\mathbb{E}(\Psi^{\mathrm{G}})$	0.16	-2.80	-13.93	-	-	-
		(51.64)	(28.90)	(19.45)	-	-	-
Shadow Price of Coal	$\mathbb{E}(\Psi^{\mathrm{C}})$	-0.25	-3.27	-16.72	-	-	-
		(54.71)	(31.21)	(27.34)	-	-	-
Shadow Price of Renewable Energy	$\mathbb{E}(\Psi^{\mathrm{RE}})$	2.92	-0.32	-8.35	-	-	-
		(38.34)	(19.91)	(3.70)	-	-	-
Shadow Price of Minerals	$\mathbb{E}(\Psi^{\mathrm{M}})$	35.87	13.23	-35.91	-	-	-
		(47.55)	(29.92)	(31.96)	-	-	-
Shadow Price of Forest ES	$\mathbb{E}(\Psi^{\mathrm{FO}})$	-4.24	-5.63	-9.63	-	-	-
		(58.54)	(31.27)	(18.37)	-	-	-
Shadow Price of Cropland	$\mathbb{E}(\Psi^{\mathrm{L}})$	5.59	0.13	-19.65	-	-	-
		(48.35)	(28.28)	(24.95)	-	-	-

Table 4: Impact of TFP uncertainty on shadow prices across different elasticity values — percentage deviations from deterministic case.

Notes: This table displays the effect of TFP uncertainty on shadow prices under two model specifications with habit formation and three values of substitution elasticity in the top CES nest. The third column corresponds to the estimated elasticity. The first column assumes complementarity, and the second an intermediate case. Results are shown as percentage deviations from the deterministic benchmark. Standard deviations are in parentheses. $\mathbb{E}(X)$ denotes the conditional mean of variable X.

Additional results are provided in the appendix: temperature shocks are analyzed in table 28, and both TFP and temperature shocks without habit formation are shown in table 27 and table 29. While temperature uncertainty has a modest impact on the SCC and shadow prices, its effects are small compared to those of TFP shocks. This is because temperature shocks only marginally affect the marginal utility of consumption, and hence the stochastic discount factor. As a result, outcomes remain similar even with habit formation. Turning to the case where TFP uncertainty is introduced without habit formation, the effects remain muted and would not meaningfully influence optimal policy. This provides a rationale for why earlier climate-economy models often downplayed the role of uncertainty in determining the SCC (Nordhaus and Moffat, 2017; Stern, 2008).

4.4.2 Uncertainty and Discoveries

In this last subsection, we analyze the effect of an unexpected discovery in fossil fuels. We study the case of gas, but the analysis would carry over with any other fossil energy. For this exercise, we rely on perturbation methods around the initial steady state, as it will allow us to cleanly decompose the channels through which a variable is impacted. We calibrate the shock to get a 10% increase in the stock of gas in impact and it goes back to zero with an auto-regressive parameter of 0.5. One could think of it as the discovery of shale gas reserves in the US, where some new reserves are progressively discovered, up to

some point.

Unanticipated "discovery shocks" in fossil-fuel availability—such as the sudden realization of vast shale or deep-sea reserves—play a pivotal role in shaping both aggregate GDP dynamics and social welfare outcomes. From a GDP perspective, abrupt supply expansions can depress global energy prices, strain the profitability of incumbent producers, and induce boom-bust investment cycles (Pindyck (2013)), while also delaying capital flows into clean-energy sectors. From a welfare standpoint, such uncertainty exacerbates the distortions identified by Weitzman (1974): consumers and producers face greater volatility in energy costs and firms leading to higher welfare costs.

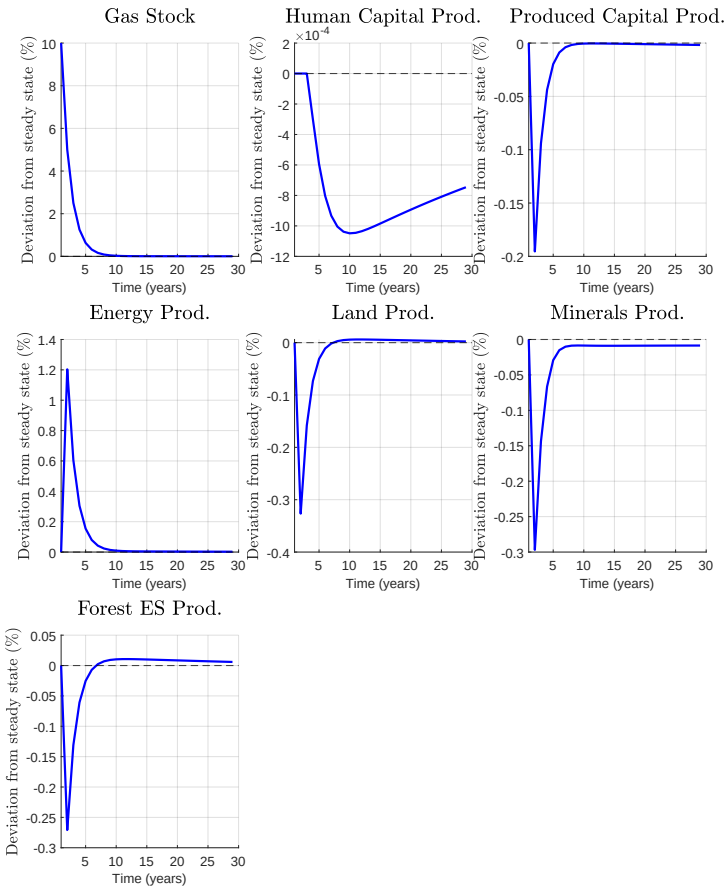

Figure 6: Impulse Response Function to a Gas Discovery

Notes: This figure shows the impulse responses of produced and natural capital production to a gas discovery shock equivalent to a 10% increase in the gas stock. Results are expressed as percentage deviations from the steady state; the zero on the x-axis represents the steady state level.

Figure 6 shows the impulse responses of all inputs in the first production nest under our baseline calibration. The first panel depicts the direct effect of the shock on the target variable: a 10% increase in the gas stock. This discovery generates a sharp rise in fossil fuel and thus the energy output, while production from all other first-nest natural capital stocks production falls. Because substitution is highly elastic, the

planner shifts production easily toward fossil inputs, drawing down other natural and man-made capital stocks and thereby amplifying climate damages via rise in emissions. As we will see below, the net effect on GDP while positive, it comes at a welfare cost due to increased climate impacts.

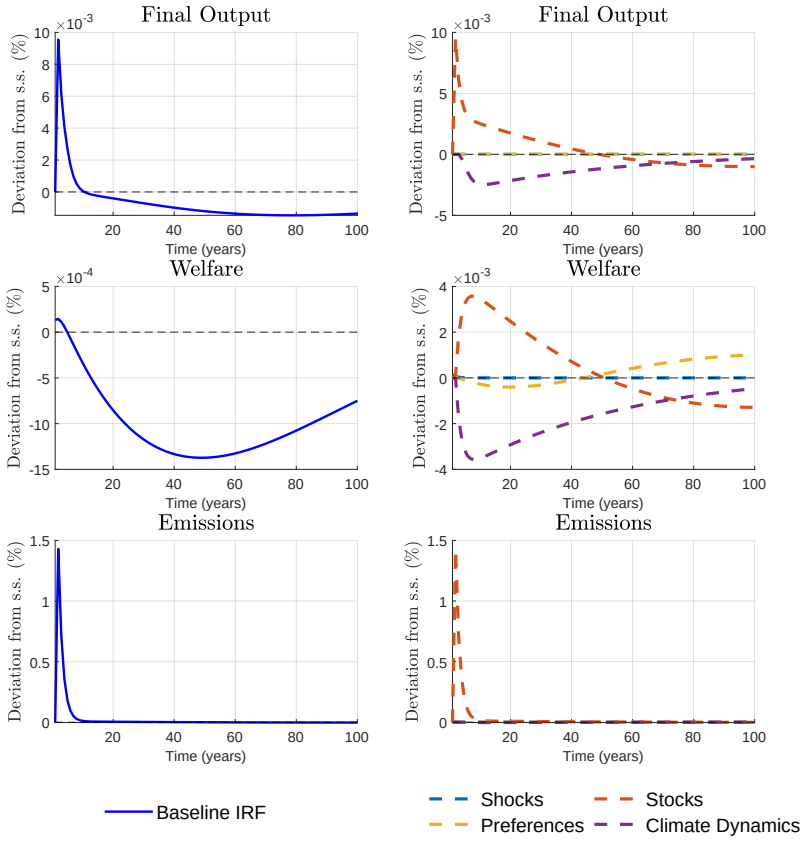

Figure 7: Impulse Response Function Decomposition

Notes: This figure shows the impulse responses of selected variables to a gas discovery shock equivalent to a 10% increase in the gas stock. The solid blue line represents the total response, while the dashed colored lines decompose the impulse response function (IRF) into contributions from individual state variables. All responses are expressed as percentage deviations from the steady state; the zero on the x-axis corresponds to the steady state level. Shocks include: TFP, Discovery, and Temperature shock (notice that only discovery shock is activated for this exercise); Stocks include all natural capital stocks but human capital; Preferences include: time preference, habits, as well as its leads and/or lags; and finally Climate Dynamics include: cumulative emissions, temperature, as well as their leads and/or lags.

We then decompose the effects of a gas discovery shock on total output, social welfare, and emissions.[25] While total output rises initially due to the sudden availability of fossil energy, the welfare impact quickly turns negative. The surge in fossil fuel use raises emissions and intensifies climate damages, as shown in

[25] We decompose the overall impact of the shock by attributing it to individual state variables in the model. For ease of interpretation, these contributions are aggregated into the categories indicated in the figure notes.

figure 7. After a few periods, the adverse welfare effects from climate damages outweigh the short-run gains from increased resource availability. Output, by contrast, continues to benefit in the near term from expanded energy stocks, although these gains are eventually reversed. Over the longer run, rising climate damages dominate the initial productivity boost from fossil energy, leading to a sustained decline in output before it gradually returns to steady state.

This decomposition highlights two key insights. First, while unexpected fossil fuel discoveries may generate short-term gains in GDP and welfare, these benefits quickly reverse as emissions accumulate and climate damages mount. Second, such discoveries can undermine the competitiveness of renewables and delay the transition to cleaner energy, particularly when production inputs are highly substitutable.

5 Conclusion

The rapid degradation of Earth's ecosystems has significant implications for economic production. In this paper, we demonstrated that incorporating natural capital dynamics and their interaction with climate dynamics in macroeconomic models is crucial for optimal allocation analysis. To calibrate our model, we used state-of-the-art climate econometric methods to estimate damage functions for each type of natural capital and provided new estimates of elasticity of substitution between various production inputs. With these estimates, we quantified the impact of including natural capital in a macroeconomic model featuring uncertainty.

Our findings indicate that the SCC is about 12 percent higher in the fully-fledged model compared to the baseline. Additionally, all shadow prices are highly sensitive to the elasticity of substitution in the final output production function and the calibration of damage functions. We also computed the mean of the shadow prices, conditional on the expectation of shocks to productivity and temperature. Accounting for the stochastic nature of productivity increases the SCC by 39 percent in our baseline parametrization. However, accounting for a moderate risk of temperature variation does not significantly impact shadow prices. Finally, we demonstrate that although fossil-fuel discoveries boost output in the short run, they lead to lower output over the long run and impose adverse welfare consequences.

In conclusion, our study highlights the importance of considering natural capital and the role of uncertainty in macroeconomic models. Ignoring natural capital can lead to substantial underestimation of the SCC and other shadow prices, ultimately affecting policy decisions and long-term sustainability.

6 Bibliography

D. Acemoglu, P. Aghion, L. Bursztyn, and D. Hemous. The environment and directed technical change. *American Economic Review*, 102(1):131–66, 2012.

E. Atalay. How important are sectoral shocks? *American Economic Journal: Macroeconomics*, 9(4):254–280, 2017.

M. Barnett, W. Brock, and L. P. Hansen. Climate Change Uncertainty Spillover in the Macroeconomy. In *NBER Macroeconomics Annual 2021, volume 36*, NBER Chapters. National Bureau of Economic Research, Inc, November 2021. URL https://ideas.repec.org/h/nbr/nberch/14556.html.

A. I. Barreca. Climate change, humidity, and mortality in the united states. *Journal of Environmental Economics and Management*, 63(1):19–34, 2012.

B. Bastien-Olvera, M. Conte, X. Dong, T. Briceno, D. Batker, J. Emmerling, M. Tavoni, F. Granella, and F. Moore. Unequal climate impacts on global values of natural capital. *Nature*, 625(7996):722–727, 2024.

B. A. Bastien-Olvera and F. C. Moore. Use and non-use value of nature and the social cost of carbon. *Nature Sustainability*, 4(2):101–108, 2021.

G. Benmir, I. Jaccard, and G. Vermandel. Green asset pricing. Technical report, ECB Working Paper, 2020.

A. Bilal and D. R. Känzig. The macroeconomic impact of climate change: Global vs. local temperature. Technical report, National Bureau of Economic Research, 2024.

M. Burke and K. Emerick. Adaptation to climate change: Evidence from us agriculture. *American Economic Journal: Economic Policy*, 8(3):106–140, 2016.

M. Burke, S. M. Hsiang, and E. Miguel. Global non-linear effect of temperature on economic production. *Nature*, 527(7577):235–239, 2015.

Y. Cai and T. S. Lontzek. The social cost of carbon with economic and climate risks. *Journal of Political Economy*, 127(6):2684–2734, 2019.

T. Carleton, A. Jina, M. Delgado, M. Greenstone, T. Houser, S. Hsiang, A. Hultgren, R. E. Kopp, K. E. McCusker, I. Nath, et al. Valuing the global mortality consequences of climate change accounting for adaptation costs and benefits. *The Quarterly Journal of Economics*, 137(4):2037–2105, 2022.

I. Choi. Unit root tests for panel data. *Journal of international money and Finance*, 20(2):249–272, 2001.

V. Corbo. Second-Order Approximations for Estimating Production Functions. In *Annals of Economic and Social Measurement, Volume 5, number 1*, NBER Chapters, pages 65–73. National Bureau of Economic Research, Inc, May 1976. URL https://ideas.repec.org/h/nbr/nberch/10428.html.

D. Cordell, J.-O. Drangert, and S. White. The story of phosphorus: global food security and food for thought. *Global environmental change*, 19(2):292–305, 2009.

P. Dasgupta. *The Economics of Biodiversity: The Dasgupta Review*. HM Treasury, London, 2021.

M. Dell, B. F. Jones, and B. A. Olken. Temperature shocks and economic growth: Evidence from the last half century. *American Economic Journal: Macroeconomics*, 4(3):66–95, 2012.

O. Deschênes and M. Greenstone. The economic impacts of climate change: evidence from agricultural output and random fluctuations in weather. *American economic review*, 97(1):354–385, 2007.

O. Deschênes and M. Greenstone. Climate change, mortality, and adaptation: Evidence from annual fluctuations in weather in the us. *American Economic Journal: Applied Economics*, 3(4):152–185, 2011.

O. Deschênes, M. Greenstone, and J. Guryan. Climate change and birth weight. *American Economic Review*, 99(2):211–217, 2009.

S. Dietz and F. Venmans. Cumulative carbon emissions and economic policy: in search of general principles. *Journal of Environmental Economics and Management*, 96:108–129, 2019.

M. A. Drupp. Limits to substitution between ecosystem services and manufactured goods and implications for social discounting. *Environmental and Resource Economics*, 69(1):135–158, 2018.

M. A. Drupp and M. C. Hänsel. Relative prices and climate policy: how the scarcity of nonmarket goods drives policy evaluation. *American Economic Journal: Economic Policy*, 13(1):168–201, 2021.

M. S. Feldstein. Alternative methods of estimating a ces production function for britain. *Economica*, 34(136): 384–394, 1967.

D. Folini, A. Friedl, F. Kübler, and S. Scheidegger. The climate in climate economics. *Review of Economic Studies*, page rdae011, 2024.

S. Giglio, T. Kuchler, J. Stroebel, and O. Wang. The economics of biodiversity loss. Technical report, National Bureau of Economic Research, 2024.

S. Giglio, T. Kuchler, J. Stroebel, and O. Wang. Nature loss and climate change: The twin-crises multiplier. In *AEA Papers and Proceedings*, volume 115, pages 409–414. American Economic Association 2014 Broadway, Suite 305, Nashville, TN 37203, 2025.

M. Golosov, J. Hassler, P. Krusell, and A. Tsyvinski. Optimal taxes on fossil fuel in general equilibrium. *Econometrica*, 82(1):41–88, 2014.

R. L. Graham, M. G. Turner, and V. H. Dale. How increasing co2 and climate change affect forests. *BioScience*, 40(8):575–587, 1990.

A. Henningsen and G. Henningsen. On estimation of the ces production function—revisited. *Economics Letters*, 115(1):67–69, 2012. URL https://EconPapers.repec.org/RePEc:eee:ecolet:v:115:y:2012:i:1:p:67-69.

A. Hoff. The linear approximation of the ces function with n input variables. *Marine Resource Economics*, 19 (3):295–306, 2004. ISSN 07381360, 23345985. URL http://www.jstor.org/stable/42629436.

S. Hsiang. Climate econometrics. *Annual Review of Resource Economics*, 8:43–75, 2016.

IPCC. Climate change and land: an ipcc special report on climate change, desertification, land degradation, sustainable land management, food security, and greenhouse gas fluxes in terrestrial ecosystems. *In press*, 2019.

I. Jaccard. Asset returns and labor supply in a production economy. *Journal of Money, Credit and Banking*, 46 (5):889–919, 2014. ISSN 00222879, 15384616.

A. Jo. Substitution between clean and dirty energy with biased technical change. *International Economic Review*, 66(2):883–902, 2025.

A. Jo and A. Miftakhova. How constant is constant elasticity of substitution? endogenous substitution between clean and dirty energy. *Journal of Environmental Economics and Management*, 125:102982, 2024.

D. P. Kingma and J. Ba. Adam: A method for stochastic optimization. *arXiv preprint arXiv:1412.6980*, 2014.

P. J. Klenow, I. B. Nath, and V. A. Ramey. How much will global warming cool global growth? Technical report, Working paper, 2023.

J. Kmenta. On estimation of the ces production function. *International Economic Review*, 8(2):180–189, 1967. ISSN 00206598, 14682354. URL http://www.jstor.org/stable/2525600.

M. Kotz, A. Levermann, and L. Wenz. The economic commitment of climate change. *Nature*, 628(8008): 551–557, 2024.

E. Lagomarsino. Estimating elasticities of substitution with nested ces production functions: Where do we stand? *Energy Economics*, 88(C):S0140988320300918, 2020. URL https://EconPapers.repec.org/RePEc:eee:eneeco:v:88:y:2020:i:c:s0140988320300918.

G. Maddala and J. B. Kadane. Estimation of returns to scale and the elasticity of substitution. *Econometrica, Journal of the Econometric Society*, pages 419–423, 1967.

H. D. Matthews, N. P. Gillett, P. A. Stott, and K. Zickfeld. The proportionality of global warming to cumulative carbon emissions. *Nature*, 459(7248):829–832, 2009.

R. P. McDonald. A simple comprehensive model for the analysis of covariance structures: Some remarks on applications. *British Journal of Mathematical and Statistical Psychology*, 33(2):161–183, 1980.

R. G. Newell, B. C. Prest, and S. E. Sexton. The gdp-temperature relationship: implications for climate change damages. *Journal of Environmental Economics and Management*, 108:102445, 2021.

W. Nordhaus. A question of balance: Weighing the options on global warming policies. Yale university press. *New Haven, CT*, 2008.

W. D. Nordhaus. To slow or not to slow: the economics of the greenhouse effect. *Economic Journal*, 101(407): 920–937, 1991.

W. D. Nordhaus. Geography and macroeconomics: New data and new findings. *Proceedings of the National Academy of Sciences*, 103(10):3510–3517, 2006.

W. D. Nordhaus and A. Moffat. A survey of global impacts of climate change: replication, survey methods, and a statistical analysis. 2017.

W. D. Nordhaus and Z. Yang. A regional dynamic general-equilibrium model of alternative climate-change strategies. *American Economic Review*, pages 741–765, 1996.

C. Papageorgiou, M. Saam, and P. Schulte. Substitution between clean and dirty energy inputs: A macroeconomic perspective. *The Review of Economics and Statistics*, 99(2):pp. 281–290, 2017. ISSN 00346535, 15309142. URL https://www.jstor.org/stable/26616117.

R. S. Pindyck. Climate change policy: what do the models tell us? *Journal of Economic Literature*, 51(3): 860–872, 2013.

H. Qian, L. Wu, and J. Fan. On estimation of deep nested ces production functions. *Available at SSRN 3247693*, 2018.

K. Ricke, L. Drouet, K. Caldeira, and M. Tavoni. Country-level social cost of carbon. *Nature Climate Change*, 8(10):895–900, 2018.

S. Roy, D. P. Mishra, R. M. Bhattacharjee, and H. Agrawal. Heat stress in underground mines and its control measures: a systematic literature review and retrospective analysis. *Mining, Metallurgy & Exploration*, 39 (2):357–383, 2022.

S. Ruder. An overview of gradient descent optimization algorithms. *arXiv preprint arXiv:1609.04747*, 2016.

R. Schaeffer, A. S. Szklo, A. F. P. de Lucena, B. S. M. C. Borba, L. P. P. Nogueira, F. P. Fleming, A. Troccoli, M. Harrison, and M. S. Boulahya. Energy sector vulnerability to climate change: A review. *Energy*, 38(1): 1–12, 2012.

W. Schlenker and M. J. Roberts. Nonlinear temperature effects indicate severe damages to us crop yields under climate change. *Proceedings of the National Academy of sciences*, 106(37):15594–15598, 2009.

K. Schubert. Macroeconomics and the environment. *Revue de l'OFCE*, (3):117–132, 2018.

R. Seidl, D. Thom, M. Kautz, D. Martin-Benito, M. Peltoniemi, G. Vacchiano, J. Wild, D. Ascoli, M. Petr, J. Honkaniemi, et al. Forest disturbances under climate change. *Nature climate change*, 7(6):395–402, 2017.

N. Stern. The economics of climate change. *American Economic Review*, 98(2):1–37, 2008.

T. Sterner and U. M. Persson. An even sterner review: Introducing relative prices into the discounting debate. *Review of environmental economics and policy*, 2008.

R. Tarsia. Heterogeneous effects of weather shocks on firm economic performance. *Available at SSRN 4672552*, 2023.

J. Thursby and C. Lovell. An investigation of the kmenta approximation to the ces function. *International Economic Review*, 19(2):363–77, 1978. URL https://EconPapers.repec.org/RePEc:ier:iecrev:v:19:y:1978:i:2:p:363-77.

C. P. Traeger. Ace—analytic climate economy. *American Economic Journal: Economic Policy*, 15(3):372–406, 2023.

I. van den Bijgaart and M. Rodriguez. Closing wells: Fossil development and abandonment in the energy transition. *Resource and Energy Economics*, 74:101387, 2023.

F. van der Ploeg and A. Rezai. Optimal carbon pricing in general equilibrium: Temperature caps and stranded assets in an extended annual dsge model. *Journal of Environmental Economics and Management*, 110:102522, 2021.

Y. Wei and Z. Jiang. Estimating parameters of structural models using neural networks. *Marketing Science*, 44(1):102–128, 2025.

M. L. Weitzman. Prices vs. quantities. *The review of economic studies*, 41(4):477–491, 1974.

Appendix A Data

A.1 Descriptive Statistics

	Statistics				
	Average	Std. Dev.	Min.	Max.	Obs.
First nest Variables					
GDP	63.21	197.79	0.1062	2045.61	2,184
Capital	280.36	878.59	0.2077	8622.27	2,184
Human Capital	557.65	2066.65	0.3627	20302.21	2,184
Ecosystem	6.56	20.03	0.0001	199.02	2,184
Cropland	12.91	44.99	0.0194	516.22	2,184
Minerals	3.32	14.02	1.86E-06	249.08	2,184
Fossil Energy	22.66	75.64	8.82E-08	716.05	2,184
Second nest Variables					
Electricity Demand	109.97	429.31	0.03	6871.14	3,478
Fossil Fuel Electricity	84.03	349.02	0.00	5035.82	3,478
Renewable Electricity	25.93	94.04	0.00	1835.32	3,478
Third nest Variables					
Oil-Gas Production	10.32	22.58	0.000025	161.98	1,152
Coal Production	7.38	24.64	0.00005	220.34	1,152

Note: The first nest variables are expressed in 10 Billion Current 2018 USD, the second and third nest variables are expressed in terawatt hours.

Table 5: Summary Statistics: CES Estimates Data

	Statistics				
	Average	Std. Dev.	Min.	Max.	Obs.
Total Cropland	40.71	3.69	29.90	50.32	1,728
Forest Ecosystem	23.34	2.37	14.01	28.32	1,704
Minerals	21.35	3.19	11.94	28.54	1,368
Coal Electricity	2.86	2.32	-4.61	8.46	1,212
Gas Electricity	2.64	1.92	-4.61	7.29	1,548
Oil Electricity	1.39	1.98	-6.21	5.52	1,523
Fossil Fuel Electricity	3.75	1.72	-4.61	8.52	1,606
Renewable Electricity	2.29	2.21	-5.52	7.51	1,616
Energy	27.02	1.43	23.89	31.28	1,728
Temperature	14.85	8.26	-4.89	28.98	1,728
Precipitation	1072.72	793.83	6.11	4226.89	1,728

Note: All values except temperature and precipitation are expressed in logarithmic values.

Table 6: Summary Statistics: Climate Damages Estimates Data

A.2 Calibration and Moments Matching

Name	Variable	Value	Sensitivity
Climate Parameters			
Climate Transient Parameters 1	ϕ_1	0.50	$\in (0.1, 2)$
Climate Transient Parameters 2	ϕ_2	0.61	-
Produced and Natural Capital Damages	β_m^h	refer to estimation	$\in (2 * \beta_m^h, 4 * \beta_m^h)$
Human Capital Damages	β_1^{AL}	- 0.02	$\in (2 * \beta_1^{AL}, 4 * \beta_1^{AL})$
Emission Intensity	ϕ_E	0.0014	-
Persistence of Temperature Shock	ρ_T	0.90	-
Temperature Shock Standard Deviation	σ_T	0.01	-
Macro Parameters			
Time preference	β	0.96	$\in (0.94, 0.99)$
Risk aversion	σ^H	2.00	-
Economy Growth Rate	γ^Γ	1.03	-
Habits adjustment level	γ^H	0.975	-
Habits level	$\bar{m}$	0.90	-
Labor hours	$\bar{L}$	0.33	-
Productivity of labor	A	2.22 * 10^3	-
GDP scale	γ_Y	0.32	-
Energy scale	γ_E	3.39	-
Fossil Energy scale	γ_F	5.13	-
Inputs weights	θ_k	refer to estimation	-
Elasticity of Substitution First nest	θ	refer to estimation	$\in (0.2, 3.5)$
Fossil Fuel Weight	σ_{FE}	refer to estimation	-
Renewable Energy Weight	σ_{RE}	refer to estimation	-
Elasticity of Substitution Second nest	σ	refer to estimation	-
Elasticity of Substitution Third nest	ϵ	refer to estimation	-
Oil, Gas, Coal Weights	ϵ_i	refer to estimation	-
Persistence of TFP Shock	ρ_A	0.90	-
TFP Shock Standard Deviation	σ_A	0.01	-
Persistence of Discovery/Investment Shock	ρ_{D_i}	0.50	-

Table 7: Calibration

Variable	Label	Target	Source
Cumulative Emission (World, Trillion tCO2)	X	1.63	Ourworldindata
Yearly Emission Flow (World, GtCO2)	E	36.77	Ourworldindata
Temperature in Celcius	T	1.00	NOAA
World GDP in Trillion $	Y^T	86.50	WB Database
Produced Capital in Trillion $	Y^K	358.50	WB Database
Human Capital in Trillion $	Y^{AL}	727.21	WB Database
Renewable Energy in Trillion $	Y^{RE}	0.54	Authors Calculation
Coal in Trillion $	Y^C	3.48	WB Database
Gas in Trillion $	Y^G	3.27	WB Database
Oil in Trillion $	Y^O	18.63	WB Database
Cropland in Trillion $	Y^L	20.86	WB Database
Minerals in Trillion $	Y^M	3.08	WB Database
Forest Ecosystem Services in Trillion $	Y^{FO}	7.36	WB Database
Oil Investment to Output Ratio in %	D^{FO}/Y^{FO}	0.46	Authors Calculations
Coal Investment to Output Ratio in %	D^C/Y^C	1.01	Authors Calculations
Gas Investment to Output Ration in %	D^G/Y^G	3.82	Authors Calculations
Renewable Investment to Output Ratio in %	D^{RE}/Y^{RE}	156.25	Authors Calculations
Minerals Investment to Output Ratio in %	D^M/Y^M	3.00	Authors Calibration
Cropland Investment to Output Ratio in %	D^L/Y^L	3.00	Authors Calibration
Forest Ecosystem Services Investment to Output Ratio in %	D^{FO}/Y^{FO}	3.00	Authors Calibration
Capital Investment to Output Ratio in %	D^K/Y^K	3.00	Authors Calibration

Table 8: Moments Matching

Notes: All the values reported in this table are perfectly matched by the model for the initial period 2018. The energy output is calculated using the electricity prices from https://www.cable.co.uk/energy/worldwide-pricing/ and quantities from OWID.

Appendix B Empirical Estimation

This section is an addendum to the empirical estimation briefly discussed above. We elaborate on the estimation methods, model specifications, and data-handling procedures employed to obtain accurate and robust parameter estimates.

B.1 Data

In this subsection, we describe the variables used for estimating the CES production functions as well as the climate damages. Moreover, we shed light on data-related challenges and the considerations necessary to address them effectively during the estimation process.

B.1.1 CES Estimation Data

Before delving into the CES production function estimation, we must deal with three key data related challenges that arise in this procedure. These affect the data utilized for the estimation. First, units must be consistent to ensure interpretability. Second, the output variable must not be a linear sum of inputs, as this implies perfect substitutability ($\sigma \to \infty$). To address unit consistency, we restrict the first-nest estimation to CWON's produced, natural, and human capital, with GDP as output. All variables are measured in constant 2018 USD. To address the second issue, for the second nest, we use OWID data with electricity demand as the output and generation from fossil and renewable sources as inputs. This is because electricity generation is a linear sum of fossil and renewable sources. Discrepancies between demand and supply are understood to be resolved through cross-country electricity trade. In the third nest, we use fossil electricity generation as the output to ensure consistency with the second nest, and use coal, oil, and gas production as inputs, since fossil-based electricity is a linear sum of these sources. This is also why CWON data is not used to estimate the third nest.

The third issue is regarding the fact that the inputs discussed above, such as human capital, are stock variables and the output, GDP, is a flow. To address this, we note that the scaling parameter $\tilde{g}_Y$ in the CES function below, which features produced and human capital, captures both productivity and the contribution of stock input to flow output. To see how, note that a stock variable can be converted to a flow by multiplying the inputs by some discount rate r.[26] This discount rate can be factored out and we can restate the new multiplicative term as $g_Y = \tilde{g_Y} r$, which helps reconcile the stock-flow mismatch.

$$Y_{i,t} = \tilde{g_Y} \left(\theta (r Y_{i,t}^K)^{\frac{\sigma-1}{\sigma}} + (1-\theta)(r Y_{i,t}^{AL})^{\frac{\sigma-1}{\sigma}} \right)^{\frac{\sigma}{\sigma-1}} \tag{23}$$

Lastly, we exclude certain CWON natural capitals from the estimation procedure, such as mangroves, fisheries, and protected areas, since these are rare across countries, making their inclusion inappropriate for a representative economy. Additionally, we do not include forest timber, as its inclusion in the CES results in an estimated production share of zero. Table 9 provides summarizes the variables used while table 5 provides the summary statistics.

[26] The CWON dataset expresses all variables as discounted stock values, using a consistent discount rate for all variables.

Category	Symbol	Description	Unit	Source
First nest Variables				
GDP	Y^T	GDP at purchaser's prices	2018 USD	World Bank
Capital	Y^K	Value of buildings and equipment	2018 USD	CWON
Human Capital	Y^{AL}	PV of future earnings for the population	2018 USD	CWON
Ecosystem	Y^{FO}	Forest ecosystem services	2018 USD	CWON
Cropland	Y^L	Agricultural Land	2018 USD	CWON
Minerals	Y^M	Composite of different minerals	2018 USD	CWON
Fossil Energy	Y^E	Oil, gas, hard and soft coal	2018 USD	CWON
Second nest Variables				
Electricity Demand	Y^E	Demand for electricity	Terawatt Hours	OWID
Fossil Fuel Electricity	Y^{FE}	Electricity generation from fossil fuels	Terawatt hours	OWID
Renewable Electricity	Y^{RE}	Electricity generation from renewables	Terawatt hours	OWID
Third nest Variables				
Oil-Gas Production	Y^G	Sum of gas and oil production	Terawatt hours	OWID
Coal Production	Y^C	Coal production	Terawatt hours	OWID

Table 9: Variable Summaries: CES Estimates Data

B.1.2 Natural Capital Climate Damages Estimation Data

In this paper, the types of natural capital considered include cropland, forest ecosystem services, minerals, and energy. Energy is further broken down as described earlier. While we use the CWON dataset for natural capital classification, their data reflect the market values of these resources, which might conflate the impact of temperature on the quantity of natural capital with its market value. To avoid this confusion, whenever possible, we used available data on the actual quantities of natural capital instead of their market valuations. For cropland, we used the Arable Land data from the World Bank, measured in hectares per capita, which we converted into hectares using population data. To obtain data on aggregate energy and its decomposition, we referred to the OWID Energy dataset as previously discussed. However, since quantity data were not available for forest ecosystem services and minerals,[27] we relied on the CWON dataset for these components. Lastly, we used ERA5 temperature and precipitation data from the Climate Change Knowledge Portal. Table 10 summarizes the variables used and their sources, while table 6 provides summary statistics.

Variable	Description	Unit	Source
Total Cropland	Arable land	Hectares	World Bank
Coal Electricity	Electricity generation from coal	Terawatt hours	OWID
Gas Electricity	Electricity generation from gas	Terawatt hours	OWID
Oil Electricity	Electricity generation from oil	Terawatt hours	OWID
Fossil Fuel Electricity	Electricity generated from oil, gas and coal	Terawatt hours	OWID
Energy	Primary energy consumption	Kilowatt Hours	OWID
Temperature	Average mean surface-air temperature	Celsius	CCKP
Precipitation	Average precipitation	mm	CCKP

Table 10: Variable Summaries: Climate Damages Estimates Data

[27] Minerals in the CWON dataset include bauxite, copper, gold, iron ore, lead, nickel, phosphate, silver, tin, and zinc.

Figure 15, figure 16, and figure 17 show the distribution of each of the aforementioned variables, which are generally symmetric with slight skews. Notably, the temperature data exhibit a left skew, while the precipitation data display a heavy right skew.[28]

B.2 Natural Capital CES Estimation

There are three main approaches to estimating CES production functions. First, Kmenta (1967) introduced a linear approximation using a second-order Taylor expansion around a unitary elasticity of substitution, which can be estimated via Ordinary Least Squares (OLS). However, as Thursby and Lovell (1978) note, the approximation error increases when the true elasticity deviates from one. In addition, Hoff (2004) points out that parameter restrictions within Kmenta's method become increasingly complex with rising number of inputs.

Second, the CES function can be estimated directly using non-linear methods. While this avoids approximation error, Henningsen and Henningsen (2012) caution that parameter estimates may fall outside bounds prescribed by economic theory. Moreover, both the linear and non-linear approaches are vulnerable to endogeneity concerns, as input choices may not be exogenous to output choices.

Third, the cost minimization approach estimates elasticity from the logarithm of input price ratios. This approach is widely used in the literature[29] and benefits from being able to use exogenous price variation to avoid endogeneity issues. However, it requires price data, which we lack for natural capital inputs. Additionally, Feldstein (1967) and Papageorgiou et al. (2017) note that this approach assumes undistorted markets, a condition we cannot verify. As such, we do not employ this method here.

Following Papageorgiou et al. (2017), we implement both Non-Linear Least Squares (NLS) and the Kmenta approximation to mitigate the limitations of each method. NLS is used to estimate all nests of the CES production function, while the Kmenta approximation is applied to the second and third nests, which each have only two inputs,[30] in line with Hoff (2004)'s recommendation. Furthermore, as inPapageorgiou et al. (2017), we note that these findings reflect associations rather than causal relationships, owing to endogeneity concerns.

We employ two non-linear least squares (NLS) methods. First, Sequential Quadratic Programming (SQP), which allows for constrained optimization and ensures parameter estimates remain consistent with economic theory. Second, we implement Adaptive Moment Estimation (Adam), a stochastic gradient descent algorithm introduced by Kingma and Ba (2014) and implemented using TensorFlow.[31] Since Adam does not support explicit parameter constraints, we reparameterize the elasticity using $\rho = \frac{\sigma-1}{\sigma}$, and following McDonald (1980), we express:

$$\rho = e^{\lambda} - 1, \tag{24}$$

$$\theta_k = \frac{1}{1 + e^{-\mu_k}}, \tag{25}$$

[28] The skewness is largely driven by the warm climates in East Asia and the Pacific, Latin America and the Caribbean in the case of temperature, and by the dry conditions in the Middle East and North Africa in the case of precipitation.

[29] See Lagomarsino (2020) for a comprehensive list of literature employing the indirect approach and other methods.

[30] For estimation, oil and gas are aggregated into a single input.

[31] For details on Adam and its implementation, see Appendix A

which ensures $\rho \in (-1, \infty)$ and $\theta_k \in [0, 1]$ without directly imposing bounds. Under this formulation, we estimate the unconstrained parameters λ and μ_k with Adam. As a robustness check for the second and third CES nests, we also estimate a third specification in which the returns-to-scale parameter is fixed using values obtained from OLS. This follows Corbo (1976) and Maddala and Kadane (1967), who show that Kmenta's approximation yields reliable estimates of this parameter.

B.2.1 Results: First nest

To estimate, we restate the final output production function in equation (5) in logarithmic terms with a returns to scale parameter υ_Y and the elasticity re-parameterized as the substitution parameter ρ_Y.

$$\ln(Y_{i,t}^T) = \ln(g_Y) - \left(\frac{\upsilon_Y}{\rho_Y}\right) \ln\left(\theta_{\mathrm{K}}(Y_{i,t}^K)^{-\rho_Y} + \theta_{AL}(Y_{i,t}^{AL})^{-\rho_Y} + \sum_k \theta_k (Y_{i,t}^k)^{-\rho_Y}\right) \tag{26}$$

Table 11 below shows that the results are similar across the two estimation methods and their specifications. Aligned with standard macroeconomic literature we observe, under all estimation specifications, that the share of human capital is the largest, followed by produced capital and natural capital related to energy. These estimates are novel as they introduce the elasticities of substitution between produced capital, human capital, and the various natural capitals, which has not been estimated previously in the literature. The estimated elasticity of substitution between these inputs, given by $\theta = \frac{1}{1+\rho_Y}$, ranges between 1.65 and 1.79.

We also estimate a CES production function with produced capital, human capital, and energy natural capital as its inputs to derive parameters for a reduced form DICE-***type*** framework (we use in the quantitative modeling section), allowing us to compare our model's results (with all natural capital) and a framework with energy only. As shown in table 12, we find that the elasticity of substitution between these three inputs ranges from 1.63 to 1.73. Additionally, we observe that human capital retains the highest share, followed by produced capital. Of particular note is that both SQP and Adam, which are two different methods, yield the same results despite starting at different initial points, indicating the robustness of our results.

The results in table 12 are closest in comparison to the elasticities estimated in Qian, Wu, and Fan (2018) between energy and non-energy composite inputs. Our results fall outside the range reported by Qian et al. (2018) who find that elasticities are complementary or substitutable with elasticity greater than 2. This difference may be attributed to the fact that Qian et al. (2018) estimate the elasticities for different KLEM structures that do not feature all inputs in a single nest.

Our estimates suggest that one can substitute between produced capital, human capital and the different natural capitals. This may be the case since our estimates reflect a representative economy over the long run where the advent and proliferation of new adaptive technology can help promote substitutability between different inputs. In fact, when doing a expanding-window estimation, we find that the elasticity of substitution increases with time as can be seen in Figure 8, lending some empirical support to the fact that improvement in adaptive technology results in higher elasticity of substitution.

	Estimation Method			
	SQP Fixed υ	ADAM Fixed υ	SQP	ADAM
θ_{K}	0.2187	0.2278	0.2455	0.2437
	(0.0198)	(0.0195)	(0.0206)	(0.0022)
θ_{AL}	0.4084	0.4261	0.5155	0.5182
	(0.0326)	(0.0293)	(0.0372)	(0.0394)
θ_{FO}	0.0404	0.0366	0.0000	0.0002
	(0.0207)	(0.0204)	(0.0000)	(0.0000)
θ_{L}	0.1257	0.1178	0.0524	0.0399
	(0.0172)	(0.0135)	(0.0218)	(0.0142)
θ_{M}	0.0318	0.0155	0.0018	0.0105
	(0.0163)	(0.0072)	(0.0048)	(0.0031)
θ_{E}	0.1750	0.1764	0.1848	0.1874
	(0.0107)	(0.0101)	(0.0156)	(0.0132)
ρ_Y	-0.4448	–	-0.3994	–
	(0.0393)	–	(0.0413)	–
λ_Y	–	0.3536	–	0.3387
	–	(0.0219)	–	(0.0226)
g_Y	0.3853	0.3565	0.3448	0.3413
	(0.0181)	(0.0147)	(0.0128)	(0.0086)
υ_Y	1.0000	1.0000	0.9553	0.9555
	–	–	(0.0046)	(0.0037)
$\theta = \frac{1}{1+\rho_Y}$	1.8012	1.7368	1.6650	1.6753
Observations	2,184	2,184	2,184	2,184
MSE	0.1031	0.1028	0.0977	0.0981

Note: Values in parentheses are standard errors from bootstrapping.

Table 11: First Nest CES Estimates

	Estimation Method			
	SQP Fixed υ	ADAM Fixed υ	SQP	ADAM
θ_{K}	0.2530	0.2531	0.2524	0.2524
	(0.0208)	(0.0215)	(0.0228)	(0.0233)
θ_{AL}	0.5414	0.5426	0.5562	0.5576
	(0.0263)	(0.0227)	(0.0275)	(0.0229)
θ_{E}	0.2056	0.2043	0.1917	0.1900
	(0.0179)	(0.0138)	(0.0174)	(0.0137)
ρ_Y	-0.4266	–	-0.3938	–
	(0.0457)	–	(0.0428)	–
λ_Y	–	0.3514	–	0.3277
	–	(0.0255)	–	(0.0235)
g_Y	0.2737	0.2739	0.3261	0.3263
	(0.0057)	(0.0049)	(0.0076)	(0.0068)
υ_Y	1.0000	1.0000	0.9469	0.9468
	–	–	(0.0025)	(0.0025)
$\theta = \frac{1}{1+\rho_Y}$	1.7439	1.7274	1.6495	1.6335
Observations	2,184	2,184	2,184	2,184
MSE	0.1114	0.1114	0.0983	0.0983

Note: Values in parentheses are standard errors from bootstrapping.

Table 12: First Nest CES Estimates (Energy Only Model)

B.2.2 Results: Second nest

For the second nest, we decompose $Y_{i,t}^{\mathrm{E}}$ from the first nest into renewable and fossil fuel energy inputs. Here, we use electricity demand as a proxy for output, relying on market clearing, and include fossil electricity generation and renewable electricity generation as inputs.[32] With two inputs for this nest, we employ both the NLS methods as well as the Kmenta-approximation methods for estimation. The NLS estimation is applied to the following equation:

[32]We do not use total electricity generation as our output because it is a simple linear sum of fossil electricity and renewable electricity generation, which would make the CES estimation redundant as it would imply perfect substitutability.

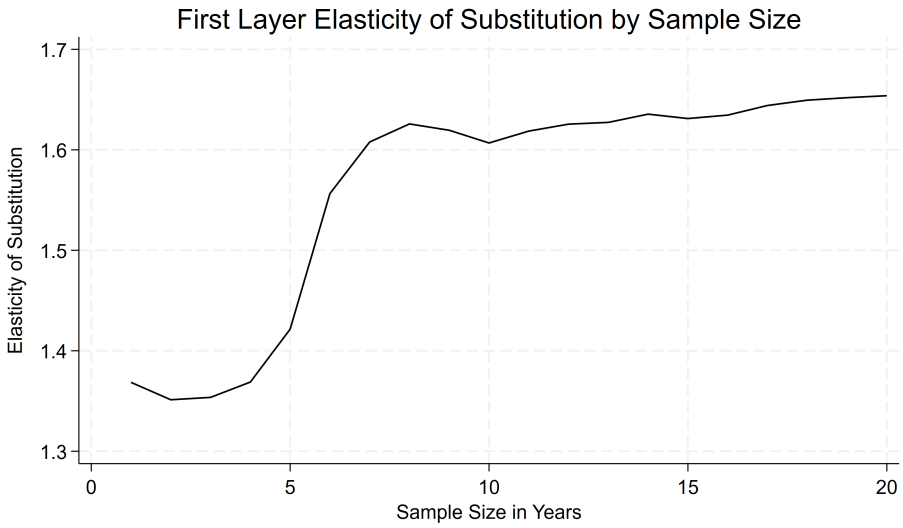

Figure 8: Evolution of Elasticity of Substitution by Sample Size

Notes: The sample size increases as we move along the year dimension. Specifically, a sample size of 1 corresponds to the year 1995, a sample size of 2 represents the years 1995–1996, and a sample size of 20 encompasses the years 1995–2014.

$$\ln(Y_{i,t}^{E}) = \ln(g_E) - \left(\frac{\upsilon_E}{\rho_E}\right) \ln\left(\sigma_{FE}(Y_{i,t}^{FE})^{-\rho_E} + \sigma_{RE}(Y_{i,t}^{RE})^{-\rho_E}\right) \tag{27}$$

Whereas, we use OLS with country fixed effects denoted by μ_i and robust standard errors to estimate the Kmenta-approximation, which follows this standard Taylor expanded expression:[33]

$$\ln(Y_{i,t}^{E}) = \beta_0 + \beta_1 \ln(Y_{i,t}^{FE}) + \beta_2 \ln(Y_{i,t}^{RE}) + \beta_3 \left(\ln(Y_{i,t}^{FE}) - \ln(Y_{i,t}^{RE})\right)^2 + \mu_i \tag{28}$$

Whereby

$$\beta_0 = \ln(g_E), \quad \beta_1 = \upsilon_E \sigma_{FE}, \quad \beta_2 = \upsilon_E \sigma_{RE}, \quad \beta_3 = \frac{-\upsilon_E \rho_E \sigma_{FE} \sigma_{RE}}{2}$$

The number of observations is lower with OLS due to missing values arising from taking logarithms of zero. Across all specifications detailed in table 13, we find that the share of fossil energy inputs in determining total energy output is consistently higher than that of renewable energy inputs, although these shares vary. These findings align with those reported by Papageorgiou et al. (2017), who observed that "clean" energy inputs account for approximately 45 percent of the total share, with variations across specifications. Furthermore, the elasticities of substitution presented below for our specifications fall within the range estimated by Qian et al. (2018), who examined various nesting structures and found that 31 percent of their estimated elasticities of substitution between clean and dirty energy inputs fell within the range of 2 to 6. Notably, 35.9 percent of their estimates were between 0 and 1, while 22.7 percent were between 1 and 2, highlighting the robustness of our results. Papageorgiou et al. (2017) reported elasticities of substitution

[33] Results of the second nest OLS estimation are available in table 15

between clean and dirty energy ranging from 1.73 to 2.81, depending on the inputs used in their production function. Our estimates using the Kmenta-approximation and NLS with fixed returns to scale parameters are consistent with their findings. Additionally, Jo (2025) found using the "indirect approach" that the elasticity of substitution between clean and dirty energy ranges from 1.9 to 3, while Jo and Miftakhova (2024) estimated it could be as high as 5, providing further support for our estimates.

	Estimation Method				
	SQP	ADAM	Kmenta-OLS	SQP Fixed υ	ADAM Fixed υ
σ_{FE}	0.5543	0.5358	0.5076	0.5738	0.5226
	(0.0063)	(0.0639)	(0.0540)	(0.0060)	(0.0602)
σ_{RE}	0.4457	0.4642	0.4924	0.4262	0.4774
	(0.0063)	(0.0639)	(0.0540)	(0.0060)	(0.0602)
ρ_E	-0.8239	–	-0.4171	-0.5811	–
	(0.0298)	–	(0.0136)	(0.0246)	–
λ_E	–	0.5907	–	–	0.5905
	–	(0.0047)	–	–	(0.0042)
g_E	2.6615	1.0322	4.0316	3.7001	1.0473
	(0.0439)	(0.0358)	(0.0575)	(0.0606)	(0.0332)
υ_E	0.9516	0.9445	0.8126	0.8126	0.8126
	(0.0048)	(0.0314)	(0.0117)	–	–
$\sigma = \frac{1}{1+\rho_E}$	5.6850	5.1329	1.7156	2.3874	5.1256
Observations	3,478	3,478	2,911	3,478	3,478
MSE	0.2025	0.0115	0.0186	0.3023	0.0153
Country Fixed Effects	No	No	136	No	No

Note: After further cleaning (e.g., removing countries with more than 15 zero entries in inputs/outputs), the NLS shares become more equitable with $\rho_E = -0.7840$ and MSE = 0.068, suggesting sensitivity to data treatment. Standard errors (in parentheses) are obtained via bootstrapping.

Table 13: Second Nest CES Estimates

B.2.3 Results: Third nest

For the third nest, we decompose fossil energy into three constituent components: oil, gas, and coal production. We use fossil electricity generation as our output variable, noting that it is a linear sum of coal, oil, and gas electricity generation and therefore these cannot be used as inputs. Recognizing that fossil electricity generation is primarily influenced by gas and coal inputs, we aggregate oil and gas production into a single input. All variables used in this analysis are measured in terawatt hours. By reducing the number of inputs from three to two, we apply both NLS and the Kmenta-approximation methods. The following expression is employed for the NLS estimation:

$$\ln(Y_{i,t}^{FE}) = \ln(g_F) - \left(\frac{\upsilon_F}{\rho_F}\right) \ln\left(\epsilon_{\mathrm{G}}(Y_{i,t}^{\mathrm{G}})^{-\rho_F} + \epsilon_C(Y_{i,t}^{\mathrm{C}})^{-\rho_F}\right) \tag{29}$$

While we employ the following expression for the Kmenta-approximation, utilizing the same parameter interpretation as discussed for the second nest's estimates:[34]

$$\ln(Y_{i,t}^{FE}) = \beta_0 + \beta_1 \ln(Y_{i,t}^{\mathrm{G}}) + \beta_2 \ln(Y_{i,t}^{\mathrm{C}}) + \beta_3(\ln(Y_{i,t}^{\mathrm{G}}) - \ln(Y_{i,t}^{\mathrm{C}}))^2 + \mu_i \tag{30}$$

Table 14 presents the varying shares of the oil-gas composite and coal production in determining fossil electricity generation across NLS and OLS methods, with both NLS methods assigning greater weight to coal production and OLS assigning equal weights. However, data on electricity production by different

[34]Third nest OLS results are available in table 16.

fossil fuels[35] suggests that oil and gas collectively contribute between 30 percent to 40 percent to global fossil electricity generation, with the remainder being coal, aligning closely with the NLS results below. These findings are innovative and indicate moderate substitutability between different energy sources, reflecting constraints imposed by existing infrastructure capabilities. Moreover, given the large differences in mean squared error (MSE), we treat the Adam results for this nest as our baseline.

	Estimation Method				
	SQP	ADAM	Kmenta-OLS	SQP Fixed υ	ADAM Fixed υ
ϵ_G	0.3716	0.3216	0.5013	0.3458	0.3990
	(0.0215)	(0.0770)	(0.0512)	(0.0397)	(0.0127)
ϵ_C	0.6284	0.6042	0.4924	0.6542	0.6010
	(0.0215)	(0.0770)	(0.0512)	(0.0397)	(0.0127)
ρ_F	-0.2145	–	-0.2162	-0.1193	–
	(0.0421)	–	(0.1014)	(0.0635)	–
λ_F	–	0.1898	–	–	0.3365
	–	(0.0760)	–	–	(0.0187)
g_F	63.1423	1.0881	52.1997	61.4013	1.2630
	(3.0628)	(0.0673)	(0.2446)	(3.1714)	(0.0399)
υ_F	0.6169	0.8021	0.4149	0.4149	0.4149
	(0.0212)	(0.1713)	(0.0425)	–	–
$\epsilon = \frac{1}{1+\rho_F}$	1.2732	1.4250	1.2643	1.1354	1.6670
Observations	1,152	1,152	1,152	1,152	1,152
MSE	1.9954	0.0150	0.1326	2.2420	0.0075
Country Fixed Effects	No	No	48	No	No

Note: Values in parentheses are standard errors from bootstrapping.

Table 14: Third Nest CES Estimates

B.3 Natural Capital Climate Damages Estimation

B.3.1 Model Selection

This section reports the model selection process we followed to identify the functional form we rely on to estimate the climate damages in section 3.2.2. As mentioned, we evaluate and discuss how the dependent and independent variables should enter the model (i.e., in levels or first differences), and which functional forms $f(\cdot)$ and $g(\cdot)$ should take (i.e., linearly or as higher-order polynomials). Regarding the first point, Burke et al. (2015) argue in their seminal paper that the GDP series is nonstationary, hence it should enter the estimation in first differences. Newell, Prest, and Sexton (2021) argue that the temperature series is also non-stationary, hence it should enter the model in first differences as well. Given the several variables in our model, we cannot assert a priori whether they are stationary or not. Therefore, we empirically test this argument using data.

Appendix B.2 reports the results of the Augmented Dickey-Fuller unit-root test[36] for all variables used in the empirical analysis. Initially, we test the variables of interest and subsequently apply the tests on the remaining detrended variables for which we did not reject the null hypothesis of nonstationarity in the first stage. We reject the null hypothesis in the test without trends for temperature, precipitation, minerals, and cropland, as well as in the test accounting for trends for forest ecosystems, gas, oil, fossil fuels, and renewable energy, indicating that these variables are either stationary or trend stationary. Conversely, we fail to reject the null hypothesis for coal and aggregate energy, which are found to be nonstationary. Therefore,

[35] See Our World in Data: Energy Mix

[36] We use the Inverse chi-squared and Modified inverse chi-squared statistics, which are more suitable for large panels (Choi, 2001).

we estimate the model from equation (20) in levels for the stationary variables and in first differences for the nonstationary variables.[37]

Regarding the specification of the damage functions $f(\cdot)$ and $g(\cdot)$, we depart from the quadratic model from Burke et al. (2015) and opt for a linear model as in Dell et al. (2012). Linear in this context refers to the order of the temperature term polynomial included in the reduced form estimation. The damage function included in the model remains non-linear as all the dependent variables are taken in logs. We do this for two reasons. First, the aim of this section is to estimate climate damages which can be used in our macroeconomic model simulation. Since the model requires global-level estimates, we consider the linear model to be better suited, as we are interested in the global average marginal effect rather than how different countries are impacted by higher temperatures. Second, the results from the models including the quadratic terms reported in section D show that the quadratic term in the second order polynomial function is often not statistically significant.

An additional aspect often discussed in the literature concerns the persistence of temperature shocks identified through lagged effects (i.e., levels versus growth effects). Kotz et al. (2024) elaborate on disentangling these effects to identify the persistence of climate impacts on economic growth using multiple lags of temperature. Given the scope of this paper and the limited time dimension of our data, we include two lags of temperature in our model.

[37] The marginal effect of an additional $1^{\circ}C$ in year t that we identify, $\frac{\partial Y_{i,t}}{\partial T_{i,t}}$, is consistent between the two estimation methods.

Appendix C Kmenta Approximation OLS Results

	Second nest Kmenta-Approximation OLS Results	
	Coefficient	[95% Conf. Interval]
$\ln(Y^{FE})$	0.4125^{***}	[0.3954, 0.4296]
	(0.0087)	
$\ln(Y^{RE})$	0.4001^{***}	[0.3850, 0.4153]
	(0.0077)	
$(\ln(Y^{FE})$ - $\ln(Y^{RE}))^2$	0.0424^{***}	[0.0399, 0.0449]
	(0.0424)	
Cons.	1.3942^{***}	[1.3380, 1.4503]
	(0.0286)	
R^2	0.9961	
N	2,911	

Table 15: Second nest Regression Results

	Third nest Kmenta-Approximation OLS Results	
	Coefficient	[95% Conf. Interval]
$\ln(Y^{\mathrm{C}})$	0.2080^{***}	[0.1469, 0.2691]
	(0.0312)	
$\ln(Y^{\mathrm{G}})$	0.2069^{***}	[0.1501, 0.2637]
	(0.0289)	
$(\ln(Y^{\mathrm{C}}) - \ln(Y^{\mathrm{G}}))^2$	0.0112^{***}	[0.0047, 0.0177]
	(0.0033)	
Cons.	3.9551^{***}	[3.8886, 4.0215]
	(0.0339)	
R^2	0.9714	
N	1,152	

Table 16: Third nest Regression Results

Appendix D Climate Damages Regression Tables

	(1) Produced Capital	(2) Produced Capital	(3) Produced Capital	(4) Produced Capital	(5) Produced Capital	(6) Produced Capital
T	-0.040***	-0.044***	-0.030**	-0.13**	-0.11***	-0.095***
	(0.0098)	(0.0096)	(0.0084)	(0.038)	(0.029)	(0.026)
P	-0.000025	-0.000010	0.000014	-0.0000063	-0.0000091	0.000034
	(0.000024)	(0.000022)	(0.000022)	(0.000090)	(0.000099)	(0.000086)
$(\ell 1)T$		-0.035***	-0.040***		-0.096***	-0.088***
		(0.0067)	(0.0088)		(0.025)	(0.023)
$(\ell 2)T$			-0.036***			-0.051**
			(0.0086)			(0.014)
T^2				0.0045**	0.0034*	0.0029*
				(0.0017)	(0.0015)	(0.0012)
P^2				3.5e-09	3.8e-09	-1.3e-09
				(0.000000016)	(0.000000020)	(0.000000019)
$(\ell 1)T^2$					0.0031**	0.0028**
					(0.0011)	(0.0011)
$(\ell 2)T^2$						0.00069***
						(0.00019)
Country FE	Yes	Yes	Yes	Yes	Yes	Yes
Year FE	Yes	Yes	Yes	Yes	Yes	Yes
R^2	0.99	0.99	0.99	0.99	0.99	0.99
N	1728	1656	1584	1728	1656	1512

Standard errors in parentheses
* $p < 0.10$, ** $p < 0.05$, *** $p < 0.01$

Table 17: Point estimates and standard errors from the regressions of weather variables on produced capital. Results from different specifications with country and year FE, standard errors clustered at the regional level as identified by the World Bank.

	(1) Cropland	(2) Cropland	(3) Cropland	(4) Cropland	(5) Cropland	(6) Cropland
T	-0.034***	-0.047***	-0.015	-0.19**	-0.16***	-0.10**
	(0.0092)	(0.0087)	(0.012)	(0.064)	(0.042)	(0.029)
P	0.000035	0.000037	0.000085	-0.000060	-0.000079	-0.0000080
	(0.000070)	(0.000068)	(0.000060)	(0.000080)	(0.000069)	(0.000085)
$(\ell 1)T$		-0.039***	-0.051***		-0.12**	-0.100**
		(0.0082)	(0.0081)		(0.042)	(0.040)
$(\ell 2)T$			-0.047***			-0.075***
			(0.010)			(0.015)
T^2				0.0075**	0.0057***	0.0041***
				(0.0022)	(0.0014)	(0.00066)
P^2				0.000000037	0.000000036	0.000000029
				(0.000000024)	(0.000000021)	(0.000000024)
$(\ell 1)T^2$					0.0043**	0.0035*
					(0.0017)	(0.0016)
$(\ell 2)T^2$						0.0012**
						(0.00037)
Country FE	Yes	Yes	Yes	Yes	Yes	Yes
Year FE	Yes	Yes	Yes	Yes	Yes	Yes
R^2	1.00	1.00	1.00	1.00	1.00	1.00
N	1728	1656	1584	1728	1656	1512

Standard errors in parentheses
* $p < 0.10$, ** $p < 0.05$, *** $p < 0.01$

Table 18: Point estimates and standard errors from the regressions of weather variables on cropland. Results from different specifications with country and year FE, standard errors clustered at the regional level as identified by the World Bank.

	(1) ΔCoal	(2) ΔCoal	(3) ΔCoal	(4) ΔCoal	(5) ΔCoal	(6) Δ Coal
ΔT	-0.013	-0.0099	-0.0037	-0.039*	-0.054	-0.053
	(0.013)	(0.020)	(0.020)	(0.020)	(0.035)	(0.036)
$(\ell 1)\Delta T$		0.0096	0.021		-0.029	-0.035
		(0.017)	(0.018)		(0.027)	(0.039)
$(\ell 2)\Delta T$			0.014**			-0.010
			(0.0041)			(0.017)
ΔP	-0.00010*	-0.00010*	-0.00011**	-0.00025**	-0.00024***	-0.00023***
	(0.000046)	(0.000045)	(0.000035)	(0.000069)	(0.000062)	(0.000060)
ΔT^2				0.0013	0.0022	0.0025
				(0.00085)	(0.0013)	(0.0015)
$(\ell 1)\Delta T^2$					0.0020	0.0029
					(0.0011)	(0.0017)
$(\ell 2)\Delta T^2$						0.0013
						(0.00086)
ΔP^2				0.000000046*	0.000000042*	0.000000035
				(0.000000020)	(0.000000018)	(0.000000018)
Country FE	Yes	Yes	Yes	Yes	Yes	Yes
Year FE	Yes	Yes	Yes	Yes	Yes	Yes
R^2	0.13	0.14	0.14	0.13	0.15	0.15
N	1155	1111	1067	1155	1111	1067

Standard errors in parentheses
* $p < 0.10$, ** $p < 0.05$, *** $p < 0.01$

Table 19: Point estimates and standard errors from the regressions of weather variables on coal. Results from different specifications in first difference with country and year FE, standard errors clustered at the regional level as identified by the World Bank.

	(1) Gas	(2) Gas	(3) Gas	(4) Gas	(5) Gas	(6) Gas
T	-0.098***	-0.100**	-0.084**	-0.36**	-0.33***	-0.31***
	(0.025)	(0.028)	(0.029)	(0.098)	(0.084)	(0.074)
P	-0.00035***	-0.00034***	-0.00026**	-0.00037*	-0.00032	-0.00015
	(0.000057)	(0.000076)	(0.000089)	(0.00018)	(0.00019)	(0.00015)
$(\ell 1)T$		-0.083***	-0.088***		-0.23***	-0.22***
		(0.020)	(0.023)		(0.054)	(0.048)
$(\ell 2)T$			-0.098***			-0.11***
			(0.017)			(0.026)
T^2				0.013**	0.011**	0.012***
				(0.0041)	(0.0034)	(0.0029)
P^2				0.000000028	6.6e-09	-3.6e-09
				(0.000000044)	(0.000000043)	(0.000000037)
$(\ell 1)T^2$					0.0074**	0.0071***
					(0.0024)	(0.0019)
$(\ell 2)T^2$						0.0016**
						(0.00044)
Country FE	Yes	Yes	Yes	Yes	Yes	Yes
Year FE	Yes	Yes	Yes	Yes	Yes	Yes
R^2	0.91	0.91	0.92	0.91	0.92	0.93
N	1548	1500	1452	1548	1500	1403

Standard errors in parentheses
* $p < 0.10$, ** $p < 0.05$, *** $p < 0.01$

Table 20: Point estimates and standard errors from the regressions of weather variables on gas. Results from different specifications with country and year FE, standard errors clustered at the regional level as identified by the World Bank.

	(1) Oil	(2) Oil	(3) Oil	(4) Oil	(5) Oil	(6) Oil
T	-0.048	-0.060	-0.041	-0.15	-0.13	-0.11
	(0.039)	(0.038)	(0.048)	(0.12)	(0.094)	(0.088)
P	-0.00032	-0.00033	-0.00035*	-0.00051	-0.00060	-0.00056
	(0.00017)	(0.00018)	(0.00017)	(0.00034)	(0.00039)	(0.00034)
$(\ell 1)T$		-0.0063	-0.011		-0.11	-0.12
		(0.052)	(0.051)		(0.082)	(0.073)
$(\ell 2)T$			0.031			0.057
			(0.032)			(0.057)
T^2				0.0050	0.0037	0.0039
				(0.0058)	(0.0046)	(0.0046)
P^2				0.000000061	0.000000074	0.000000053
				(0.000000057)	(0.000000064)	(0.000000054)
$(\ell 1)T^2$					0.0051	0.0063
					(0.0049)	(0.0047)
$(\ell 2)T^2$						-0.00098
						(0.0014)
Country FE	Yes	Yes	Yes	Yes	Yes	Yes
Year FE	Yes	Yes	Yes	Yes	Yes	Yes
R^2	0.89	0.89	0.89	0.89	0.89	0.90
N	1523	1473	1423	1523	1473	1373

Standard errors in parentheses
* $p < 0.10$, ** $p < 0.05$, *** $p < 0.01$

Table 21: Point estimates and standard errors from the regressions of weather variables on oil. Results from different specifications with country and year FE, standard errors clustered at the regional level as identified by the World Bank.

	(1) Fossil Fuel	(2) Fossil Fuel	(3) Fossil Fuel	(4) Fossil Fuel	(5) Fossil Fuel	(6) Fossil Fuel
T	-0.080***	-0.084***	-0.063**	-0.33***	-0.28***	-0.25***
	(0.019)	(0.018)	(0.020)	(0.086)	(0.067)	(0.062)
P	-0.00016*	-0.00013*	-0.000091	-0.00033**	-0.00035**	-0.00029*
	(0.000070)	(0.000068)	(0.000080)	(0.00013)	(0.00012)	(0.00014)
$(\ell 1)T$		-0.054**	-0.057**		-0.21***	-0.19***
		(0.016)	(0.019)		(0.045)	(0.041)
$(\ell 2)T$			-0.039**			-0.041
			(0.015)			(0.024)
T^2				0.012***	0.0095***	0.0090***
				(0.0025)	(0.0019)	(0.0018)
P^2				0.000000070	0.000000068	0.000000058
				(0.000000037)	(0.000000035)	(0.000000037)
$(\ell 1)T^2$					0.0075***	0.0072***
					(0.0010)	(0.0011)
$(\ell 2)T^2$						0.00057
						(0.00040)
Country FE	Yes	Yes	Yes	Yes	Yes	Yes
Year FE	Yes	Yes	Yes	Yes	Yes	Yes
R^2	0.97	0.97	0.97	0.97	0.97	0.97
N	1606	1555	1504	1606	1555	1453

Standard errors in parentheses
* $p < 0.10$, ** $p < 0.05$, *** $p < 0.01$

Table 22: Point estimates and standard errors from the regressions of weather variables on fossil fuel. Results from different specifications with country and year FE, standard errors clustered at the regional level as identified by the World Bank.

	(1) Δ Agg. Energy	(2) Δ Agg. Energy	(3) Δ Agg. Energy	(4) Δ Agg. Energy	(5) Δ Agg. Energy	(6) Δ Agg. Energy
ΔT	-0.014***	-0.015***	-0.016***	-0.013***	-0.016***	-0.017***
	(0.0016)	(0.0027)	(0.0035)	(0.0025)	(0.0027)	(0.0030)
$(\ell 1)\Delta T$		-0.0032	-0.0056		0.0024	-0.0012
		(0.0017)	(0.0034)		(0.0029)	(0.0032)
$(\ell 2)\Delta T$			-0.0013			-0.0028
			(0.0024)			(0.0023)
ΔP	0.0000023	0.0000017	0.0000046	0.000011	0.0000093	0.000018
	(0.000012)	(0.000012)	(0.000013)	(0.000028)	(0.000031)	(0.000029)
ΔT^2				-0.0000063	0.000041	0.00010
				(0.00018)	(0.00019)	(0.00019)
$(\ell 1)\Delta T^2$					-0.00025**	-0.00020
					(0.00010)	(0.00014)
$(\ell 2)\Delta T^2$						0.000063
						(0.000097)
ΔP^2				-2.4e-09	-1.5e-09	-3.1e-09
				(6.6e-09)	(7.0e-09)	(5.9e-09)
Country FE	Yes	Yes	Yes	Yes	Yes	Yes
Year FE	Yes	Yes	Yes	Yes	Yes	Yes
R^2	0.24	0.25	0.26	0.24	0.25	0.26
N	1656	1584	1512	1656	1584	1512

Standard errors in parentheses
* $p < 0.10$, ** $p < 0.05$, *** $p < 0.01$

Table 23: Point estimates and standard errors from the regressions of weather variables on energy. Results from different specifications in first difference with country and year FE, standard errors clustered at the regional level as identified by the World Bank.

	(1) Ren. Energy	(2) Ren. Energy	(3) Ren. Energy	(4) Ren. Energy	(5) Ren. Energy	(6) Ren. Energy
T	-0.036	-0.028	-0.062**	-0.0071	-0.027	-0.077
	(0.022)	(0.021)	(0.020)	(0.064)	(0.052)	(0.058)
P	0.00024	0.00027*	0.00022**	0.00062**	0.00065**	0.00044***
	(0.00013)	(0.00012)	(0.000082)	(0.00022)	(0.00019)	(0.00011)
$(\ell 1)T$		-0.033	-0.029		0.033	-0.0090
		(0.018)	(0.018)		(0.061)	(0.057)
$(\ell 2)T$			-0.045			-0.044
			(0.024)			(0.029)
T^2				-0.0012	0.000093	0.00087
				(0.0022)	(0.0017)	(0.0022)
P^2				-0.000000097*	-0.000000093*	-0.000000057*
				(0.000000047)	(0.000000040)	(0.000000026)
$(\ell 1)T^2$					-0.0035	-0.0029
					(0.0023)	(0.0022)
$(\ell 2)T^2$						-0.0000042
						(0.00078)
Country FE	Yes	Yes	Yes	Yes	Yes	Yes
Year FE	Yes	Yes	Yes	Yes	Yes	Yes
R^2	0.96	0.96	0.96	0.96	0.96	0.96
N	1616	1549	1483	1616	1549	1416

Standard errors in parentheses
* $p < 0.10$, ** $p < 0.05$, *** $p < 0.01$

Table 24: Point estimates and standard errors from the regressions of weather variables on renewable energy. Results from different specifications with country and year FE, standard errors clustered at the regional level as identified by the World Bank.

	(1) Forest Eco.	(2) Forest Eco.	(3) Forest Eco.	(4) Forest Eco.	(5) Forest Eco.	(6) Forest Eco.
T	-0.0059	-0.0087***	-0.011**	-0.0098	-0.0087	-0.011
	(0.0047)	(0.0023)	(0.0036)	(0.033)	(0.025)	(0.024)
P	-0.0000022	-0.0000084	-0.000012	0.000018	0.000020	-0.0000092
	(0.000020)	(0.000021)	(0.000015)	(0.000067)	(0.000075)	(0.000071)
$(\ell 1)T$		-0.0087	-0.011**		-0.014	-0.018
		(0.0047)	(0.0038)		(0.024)	(0.023)
$(\ell 2)T$			-0.0078			-0.012
			(0.0070)			(0.010)
T^2				0.00020	0.000022	-0.000083
				(0.0018)	(0.0013)	(0.0011)
P^2				-4.8e-09	-7.2e-09	2.3e-09
				(0.000000014)	(0.000000019)	(0.000000017)
$(\ell 1)T^2$					0.00023	0.00021
					(0.0012)	(0.0011)
$(\ell 2)T^2$						-0.000013
						(0.00031)
Country FE	Yes	Yes	Yes	Yes	Yes	Yes
Year FE	Yes	Yes	Yes	Yes	Yes	Yes
R^2	1.00	1.00	1.00	1.00	1.00	1.00
N	1704	1633	1562	1704	1633	1491

Standard errors in parentheses
* $p < 0.10$, ** $p < 0.05$, *** $p < 0.01$

Table 25: Point estimates and standard errors from the regressions of weather variables on forest ecosystem. Results from different specifications with country and year FE, standard errors clustered at the regional level as identified by the World Bank.

	(1) Minerals	(2) Minerals	(3) Minerals	(4) Minerals	(5) Minerals	(6) Minerals
T	-0.075***	-0.064***	-0.027	-0.33**	-0.25**	-0.19*
	(0.016)	(0.012)	(0.017)	(0.11)	(0.080)	(0.083)
P	0.00013	0.00012	0.00014	0.00073	0.00055	0.00045
	(0.00012)	(0.00011)	(0.00013)	(0.00052)	(0.00055)	(0.00081)
$(\ell 1)T$		-0.095**	-0.082**		-0.32***	-0.28**
		(0.028)	(0.026)		(0.072)	(0.080)
$(\ell 2)T$			-0.16***			-0.20**
			(0.027)			(0.062)
T^2				0.013**	0.0097**	0.0088**
				(0.0038)	(0.0032)	(0.0034)
P^2				-0.00000012	-0.000000096	-0.000000076
				(0.00000010)	(0.00000011)	(0.00000015)
$(\ell 1)T^2$					0.011**	0.011**
					(0.0032)	(0.0040)
$(\ell 2)T^2$						0.0027
						(0.0015)
Country FE	Yes	Yes	Yes	Yes	Yes	Yes
Year FE	Yes	Yes	Yes	Yes	Yes	Yes
R^2	0.92	0.93	0.93	0.92	0.93	0.93
N	1368	1311	1254	1368	1311	1197

Standard errors in parentheses
* $p < 0.10$, ** $p < 0.05$, *** $p < 0.01$

Table 26: Point estimates and standard errors from the regressions of weather variables on minerals. Results from different specifications with country and year FE, standard errors clustered at the regional level as identified by the World Bank.

Appendix E Model Results

E.1 Shadow Prices Sensitivity Analysis

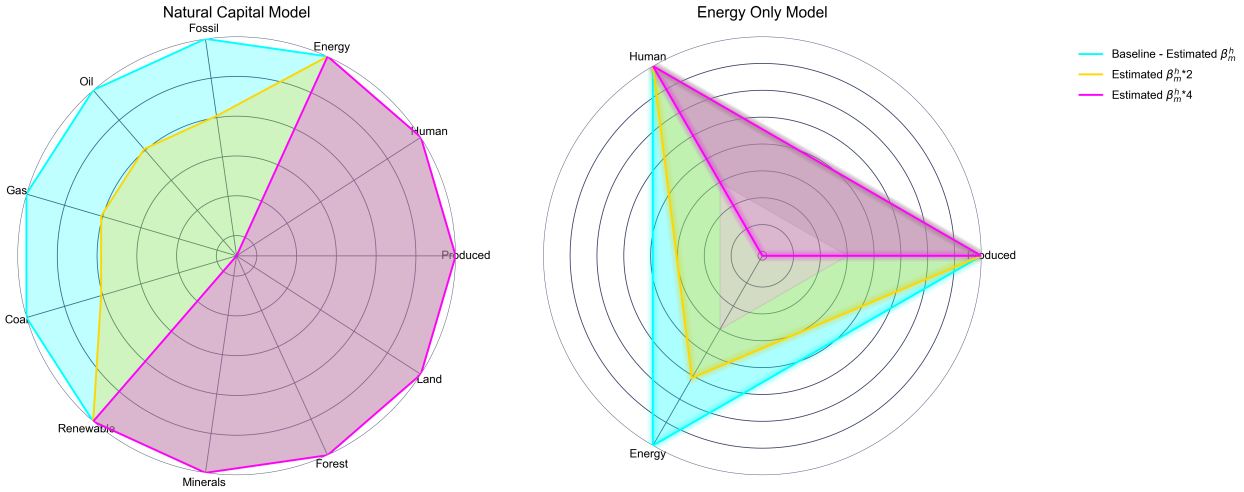

Figure 9: Shadow Prices Sensitivity To Climate Damages

Notes: This figure shows production factors' shadow prices under two different model specifications across three parameter values representing distinct scenarios. The baseline case shadow prices are normalized to one and the center of the circle correspond the lowest shadow price value.

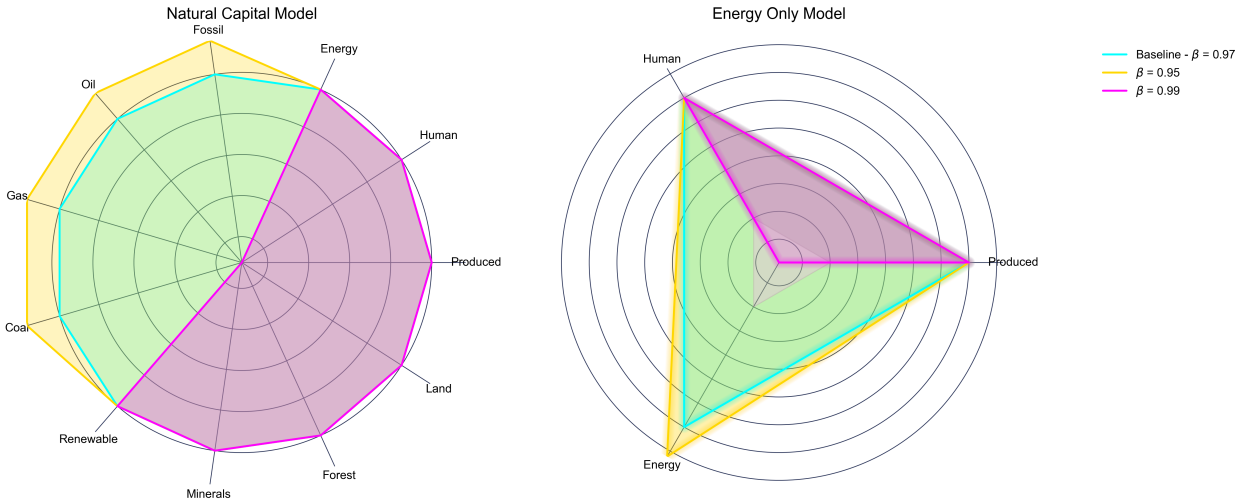

Figure 10: Natural Shadow Prices Sensitivity To Discount Rate

Notes: This figure shows production factors' shadow prices under two different model specifications across three parameter values representing distinct scenarios. The baseline case shadow prices are normalized to one and the center of the circle correspond the lowest shadow price value.

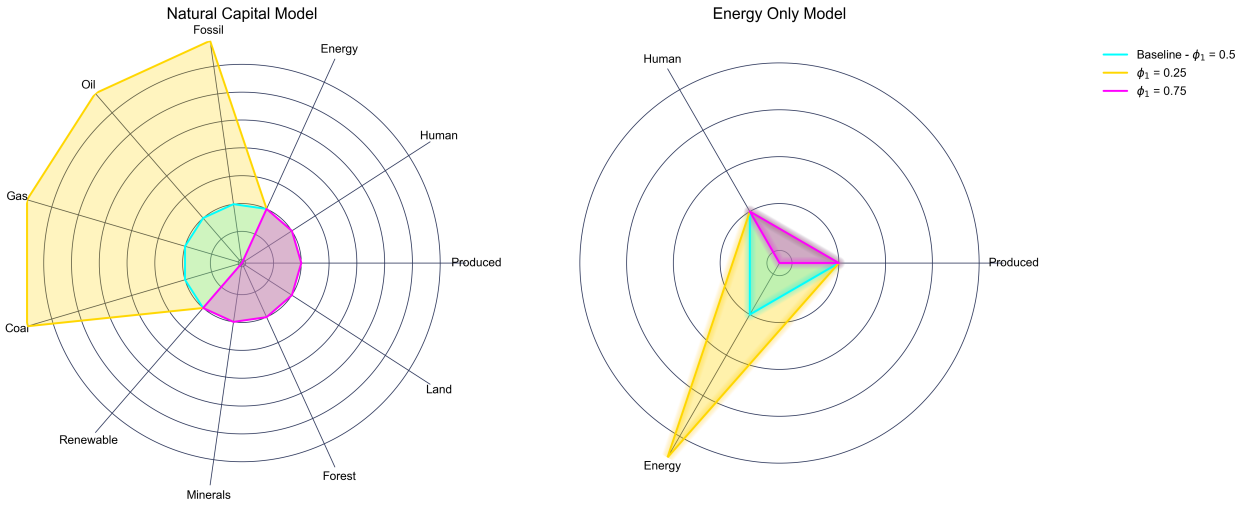

Figure 11: Natural Shadow Prices Sensitivity To Climate Sensitivity

Notes: This figure shows production factors' shadow prices under two different model specifications across three parameter values representing distinct scenarios. The baseline case shadow prices are normalized to one and the center of the circle correspond the lowest shadow price value.

E.2 Long-run Dynamics

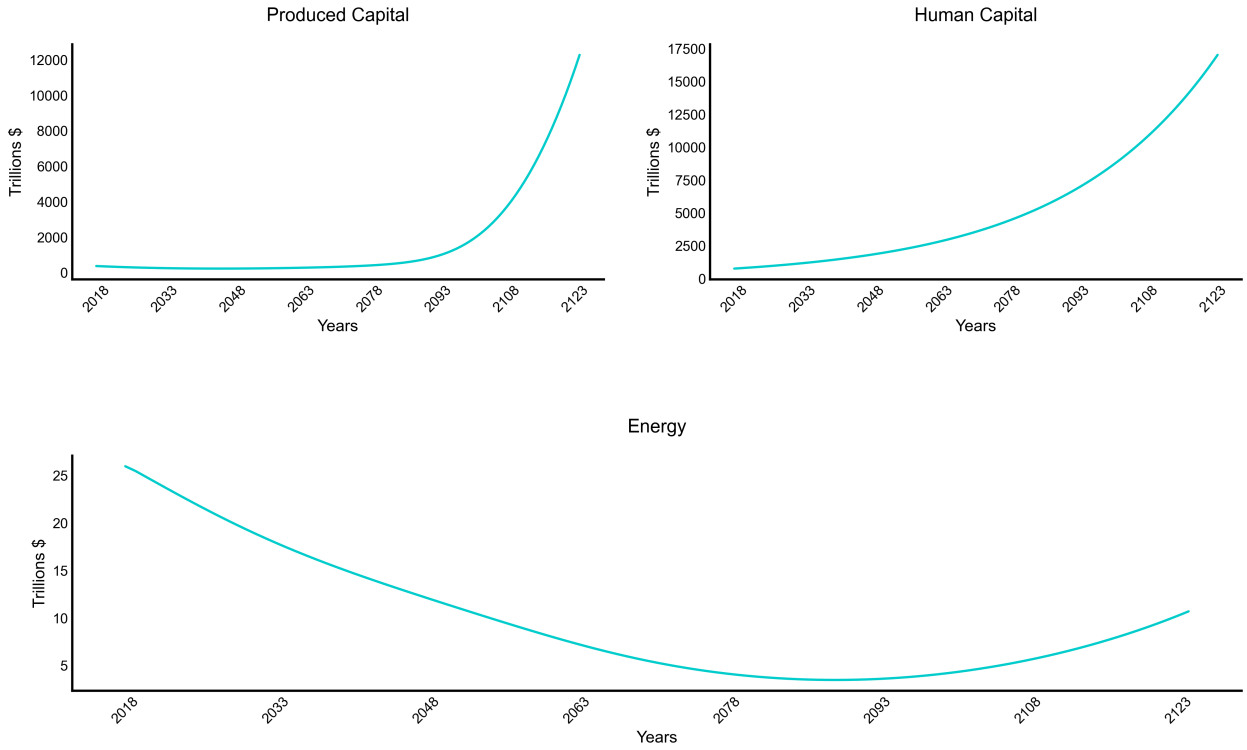

Figure 12: Long-Run Transition: Produced Capital, Human Capital, and Energy

Notes: This figure illustrates the long-run transition over 107 years (up to 2125) with a 3 percent growth rate.

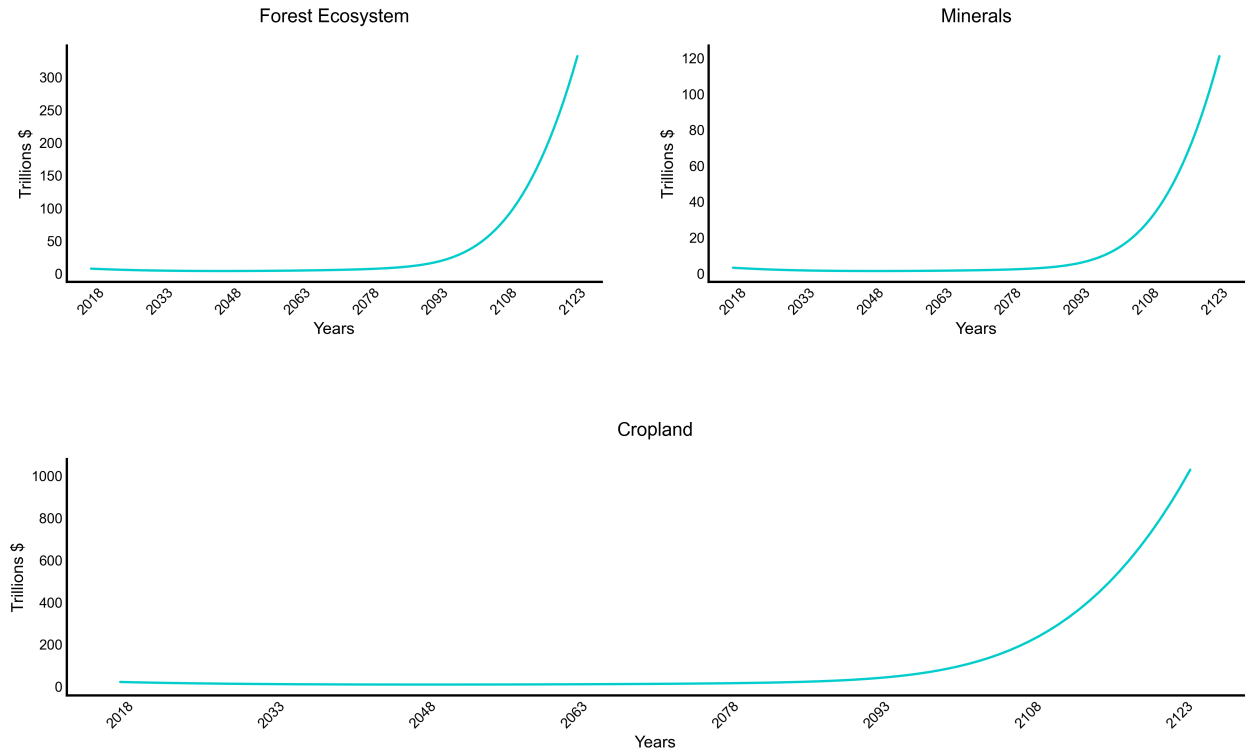

Figure 13: Long-Run Transition: Natural Capital Components

Notes: This figure illustrates the long-run transition over 107 years (up to 2125) with a 3 percent growth rate.

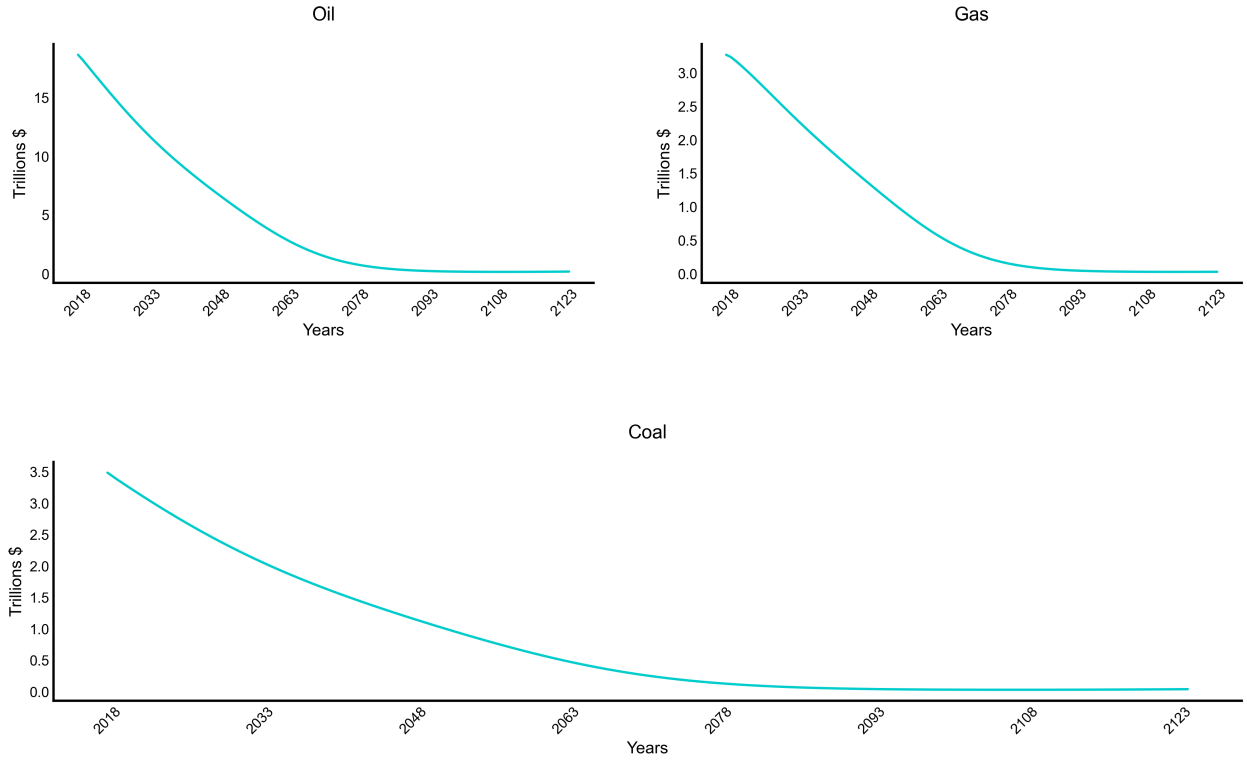

Figure 14: Long-Run Transition: Fossil Fuels Components

Notes: This figure illustrates the long-run transition over 107 years (up to 2125) with a 3 percent growth rate.

E.3 Uncertainty and Shadow Prices

Name	Variable	All Natural Capital			Only Energy		
		$\theta = 0.85$	$\theta = 0.99$	$\theta = 1.70$	$\theta = 0.85$	$\theta = 0.99$	$\theta = 1.70$
Shadow Price of Emission	$\mathbb{E}(V^{\mathrm{E}})$	0.04	0.03	0.13	0.02	0.01	0.06
		(3.27)	(3.26)	(3.91)	(3.03)	(3.19)	(3.93)
Shadow Price of Energy	$\mathbb{E}(\Psi^{\mathrm{E}})$	0.02	0.02	0.04	0.03	0.03	0.01
		(2.30)	(2.29)	(2.06)	(3.06)	(3.26)	(3.26)
Shadow Price of Fossil	$\mathbb{E}(\Psi^{\mathrm{FE}})$	0.01	0.02	-0.02	-	-	-
		(2.96)	(3.11)	(3.67)	-	-	-
Shadow Price of Oil	$\mathbb{E}(\Psi^{\mathrm{O}})$	0.01	0.02	-0.02	-	-	-
		(2.94)	(3.08)	(3.54)	-	-	-
Shadow Price of Gas	$\mathbb{E}(\Psi^{\mathrm{G}})$	0.01	0.02	-0.01	-	-	-
		(2.87)	(2.97)	(3.03)	-	-	-
Shadow Price of Coal	$\mathbb{E}(\Psi^{\mathrm{C}})$	0.01	0.01	-0.02	-	-	-
		(3.00)	(3.16)	(3.92)	-	-	-
Shadow Price of Renewable Energy	$\mathbb{E}(\Psi^{\mathrm{RE}})$	0.02	0.03	0.02	-	-	-
		(2.25)	(2.17)	(1.19)	-	-	-
Shadow Price of Minerals	$\mathbb{E}(\Psi^{\mathrm{M}})$	0.15	0.18	0.06	-	-	-
		(3.17)	(3.29)	(3.52)	-	-	-
Shadow Price of Forest ES	$\mathbb{E}(\Psi^{\mathrm{FO}})$	-0.01	-0.01	-0.03	-	-	-
		(2.92)	(3.00)	(2.87)	-	-	-
Shadow Price of Cropland	$\mathbb{E}(\Psi^{\mathrm{L}})$	0.04	0.05	-0.01	-	-	-
		(2.79)	(2.92)	(3.29)	-	-	-

Table 27: Uncertainty cost of TFP shock for different θ values – percentage change with respect to deterministic case (case without habits)

Notes: This table displays the impact of TFP uncertainty on shadow prices under our two different model specifications and three cases for elasticity of substitution in the first nest. The third column corresponds to the estimated elasticity. The first column assumes an elasticity lower than unity, and the second one is an intermediate case. Results are reported as percentage deviations from the deterministic case. Standard deviations are reported in parentheses. $\mathbb{E}$(X) refers to the expectation of the shadow price X.

Name	Variable	All Natural Capital			Only Energy		
		$\theta = 0.85$	$\theta = 0.99$	$\theta = 1.70$	$\theta = 0.85$	$\theta = 0.99$	$\theta = 1.70$
Shadow Price of Emission	$\mathbb{E}(V^{\mathrm{E}})$	-0.10	-0.11	-0.33	-0.09	-0.09	-0.17
		(1.19)	(1.18)	(1.18)	(1.19)	(1.19)	(1.16)
Shadow Price of Energy	$\mathbb{E}(\Psi^{\mathrm{E}})$	-0.01	-0.01	-0.07	0.01	0.01	0.05
		(0.13)	(0.15)	(0.37)	(0.10)	(0.13)	(0.35)
Shadow Price of Fossil	$\mathbb{E}(\Psi^{\mathrm{FE}})$	0.01	0.01	0.11	-	-	-
		(0.18)	(0.19)	(0.51)	-	-	-
Shadow Price of Oil	$\mathbb{E}(\Psi^{\mathrm{O}})$	0.01	0.01	0.11	-	-	-
		(0.18)	(0.19)	(0.51)	-	-	-
Shadow Price of Gas	$\mathbb{E}(\Psi^{\mathrm{G}})$	0.01	0.01	0.10	-	-	-
		(0.18)	(0.19)	(0.50)	-	-	-
Shadow Price of Coal	$\mathbb{E}(\Psi^{\mathrm{C}})$	0.01	0.01	0.11	-	-	-
		(0.18)	(0.19)	(0.52)	-	-	-
Shadow Price of Renewable Energy	$\mathbb{E}(\Psi^{\mathrm{RE}})$	0.01	0.01	0.11	-	-	-
		(0.09)	(0.07)	(0.12)	-	-	-
Shadow Price of Minerals	$\mathbb{E}(\Psi^{\mathrm{M}})$	0.03	0.05	0.43	-	-	-
		(0.15)	(0.13)	(0.47)	-	-	-
Shadow Price of Forest ES	$\mathbb{E}(\Psi^{\mathrm{FO}})$	0.00	0.00	0.04	-	-	-
		(0.12)	(0.10)	(0.15)	-	-	-
Shadow Price of Cropland	$\mathbb{E}(\Psi^{\mathrm{L}})$	0.01	0.02	0.17	-	-	-
		(0.12)	(0.10)	(0.24)	-	-	-

Table 28: Uncertainty cost of Temperature shock for different θ values – percentage change with respect to deterministic case

Notes: This table displays the impact of temperature uncertainty on shadow prices under our two different model specifications with habit formation and three cases for elasticity of substitution in the first nest. The third column corresponds to the estimated elasticity. The first column assumes an elasticity lower than unity, and the second one is an intermediate case. Results are reported as percentage deviations from the deterministic case. Standard deviations are reported in parentheses. $\mathbb{E}$(X) refers to the expectation of the shadow price X.

Name	Variable	All Natural Capital			Only Energy		
		$\theta = 0.85$	$\theta = 0.99$	$\theta = 1.70$	$\theta = 0.85$	$\theta = 0.99$	$\theta = 1.70$
Shadow Price of Emission	$\mathbb{E}(V^{\mathrm{E}})$	-0.10	-0.11	-0.34	-0.09	-0.09	-0.17
		(1.18)	(1.18)	(1.20)	(1.18)	(1.18)	(1.18)
Shadow Price of Energy	$\mathbb{E}(\Psi^{\mathrm{E}})$	-0.01	-0.01	-0.07	0.01	0.01	0.05
		(0.12)	(0.15)	(0.38)	(0.10)	(0.13)	(0.33)
Shadow Price of Fossil	$\mathbb{E}(\Psi^{\mathrm{FE}})$	0.01	0.01	0.11	-	-	-
		(0.15)	(0.18)	(0.50)	-	-	-
Shadow Price of Oil	$\mathbb{E}(\Psi^{\mathrm{O}})$	0.01	0.01	0.11	-	-	-
		(0.15)	(0.18)	(0.50)	-	-	-
Shadow Price of Gas	$\mathbb{E}(\Psi^{\mathrm{G}})$	0.01	0.01	0.11	-	-	-
		(0.15)	(0.18)	(0.49)	-	-	-
Shadow Price of Coal	$\mathbb{E}(\Psi^{\mathrm{C}})$	0.01	0.01	0.11	-	-	-
		(0.15)	(0.18)	(0.50)	-	-	-
Shadow Price of Renewable Energy	$\mathbb{E}(\Psi^{\mathrm{RE}})$	0.01	0.01	0.11	-	-	-
		(0.06)	(0.06)	(0.11)	-	-	-
Shadow Price of Minerals	$\mathbb{E}(\Psi^{\mathrm{M}})$	0.03	0.05	0.44	-	-	-
		(0.09)	(0.11)	(0.45)	-	-	-
Shadow Price of Forest ES	$\mathbb{E}(\Psi^{\mathrm{FO}})$	0.00	0.00	0.04	-	-	-
		(0.07)	(0.08)	(0.09)	-	-	-
Shadow Price of Cropland	$\mathbb{E}(\Psi^{\mathrm{L}})$	0.01	0.02	0.18	-	-	-
		(0.08)	(0.08)	(0.20)	-	-	-

Table 29: Uncertainty cost of temperature shocks for different θ values – percentage change with respect to deterministic case (case without habits)

Notes: This table displays the impact of temperature uncertainty on shadow prices under our two different model specifications and three cases for elasticity of substitution in the first nest. The third column corresponds to the estimated elasticity. The first column assumes an elasticity lower than unity, and the second one is an intermediate case. Results are reported as percentage deviations from the deterministic case. Standard deviations are reported in parentheses. $\mathbb{E}$(X) refers to the expectation of the shadow price X.

ONLINE APPENDIX
(not for publication)

A Adam: A Stochastic Gradient Descent Method

Adam is a stochastic gradient descent (SGD) algorithm variant introduced by Kingma and Ba (2014). It is implemented using TensorFlow, a popular machine learning library.[38] While most of the literature relies on linear, non-linear, or indirect econometric approaches to estimate CES elasticities, Qian et al. (2018) employ machine learning methods for CES parameter estimation, specifically using Adadelta, another widely used SGD method. This work is the closest to our proposed estimation using Adam.

To respect the bounds of the parameters, constrained gradient descent requires a projection step to ensure that the parameters fall within the feasible set. However, this can be computationally expensive and face convergence issues, proving to be particularly challenging for the share and the elasticity of substitution parameters. Unlike SQP, we cannot introduce explicit constraints and as such, following McDonald (1980), we reparameterize the elasticity and each of the k share parameters as follows:

$$\rho = e^{\lambda} - 1 \tag{31}$$

$$\theta_k = \frac{1}{1 + e^{-\mu_k}} \tag{32}$$

This removes the need to explicitly constrain λ and μ_j while ensuring that $\rho \in (-1, \infty)$ and $\theta_k \in [0, 1]$. Ultimately, the objective of the problem is to minimize the sum of squared residuals (SSR) shown below where $Y_{i,t}^k$ denotes the inputs, γ is an efficiency parameter and f represents a production function, which in our case is a CES production function.

$$\min_{\gamma,\lambda,\mu} SSR_{i,t} = \min_{\gamma,\lambda,\mu} \sum_{t=1}^{T} (Y_{i,t} - f(\gamma, Y_{i,t}^k, \lambda, \mu_k))^2 \tag{33}$$

We use Adam to find the parameters that minimize SSR by updating them as shown below where t denotes the timestep in the optimization procedure and θ denotes the parameters. Adam differs from regular SGD since it computes adaptive learning rates for the parameters and updates these rates by computing two exponentially decaying averages of the first and second moments of past gradients. In doing so, it combines the features of Adadelta and AdaGrad methods.[39] Here, following Kingma and Ba (2014), we provide a brief exposition of the algorithm (refer to Kingma and Ba (2014) for more details):

1. Initialize m_0 and v_0, the first and second moment respectively as a vector of zeros. Set the step-size/learning rate δ.

[38] Adam belongs to a broader class of adaptive learning rate algorithms, which includes AdaGrad, RMSProp, and Adadelta.
[39] See Ruder (2016) for an overview of different SGD methods.

2. Derive gradients for a given parameter given by $g_t = \nabla_\theta r_t(\theta_{t-1})$ where r_t is the objective function as defined above.

3. Update the first (biased) moment as $m_t = \beta_1 \cdot m_{t-1} + (1 - \beta_1) g_t$ where β_1 is an exponential decay rate set at default 0.9.

4. Update the second (biased) moment as $v_t = \beta_2 \cdot v_{t-1} + (1 - \beta_2) g_t^2$ where β_2 is another exponential decay rate set at default 0.99.

5. Compute the bias-corrected versions of the first and second raw moment estimates as $\hat{m}_t = \frac{m_t}{(1-\beta_1^t)}$ and $\hat{v}_t = \frac{v_t}{(1-\beta_2^t)}$ respectively. This is to correct the moments' bias toward zero given their initialization.

6. Update the parameters as $\theta_t = \theta_{t-1} - \delta \frac{\hat{m}_t}{\sqrt{\hat{v}_t} + \epsilon}$ where $\epsilon = 10^{-8}$ to prevent division by zero.

As discussed in Qian et al. (2018), the benefits of using machine learning tools such as TensorFlow is that it uses automatic differentiation to calculate the gradients of complex objective functions.

B Climate Damages Estimation

B.1 Density Figures for Natural Capitals

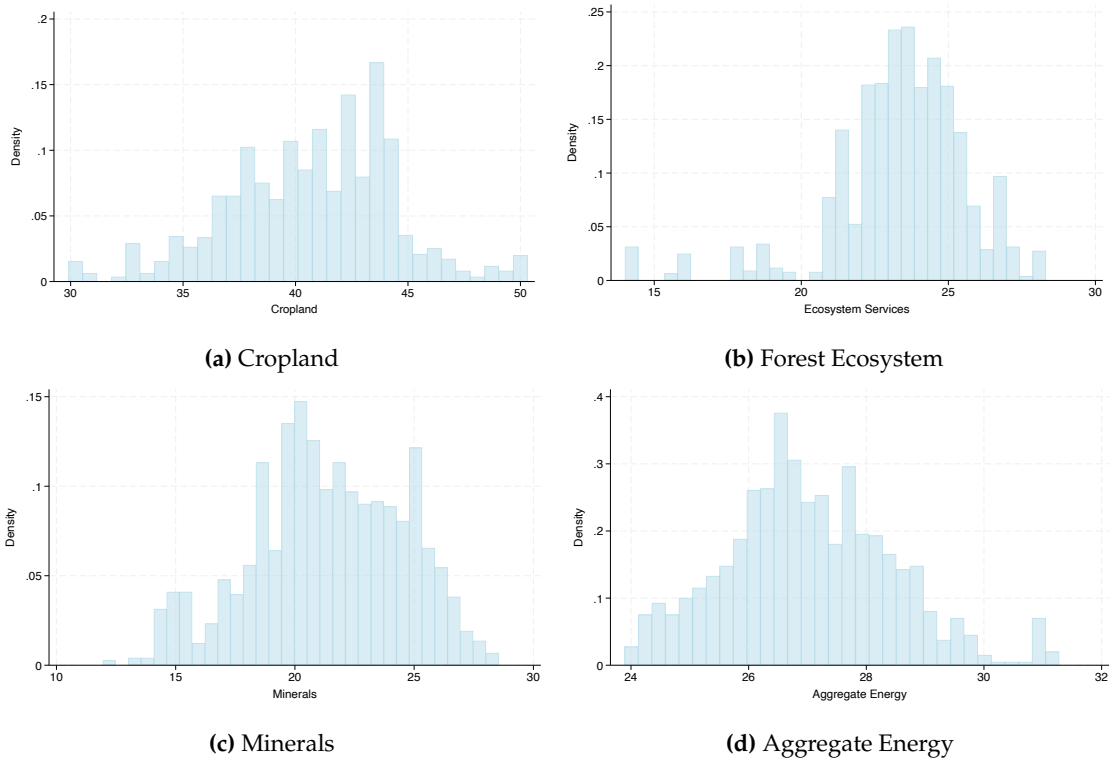

(a) Cropland

(b) Forest Ecosystem

(c) Minerals

(d) Aggregate Energy

Figure 15: Density distributions for the variables in nest one.

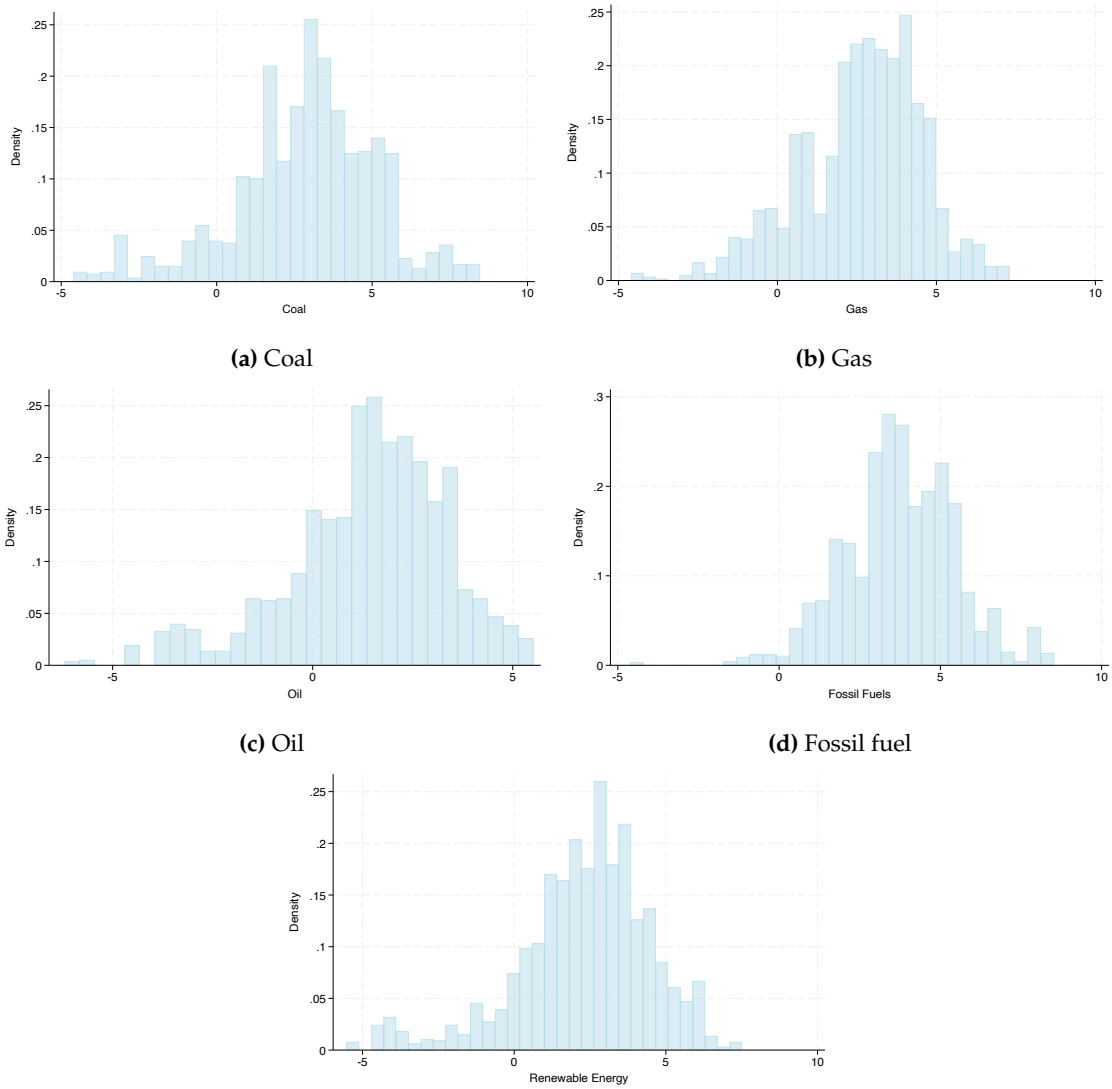

(a) Coal

(b) Gas

(c) Oil

(d) Fossil fuel

(e) Renewable energy

Figure 16: Density distributions for the variables in nests two and three.

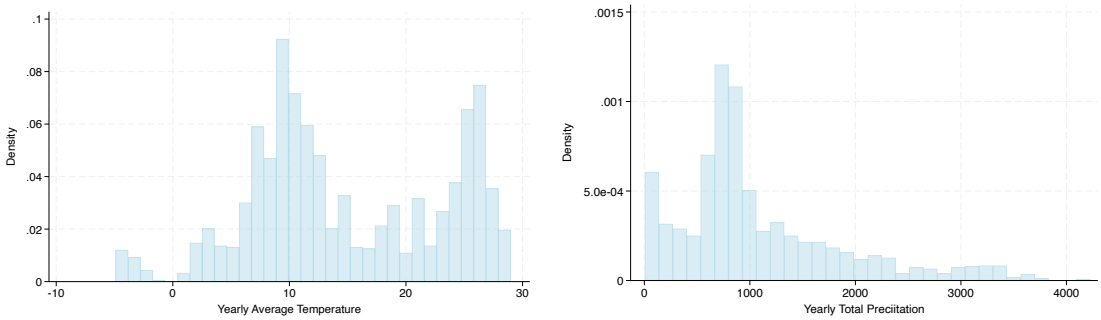

(a) Temperature **(b)** Precipitation

Figure 17: Density distributions for the climate variables

B.2 Stationarity Tests

	Statistic	p-value
Inverse chi-squared	471.278	0.000
Inverse normal	-14.789	0.000
Inverse logit	-13.906	0.000
Modified inv. chi-squared	19.285	0.000

Table 30: Panel unit-root Augmented Dickey Fueller tests results for yearly average temperature. Test statistics and p-values reported.

	Statistic	p-value
Inverse chi-squared	758.425	0.000
Inverse normal	-24.403	0.000
Inverse logit	-20.220	0.000
Modified inv. chi-squared	36.205	0.000

Table 31: Panel unit-root Augmented Dickey Fueller tests results for yearly total precipitation. Test statistics and p-values reported.

	Statistic	p-value
Inverse chi-squared	117.617	0.933
Inverse normal	0.741	0.770
Inverse logit	0.659	0.745
Modified inv. chi-squared	-1.447	0.926

Table 32: Panel unit-root Augmented Dickey Fueller tests results for coal. Test statistics and p-values reported. Model with trends.

	Statistic	p-value
Inverse chi-squared	198.550	0.001
Inverse normal	-1.353	0.088
Inverse logit	-0.908	0.182
Modified inv. chi-squared	3.356	0.000

Table 33: Panel unit-root Augmented Dickey Fueller tests results for gas. Test statistics and p-values reported. Model with trends.

	Statistic	p-value
Inverse chi-squared	277.578	0.000
Inverse normal	-5.132	0.000
Inverse logit	-4.556	0.000
Modified inv. chi-squared	7.871	0.000

Table 34: Panel unit-root Augmented Dickey Fueller tests results for oil. Test statistics and p-values reported. Model with trends.

	Statistic	p-value
Inverse chi-squared	185.915	0.011
Inverse normal	-1.235	0.109
Inverse logit	-1.129	0.130
Modified inv. chi-squared	2.470	0.007

Table 35: Panel unit-root Augmented Dickey Fueller tests results for fossil fuel. Test statistics and p-values reported. Model with trends.

	Statistic	p-value
Inverse chi-squared	163.741	0.124
Inverse normal	-0.798	0.213
Inverse logit	-0.604	0.273
Modified inv. chi-squared	1.163	0.122

Table 36: Panel unit-root Augmented Dickey Fueller tests results for gas aggregate energy. Test statistics and p-values reported. Model with trends.

	Statistic	p-value
Inverse chi-squared	186.098	0.010
Inverse normal	-0.264	0.396
Inverse logit	-0.018	0.493
Modified inv. chi-squared	2.481	0.007

Table 37: Panel unit-root Augmented Dickey Fueller tests results for renewable electricity. Test statistics and p-values reported. Model with trends.

	Statistic	p-value
Inverse chi-squared	182.514	0.016
Inverse normal	-0.861	0.195
Inverse logit	-0.615	0.269
Modified inv. chi-squared	2.269	0.012

Table 38: Panel unit-root Augmented Dickey Fueller tests results for forest ecosystem. Test statistics and p-values reported. Model with trends.

	Statistic	p-value
Inverse chi-squared	169.586	0.071
Inverse normal	-3.196	0.001
Inverse logit	-2.225	0.013
Modified inv. chi-squared	1.508	0.066

Table 39: Panel unit-root Augmented Dickey Fueller tests results for minerals. Test statistics and p-values reported.

	Statistic	p-value
Inverse chi-squared	262.336	0.000
Inverse normal	-1.380	0.084
Inverse logit	0.793	0.786
Modified inv. chi-squared	6.973	0.000

Table 40: Panel unit-root Augmented Dickey Fueller tests results for cropland. Test statistics and p-values reported.

C Non-Detrended Economy

C.1 Social Planner Equilibrium: Complete Model

Consistent with the model section, the following notations are used:
$i \in \left\{Y_t^O, Y_t^G, Y_t^C\right\}$
$j \in \left\{Y_t^K, Y_t^M, Y_t^L, Y_t^{FO}\right\}$
$k \in \left\{Y_t^K, Y_t^{AL}, Y_t^E, Y_t^L, Y_t^M, Y_t^{FO}\right\}$
$h \in \{i\} \cup \{j\} \cup \{RE\}$

The social planner face the following maximization problem:

$$
\begin{aligned}
\mathcal{L} = \mathbb{E}_0 \sum_{t=0}^{\infty} \beta^t \Bigg\{ & \frac{\left(C_t - \gamma_H H_t\right)^{1-\sigma^H}}{1-\sigma} \\
& + \lambda_t^C \left[Y_t^T - C_t - \sum_h D_t^h \right] \\
& + \lambda_t^C \lambda_t^H \left[H_{t+1} - \bar{m} H_t - (1-\bar{m}) C_t \right] \\
& + \lambda_t^C V_t^T \left[T_{t+1} - T_t - \epsilon_t^T \phi_1 \left(\phi_2 X_t - T_t \right) \right] \\
& + \lambda_t^C V_t^X \left[X_{t+1} - X_t - E_t \right] \\
& + \lambda_t^C V_t^E \left[E_t - \phi_E Y_t^{\mathrm{FE}} \right] \\
& + \lambda_t^C \Psi_t^{\mathrm{AL}} \left[e^{d_{\mathrm{AL}}(\cdot)} A_t L_t - Y_t^{\mathrm{AL}} \right] \\
& + \sum_h \lambda_t^C \Psi_t^h \left[e^{d_h(\cdot)} S_t^h - Y_t^h \right] \\
& + \sum_h \lambda_t^C \mathcal{R}_t^h \left[S_t^h + \epsilon_t^{D_h} \alpha_h D_t^h - \delta_h S_t^h - S_{t+1}^h \right] \\
& + \lambda_t^C \Psi_t^{\mathrm{FE}} \left[g_{\mathrm{FE}} \left(\sum_i \epsilon_i \left(Y_t^i \right)^{\frac{\epsilon-1}{\epsilon}} \right)^{\frac{\epsilon}{1-\epsilon}} - Y_t^{\mathrm{FE}} \right] \\
& + \lambda_t^C \Psi_t^{\mathrm{E}} \left[g_E \left(\sigma_{\mathrm{FE}} \left(Y_t^{\mathrm{FE}} \right)^{\frac{\sigma-1}{\sigma}} + \sigma_{\mathrm{RE}} \left(Y_t^{\mathrm{RE}} \right)^{\frac{\sigma-1}{\sigma}} \right)^{\frac{\sigma}{1-\sigma}} - Y_t^{\mathrm{E}} \right] \\
& + \lambda_t^C \Psi_t^T \left[\epsilon_t^A g_Y \left(\sum_k \gamma_k \left(Y_t^k \right)^{\frac{\theta-1}{\theta}} \right)^{\frac{\theta}{1-\theta}} - Y_t^T \right] \Bigg\}
\end{aligned}
$$

This yields the first order conditions (FOCs) with respect to:
$K_{t+1}, H_{t+1}, X_{t+1}, T_{t+1}, C_t, E_t, Y_t^{\mathrm{AL}}, Y_t^h, Y_t^{\mathrm{FE}}, Y_t^{\mathrm{RE}}, Y_t^{\mathrm{E}}, Y_t^T, S_{t+1}^h, D_t^h$

The FOCs read as:

$$[C_t] : (C_t - \gamma_H H_t)^{-\sigma^H} = \lambda_t^C + \lambda_t^C \lambda_t^H (1 - \bar{m})$$

$$[H_{t+1}] : \lambda_t^C \lambda_t^H = \beta \mathbb{E}_t \left\{ \gamma_H (C_{t+1} - H_{t+1})^{-\sigma} + \bar{m} \lambda_{t+1}^C \lambda_{t+1}^H \right\}$$

$$[X_{t+1}] : \lambda_t^C V_t^X = \beta \mathbb{E}_t \left\{ \lambda_{t+1}^C \left[V_{t+1}^X + \epsilon_{t+1}^T \phi_1 \phi_2 V_{t+1}^T \right] \right\}$$

$$[T_{t+1}] : V_t^T = \beta \mathbb{E}_t \left\{ \frac{\lambda_{t+1}^C}{\lambda_t^C} \left[(1 - \epsilon_{t+1}^T \phi_1) \right] V_{t+1}^T \right\} - \sum_h \sum_m \mathbb{E}_{t+m} \left\{ \left[\left(\prod_{o=0}^{m-1} \beta \frac{\lambda_{t+1+o}^C}{\lambda_{t+o}^C} \right) \Psi_{t+m}^h \beta_m^h Y_{t+m}^h \right] \right\}$$

$$[E_t] : V_t^X = V_t^E$$

$$\left[S_{t+1}^h \right] : \mathcal{R}_t^h = \mathbb{E}_t \left\{ \beta \frac{\lambda_{+1}^C}{\lambda_t^C} \left[(1 - \delta_h) \mathcal{R}_{t+1}^h + e^{d_h (T_{t+1})} \Psi_{t+1}^h \right] \right\}$$

$$\left[D_t^h \right] : \mathcal{R}_t^h = \frac{1}{\epsilon_t^{D_h} \alpha_h}$$

$$\left[Y_t^{\text{AL}} \right] : \Psi_t^{\text{AL}} = \Psi_t^T \gamma_{\text{AL}} \left(Y_t^{\text{AL}} \right)^{-\frac{1}{\theta}} \left(Y_t^T \right)^{\frac{1}{\theta}} \left(\epsilon_t^A g_Y \right)^{\frac{\theta - 1}{\theta}}$$

$$\left[Y_t^i \right] : \Psi_t^i = \Psi_t^{\text{FE}} \epsilon_i \left(Y_t^i \right)^{-\frac{1}{\epsilon}} \left(Y_t^{\text{FE}} \right)^{\frac{1}{\epsilon}} g_{\text{FE}}^{\frac{\epsilon - 1}{\epsilon}}$$

$$\left[Y_t^j \right] : \Psi_t^j = Y_t^T \gamma_j \left(Y_t^j \right)^{-\frac{1}{\theta}} \left(Y_t^T \right)^{\frac{1}{\theta}} \left(\epsilon_t^A g_Y \right)^{\frac{\theta - 1}{\theta}}$$

$$\left[Y_t^{\text{FE}} \right] : \Psi_t^{\text{FE}} = \Psi_t^{\text{E}} \sigma_{\text{FE}} \left(Y_t^{\text{FE}} \right)^{-\frac{1}{\sigma}} \left(Y_t^{\text{E}} \right)^{\frac{1}{\sigma}} g_E^{\frac{\sigma - 1}{\sigma}} - \phi_E V_t^E$$

$$\left[Y_t^{\text{RE}} \right] : \Psi_t^{\text{RE}} = \Psi_t^{\text{E}} \sigma_{\text{RE}} \left(Y_t^{\text{RE}} \right)^{-\frac{1}{\sigma}} \left(Y_t^E \right)^{\frac{1}{\sigma}} g_E^{\frac{\sigma - 1}{\sigma}}$$

$$\left[Y_t^{\text{E}} \right] : \Psi_t^{\text{E}} = \Psi_t^{\text{T}} \sigma_{\text{E}} \left(Y_t^{\text{E}} \right)^{-\frac{1}{\theta}} \left(Y_t^T \right)^{\frac{1}{\theta}} \left(\epsilon_t^A g_Y \right)^{\frac{\theta - 1}{\theta}}$$

$$\left[Y_t^{\text{T}} \right] : \Psi_t^T = 1$$

C.2 Social Planner Equilibrium: Model with Fossil Energy Only

The social planner problem for the reduced form model with fossil fuel energy only reads as:

$$
\begin{aligned}
\mathcal{L} = \mathbb{E}_0 \sum_{t=0}^{\infty} \beta^t \Bigg\{ & \frac{(C_t - \gamma_H H_t)^{1-\sigma}}{1-\sigma^H} \\
& + \lambda_t^C \left[Y_t^T - C_t - D_t^{\mathrm{K}} - D_t^{\mathrm{FE}} \right] \\
& + \lambda_t^C \lambda_t^H \left[H_{t+1} - \bar{m} H_t - (1-\bar{m}) C_t \right] \\
& + \lambda_t^C V_t^T \left[T_{t+1} - T_t - \epsilon_t^T \phi_1 \left(\phi_2 X_t - T_t \right) \right] \\
& + \lambda_t^C V_t^X \left[X_{t+1} - X_t - E_t \right] \\
& + \lambda_t^C V_t^E \left[E_t - \phi_E Y_t^{\mathrm{FE}} \right] \\
& + \lambda_t^C \Psi_t^{\mathrm{AL}} \left[e^{d_{\mathrm{AL}}(\cdot)} A_t L_t - Y_t^{\mathrm{AL}} \right] \\
& + \lambda_t^C \Psi_t^{\mathrm{K}} \left[e^{d_{\mathrm{K}}(\cdot)} S_t^{\mathrm{K}} - Y_t^{\mathrm{K}} \right] \\
& + \lambda_t^C \Psi_t^{\mathrm{FE}} \left[e^{d_{\mathrm{FE}}(\cdot)} S_t^{\mathrm{FE}} - Y_t^{\mathrm{FE}} \right] \\
& + \lambda_t^C \mathcal{R}_t^{\mathrm{K}} \left[S_t^{\mathrm{K}} + \epsilon_t^{D_K} \alpha_K D_t^{\mathrm{K}} - \delta_{\mathrm{K}} S_t^{\mathrm{K}} - S_{t+1}^{\mathrm{K}} \right] \\
& + \lambda_t^C \mathcal{R}_t^{\mathrm{FE}} \left[S_t^{\mathrm{FE}} + \epsilon_t^{D_{FE}} \alpha_{\mathrm{FE}} D_t^{\mathrm{FE}} - \delta_{\mathrm{FE}} S_t^{\mathrm{FE}} - S_{t+1}^{\mathrm{FE}} \right] \\
& + \lambda_t^C \Psi_t^T \left[\epsilon_t^A g_Y \left(\gamma_{\mathrm{K}} \left(Y_t^{\mathrm{K}} \right)^{\frac{\theta-1}{\theta}} + \gamma_{\mathrm{FE}} \left(Y_t^{\mathrm{FE}} \right)^{\frac{\theta-1}{\theta}} + \gamma_{\mathrm{AL}} \left(Y_t^{\mathrm{AL}} \right)^{\frac{\theta-1}{\theta}} \right)^{\frac{\theta}{1-\theta}} - Y_t^{\mathrm{T}} \right] \Bigg\}
\end{aligned}
$$

In the following, we present all first-order conditions (FOCs). Notice that the FOCs with respect to: $T_{t+1}, Y_t^T, Y_t^{\mathrm{FE}}, S_{t+1}^{\mathrm{FE}}, D_t^{\mathrm{FE}}$ differ from those in the full model case, while the remaining FOCs (with respect to $H_{t+1}, X_{t+1}, C_t, E_t, Y_t^{\mathrm{AL}}, Y_t^{\mathrm{K}}, S_{t+1}^{\mathrm{K}}, D_t^{\mathrm{K}}$) remain similar to those in the full-scale model with all natural capital.

The FOCs read as:

$$[C_t] : (C_t - \gamma_H H_t)^{-\sigma} = \lambda_t^C + \lambda_t^C \lambda_t^H (1 - \bar{m})$$

$$[H_{t+1}] : \lambda_t^C \lambda_t^H = \beta \mathbb{E}_t \left\{ \gamma_H (C_{t+1} - H_{t+1})^{-\sigma} + \bar{m} \lambda_{t+1}^C \lambda_{t+1}^H \right\}$$

$$[X_{t+1}] : \lambda_t^C V_t^X = \beta \mathbb{E}_t \left\{ \lambda_{t+1}^C \left[V_{t+1}^X + \epsilon_{t+1}^T \phi_1 \phi_2 V_{t+1}^T \right] \right\}$$

$$[T_{t+1}] : V_t^T = \beta \mathbb{E}_t \left\{ \frac{\lambda_{t+1}^C}{\lambda_t^C} \left[(1 - \epsilon_{t+1}^T \phi_1) \right] V_{t+1}^T \right\} - \sum_h \sum_m \mathbb{E}_{t+m} \left\{ \left[\left(\prod_{o=0}^{m-1} \beta \frac{\lambda_{t+1+o}^C}{\lambda_{t+o}^C} \right) \Psi_{t+m}^h \beta_m^h Y_{t+m}^h \right] \right\}$$

$$[E_t] : V_t^X = V_t^E$$

$$\left[S_{t+1}^{\mathrm{K}} \right] : \mathcal{R}_t^{\mathrm{K}} = \mathbb{E}_t \left\{ \beta \frac{\lambda_{+1}^C}{\lambda_t^C} \left[(1 - \delta_{\mathrm{K}}) \mathcal{R}_{t+1}^{\mathrm{K}} + e^{d_{\mathrm{K}}(T_{t+1})} \Psi_{t+1}^{\mathrm{K}} \right] \right\}$$

$$\left[S_{t+1}^{\mathrm{FE}} \right] : \mathcal{R}_t^{\mathrm{FE}} = \mathbb{E}_t \left\{ \beta \frac{\lambda_{+1}^C}{\lambda_t^C} \left[(1 - \delta_{\mathrm{FE}}) \mathcal{R}_{t+1}^{\mathrm{FE}} + e^{d_{\mathrm{FE}}(T_{t+1})} \Psi_{t+1}^{\mathrm{FE}} \right] \right\}$$

$$\left[D_t^{\mathrm{K}} \right] : \mathcal{R}_t^{\mathrm{K}} = \frac{1}{\epsilon_t^{D_K} \alpha_{\mathrm{K}}}$$

$$\left[D_t^{\mathrm{FE}} \right] : \mathcal{R}_t^{\mathrm{FE}} = \frac{1}{\epsilon_t^{D_F E} \alpha_{\mathrm{FE}}}$$

$$\left[Y_t^{\mathrm{AL}} \right] : \Psi_t^{\mathrm{AL}} = \Psi_t^T \gamma_{\mathrm{AL}} \left(Y_t^{\mathrm{AL}} \right)^{-\frac{1}{\theta}} \left(Y_t^T \right)^{\frac{1}{\theta}} \left(\epsilon_t^A g_Y \right)^{\frac{\theta - 1}{\theta}}$$

$$\left[Y_t^{\mathrm{FE}} \right] : \Psi_t^{\mathrm{FE}} = \Psi_t^{\mathrm{T}} \gamma_{\mathrm{FE}} \left(Y_t^{\mathrm{FE}} \right)^{-\frac{1}{\theta}} \left(Y_t^{\mathrm{T}} \right)^{\frac{1}{\theta}} \left(\epsilon_t^A g_Y \right)^{\frac{\theta - 1}{\theta}} - \phi_E V_t^E$$

$$\left[Y_t^{\mathrm{T}} \right] : \Psi_t^T = 1$$

where h here is produced capital, fossil energy, and labor production.

D Stationary Equilibrium

D.1 The Balanced Growth Path: (For Both Models)

In this section, we present the detrended model around its balanced growth path (BGP). We denote all stationary variables with lower case letters (e.g. x_t), while variables following the trend will be referred with capital letters (e.g. X_t).

Consistent with the model section, the following notations are used:
$i \in \left\{Y_t^O, Y_t^G, Y_t^C\right\}$
$j \in \left\{Y_t^M, Y_t^L, Y_t^{FO}\right\}$
$k \in \left\{Y_t^K, Y_t^E, Y_t^L, Y_t^M, Y_t^{FO}\right\}$
$h \in \{i\} \cup \{j\} \cup \{RE\}$

Labor-augmenting technological change is subject to an exogenous growth process Γ_t such that $\Gamma_t = \gamma^\Gamma \Gamma_{t-1}$[40] and where:

$$Y_t^{AL} = e^{d(\cdot)} A(\Gamma_t \bar{L}) \tag{34}$$

where both $\bar{A}$ and $\bar{L}$ are stationary variables. Thus,

$$y_t^{AL} = e^{d(\cdot)} A\bar{L} \tag{35}$$

and where $y_t^{AL} = \frac{Y_t^{AL}}{\Gamma_t}$ where for simplicity we set $A_t = \bar{A}$.

Similarly, aggregate output reads as:

$$Y_t^T = \epsilon_t^A g_Y \left(\sum_k \gamma_k \left(Y_t^k\right)^{\frac{\theta-1}{\theta}} + \gamma_{AL} \left(Y_t^{AL}\right)^{\frac{\theta-1}{\theta}} \right)^{\frac{\theta}{1-\theta}} \tag{36}$$

The detrended output reads as:

$$y_t^T = \epsilon_t^A g_Y \left(\sum_k \gamma_k \left(y_t^k\right)^{\frac{\theta-1}{\theta}} + \gamma_{AL} \left(y_t^{AL}\right)^{\frac{\theta-1}{\theta}} \right)^{\frac{\theta}{1-\theta}} \tag{37}$$

where $y_t^T = \frac{Y_t^T}{\Gamma_t}$ and $y_t^k = \frac{Y_t^k}{\Gamma_t}$

As such all capitals in the economy grow at rate γ^Γ with:

$$\gamma^\Gamma s_{t+1}^h = \epsilon_t^{D_h} \alpha_h d_t^h + (1 - \delta_h) s_t^h \tag{38}$$

where $d_t^h = \frac{D_t^h}{\Gamma_t}$ and $s_t^h = \frac{S_t^h}{\Gamma_t}$.

[40] Where $\gamma^\Gamma = 1 + \tilde{\gamma}^\Gamma$, with $\tilde{\gamma}^\Gamma = 3\%$ in our simulations.

Since fossil energy grows at rate γ^{Γ}, so do CO_2 emissions:

$$e_t = \phi_E y_t^F \tag{39}$$

with $e_t = \frac{E_t}{\Gamma_t}$.

Cumulative emissions and temperature will also follow the same economy growth rate:

$$\gamma^{\Gamma} x_{t+1} = x_t + e_t \tag{40}$$

$$\gamma^{\Gamma} t_{t+1} = \epsilon_t^T \phi_1 (\phi_2 x_t - t_t) + t_t \tag{41}$$

The damage functions are stationary with $\tilde{\beta}_m^h = \beta_m^h \Gamma_{t-m}$:[41]

$$d(\cdot) = \sum_m \tilde{\beta}_m^h t_{t-m} \tag{42}$$

The de-trending of the remaining output variables is straightforward:

$$y_t^h = e^{d_h(\cdot)} s_t^h. \tag{43}$$

Finally the detrended utility function reads as:

$$\mathbb{E}_0 \sum_{t=0}^{\infty} \tilde{\beta}^t \left\{ \frac{(c_t - \gamma_H h_t)^{1-\sigma^H}}{1-\sigma} \right\} \tag{44}$$

where $\tilde{\beta}^t = \beta^t \Gamma_t^{1-\sigma}$.

The habits formation reads as:

$$\gamma^{\Gamma} h_{t+1} = \bar{m} h_t + (1 - \bar{m}) c_t. \tag{45}$$

In the case of the model with fossil fuel only, please notice that all variables are detrended similarly to the full model. Essentially, the model with fossil fuel only is a special case of the large model with different natural capitals.

D.2 The Social Planner

The social planner face the same maximization problem presented above:

[41] An assumption we will make when focusing on the long-run transitions is: $\tilde{\beta}_m^h \approx \beta_m^h$ in order to make sure damages are not decreasing overtime.

$$
\begin{aligned}
\mathcal{L} = \mathbb{E}_0 \sum_{t=0}^{\infty} \tilde{\beta}^t \Bigg\{ & \frac{\left(c_t - \gamma_H h_t\right)^{1-\sigma^H}}{1-\sigma} \\
& + \lambda_t^C \left[y_t^T - c_t - \sum_h d_t^h \right] \\
& + \lambda_t^C \lambda_t^H \left[\gamma^\Gamma h_{t+1} - \bar{m} h_t - (1-\bar{m}) c_t \right] \\
& + \lambda_t^C v_t^T \left[\gamma^\Gamma t_{t+1} - t_t - \epsilon_t^T \phi_1 \left(\phi_2 x_t - t_t \right) \right] \\
& + \lambda_t^C v_t^X \left[\gamma^\Gamma x_{t+1} - x_t - e_t \right] \\
& + \lambda_t^C v_t^E \left[e_t - \phi_E y_t^{\text{FE}} \right] \\
& + \lambda_t^C \psi_t^{\text{AL}} \left[e^{d_{\text{AL}}(\cdot)} \bar{A} \bar{L} - y_t^{\text{AL}} \right] \\
& + \sum_h \lambda_t^C \psi_t^h \left[e^{d_h(\cdot)} s_t^h - y_t^h \right] \\
& + \sum_h \lambda_t^C r_t^h \left[s_t^h + \epsilon_t^{D_h} \alpha_h d_t^h - \delta_h s_t^h - \gamma^\Gamma s_{t+1}^h \right] \\
& + \lambda_t^C \psi_t^{\text{FE}} \left[g_{\text{FE}} \left(\sum_i \epsilon_i \left(y_t^i \right)^{\frac{\epsilon-1}{\epsilon}} \right)^{\frac{\epsilon}{1-\epsilon}} - y_t^{\text{FE}} \right] \\
& + \lambda_t^C \psi_t^{\text{E}} \left[g_E \left(\sigma_{\text{FE}} \left(y_t^{\text{FE}} \right)^{\frac{\sigma-1}{\sigma}} + \sigma_{\text{RE}} \left(y_t^{\text{RE}} \right)^{\frac{\sigma-1}{\sigma}} \right)^{\frac{\sigma}{1-\sigma}} - y_t^{\text{E}} \right] \\
& + \lambda_t^C \psi_t^T \left[\epsilon_t^A g_Y \left(\sum_k \gamma_k \left(y_t^k \right)^{\frac{\theta-1}{\theta}} \right)^{\frac{\theta}{1-\theta}} - y_t^T \right] \Bigg\}
\end{aligned}
$$

This yields the first order conditions (FOCs) with respect to:
$k_{t+1}, h_{t+1}, x_{t+1}, t_{t+1}, c_t, e_t, y_t^{\text{AL}}, y_t^h, y_t^{\text{FE}}, y_t^{\text{RE}}, y_t^{\text{E}}, y_t^T, s_{t+1}^h, d_t^h$

The FOCs read as:

$$[c_t] : (c_t - \gamma_H h_t)^{-\sigma^H} = \lambda_t^C + \lambda_t^C \lambda_t^H (1 - \bar{m})$$

$$[h_{t+1}] : \gamma^\Gamma \lambda_t^C \lambda_t^H = \tilde{\beta} \mathbb{E}_t \left\{ \gamma_H (c_{t+1} - h_{t+1})^{-\sigma} + \bar{m} \lambda_{t+1}^C \lambda_{t+1}^H \right\}$$

$$[x_{t+1}] : \gamma^\Gamma \lambda_t^C v_t^X = \tilde{\beta} \mathbb{E}_t \left\{ \lambda_{t+1}^C \left[v_{t+1}^X + \epsilon_{t+1}^T \phi_1 \phi_2 v_{t+1}^T \right] \right\}$$

$$[t_{t+1}] : \gamma^\Gamma v_t^T = \tilde{\beta} \mathbb{E}_t \left\{ \frac{\lambda_{t+1}^C}{\lambda_t^C} \left[(1 - \epsilon_{t+1}^T \phi_1) \right] v_{t+1}^T \right\} - \sum_h \sum_m \mathbb{E}_{t+m} \left\{ \left[\left(\prod_{o=0}^{m-1} \tilde{\beta} \frac{\lambda_{t+1+o}^C}{\lambda_{t+o}^C} \right) \psi_{t+m}^h \tilde{\beta}_m^h y_{t+m}^h \right] \right\}$$

$$[e_t] : v_t^X = v_t^E$$

$$\left[s_{t+1}^h \right] : \gamma^\Gamma r_t^h = \mathbb{E}_t \left\{ \tilde{\beta} \frac{\lambda_{+1}^C}{\lambda_t^C} \left[(1 - \delta_h) r_{t+1}^h + e^{d_h(T_{t+1})} \psi_{t+1}^h \right] \right\}$$

$$\left[d_t^h \right] : r_t^h = \frac{1}{\epsilon_t^{D_h} \alpha_h}$$

$$\left[y_t^{\text{AL}} \right] : \psi_t^{\text{AL}} = \psi_t^T \gamma_{\text{AL}} \left(y_t^{\text{AL}} \right)^{-\frac{1}{\theta}} \left(y_t^T \right)^{\frac{1}{\theta}} \left(\epsilon_t^A g_Y \right)^{\frac{\theta - 1}{\theta}}$$

$$\left[y_t^i \right] : \psi_t^i = \psi_t^{\text{FE}} \epsilon_i \left(y_t^i \right)^{-\frac{1}{\epsilon}} \left(y_t^{\text{FE}} \right)^{\frac{1}{\epsilon}} g_{\text{FE}}^{\frac{\epsilon - 1}{\epsilon}}$$

$$\left[y_t^j \right] : \psi_t^j = y_t^T \gamma_j \left(y_t^j \right)^{-\frac{1}{\theta}} \left(y_t^T \right)^{\frac{1}{\theta}} \left(\epsilon_t^A g_Y \right)^{\frac{\theta - 1}{\theta}}$$

$$\left[y_t^{\text{FE}} \right] : \psi_t^{\text{E}} = \psi_t^{\text{E}} \sigma_{\text{FE}} \left(y_t^{\text{FE}} \right)^{-\frac{1}{\sigma}} \left(y_t^{\text{E}} \right)^{\frac{1}{\sigma}} g_E^{\frac{\sigma - 1}{\sigma}} - \phi_E v_t^E$$

$$\left[y_t^{\text{RE}} \right] : \psi_t^{\text{RE}} = \psi_t^{\text{E}} \sigma_{\text{RE}} \left(y_t^{\text{RE}} \right)^{-\frac{1}{\sigma}} \left(y_t^E \right)^{\frac{1}{\sigma}} g_E^{\frac{\sigma - 1}{\sigma}}$$

$$\left[y_t^{\text{E}} \right] : \psi_t^{\text{E}} = \psi_t^{\text{T}} \sigma_{\text{E}} \left(y_t^{\text{E}} \right)^{-\frac{1}{\theta}} \left(y_t^T \right)^{\frac{1}{\theta}} \left(\epsilon_t^A g_Y \right)^{\frac{\theta - 1}{\theta}}$$

$$\left[y_t^{\text{T}} \right] : \psi_t^T = 1$$

Notice that the fossil energy only model's detrended equilibrium FOC(s) remain similar to the non-detrended case and will be adjusted similar to what we presented in the case of the full detrended model presented just above.